Cell

Article

Engineered nucleocytosolic vehicles for loading of programmable editors

Graphical abstract

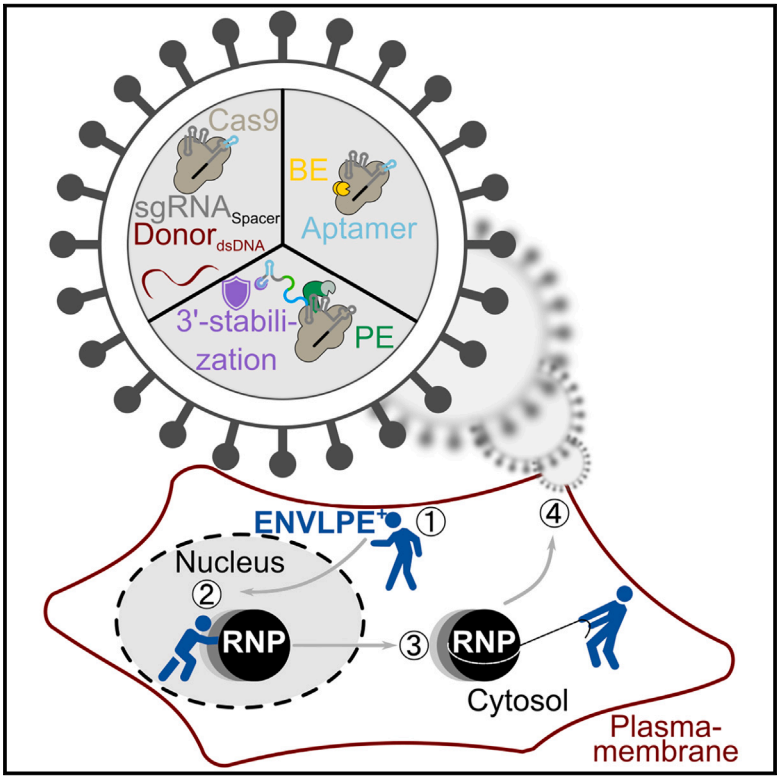

Highlights

- Nucleocytosolic shuttling allows modular loading of gene editors into VLPs via aptamers
- ENVLPE$^+$ VLPs achieve superior per-particle editing efficiency compared with previous VLPs
- 3′-pegRNA protection with Csy4 improves prime editing efficiency in VLP-based delivery
- ENVLPE$^+$ efficiently restores gene function in mouse models of inherited eye disease

Authors

Julian Geilenkeuser, Niklas Armbrust, Emily Steinmaßl, ..., Krzysztof Palczewski, Gil Gregor Westmeyer, Dong-Jiunn Jeffery Truong

Correspondence

gil.westmeyer@tum.de (G.G.W.), jeffery.truong@helmholtz-munich.de (D.-J.J.T.)

In brief

Engineered nucleocytosolic vehicles for loading of programmable editors (ENVLPE) with enhanced CRISPR ribonucleoprotein (RNP) loading and stabilization enable the efficient delivery of gene-editing effectors, such as nuclease, base, and prime editors. ENVLPE$^+$ outperforms existing VLP systems for *ex vivo* and *in vivo* gene editing, including the restoration of gene function in retinal disease models.

Geilenkeuser et al., 2025, Cell *188*, 1–19
May 15, 2025
https://doi.org/10.1016/j.cell.2025.03.015

CellPress

Cell

CellPress
OPEN ACCESS

Article

Engineered nucleocytosolic vehicles for loading of programmable editors

Julian Geilenkeuser,[1,2,10] Niklas Armbrust,[1,2,10] Emily Steinmaßl,[1,2] Samuel W. Du,[3,4] Sebastian Schmidt,[1,2,5] Eva Maria Hildegard Binder,[1,2] Yuchun Li,[1,2] Niklas Wilhelm Warsing,[1,2] Stephanie Victoria Wendel,[1,2] Florian von der Linde,[1,2] Elisa Marie Schiele,[1,2] Xiya Niu,[1] Luisa Stroppel,[1,2] Oleksandr Berezin,[1,2] Tobias Heinrich Santl,[1,2] Tanja Orschmann,[1,5] Keith Nelson,[1,2] Christoph Gruber,[5] Grazyna Palczewska,[3] Carolline Rodrigues Menezes,[3,4] Eleonora Risaliti,[3,4] Zachary J. Engfer,[3,4] Naile Koleci,[6] Andrea Schmidts,[6] Arie Geerlof,[7] Krzysztof Palczewski,[3,4,8,9] Gil Gregor Westmeyer,[1,2,*] and Dong-Jiunn Jeffery Truong[1,2,11,*]

[1]Institute for Synthetic Biomedicine, Helmholtz Munich, Neuherberg, Germany
[2]Department of Bioscience, TUM School of Natural Sciences, Technical University of Munich, Munich, Germany
[3]Gavin Herbert Eye Institute – Center for Translational Vision Research, Department of Ophthalmology, University of California, Irvine, Irvine, CA, USA
[4]Department of Physiology & Biophysics, University of California, Irvine, Irvine, CA, USA
[5]Institute of Developmental Genetics, Helmholtz Munich, Neuherberg, Germany
[6]Department of Medicine III: Hematology/Oncology, Klinikum rechts der Isar of the Technical University of Munich, TUM School of Medicine and Health, Munich, Germany
[7]Institute of Structural Biology, Helmholtz Munich, Neuherberg, Germany
[8]Department of Chemistry, University of California, Irvine, Irvine, CA, USA
[9]Department of Molecular Biology and Biochemistry, University of California, Irvine, Irvine, CA, USA
[10]These authors contributed equally
[11]Lead contact
*Correspondence: gil.westmeyer@tum.de (G.G.W.), jeffery.truong@helmholtz-munich.de (D.-J.J.T.)
https://doi.org/10.1016/j.cell.2025.03.015

SUMMARY

Advanced gene editing methods have accelerated biomedical discovery and hold great therapeutic promise, but safe and efficient delivery of gene editors remains challenging. In this study, we present a virus-like particle (VLP) system featuring nucleocytosolic shuttling vehicles that retrieve pre-assembled Cas-effectors via aptamer-tagged guide RNAs. This approach ensures preferential loading of fully assembled editor ribonucleoproteins (RNPs) and enhances the efficacy of prime editing, base editing, *trans*-activators, and nuclease activity coupled to homology-directed repair in multiple immortalized, primary, stem cell, and stem-cell-derived cell types. We also achieve additional protection of inherently unstable prime editing guide RNAs (pegRNAs) by shielding the 3′-exposed end with Csy4/Cas6f, further enhancing editing performance. Furthermore, we identify a minimal set of packaging and budding modules that can serve as a platform for bottom-up engineering of enveloped delivery vehicles. Notably, our system demonstrates superior per-VLP editing efficiency in primary T lymphocytes and two mouse models of inherited retinal disease, highlighting its therapeutic potential.

INTRODUCTION

The rapid development of various gene editing technologies over the past decade has revolutionized the field of molecular biology, allowing the precise manipulation of virtually any gene with single nucleotide precision. In particular, the recent development of base editors[1–8] and prime editors,[9] which mediate single-nucleotide conversions, deletions/insertions, or even whole gene insertions,[10,11] all without the need for mutagenic double-stranded DNA breaks (DSBs), represents a substantial advance toward genome editing. However, the efficient and safe delivery of these editing complexes remains challenging.

Viral vectors, particularly adeno-associated viruses (AAVs), are widely used for *in vivo* genome editing. Despite their safety and efficacy, AAVs have limitations, such as constrained cargo capacity, potential immunogenicity, and the risk of insertional mutagenesis and unintended mutations at on- and off-target sites due to their long persistence. Other viral vectors, including lentiviruses commonly employed in chimeric antigen receptor (CAR)-T cell therapies, integrate into the host genome, which may raise safety concerns due to insertional mutagenesis causing potential malignancy.[12]

Regardless of the delivery method, prolonged expression of genome editors can increase the risk of off-target effects

Please cite this article in press as: Geilenkeuser et al., Engineered nucleocytosolic vehicles for loading of programmable editors, Cell (2025), https://doi.org/10.1016/j.cell.2025.03.015

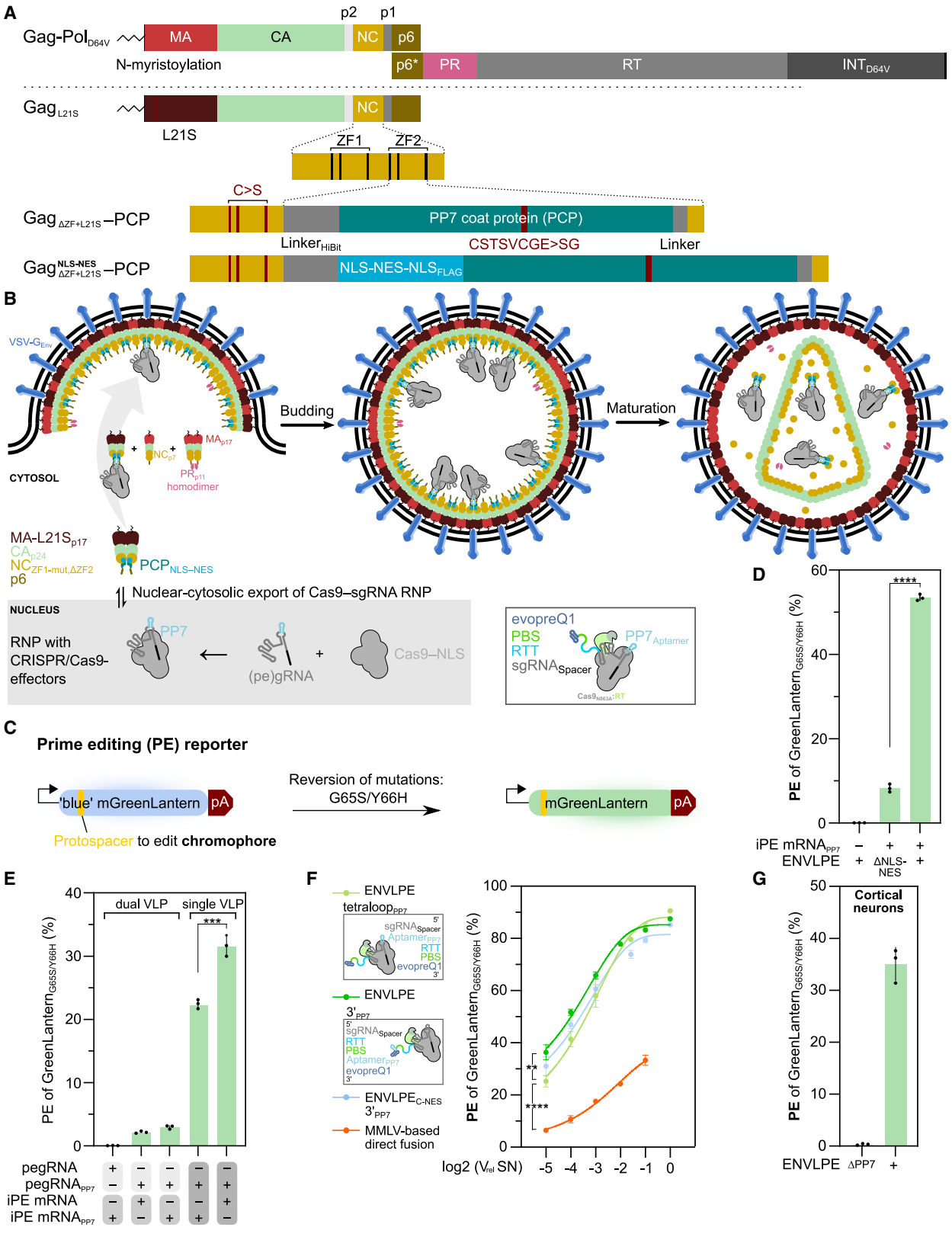

(legend on next page)

Please cite this article in press as: Geilenkeuser et al., Engineered nucleocytosolic vehicles for loading of programmable editors, Cell (2025), https://doi.org/10.1016/j.cell.2025.03.015

and immune responses. Therefore, there is a need for delivery systems that allow the cargo to persist only for a limited duration, enough to execute the desired edit but short enough to circumvent the harmful impacts of long-term expression.

In this context, lipid nanoparticles (LNPs) have gained attention as non-viral delivery vehicles for nucleic acids.[12] However, they often have limited cell-type specificity and require complex formulation and optimization for efficient delivery.

In contrast, virus-like particle (VLP) systems offer several advantages, including their capacity for pseudotyping,[13–16] enabling modulation of cell or tissue tropism by exploiting the diversity of known viruses with different tropisms. This facilitates the re-engineering of glycoproteins to target specific cell types or tissues, further enhancing the versatility and applicability of VLP systems. Importantly, VLP systems can package and deliver genome editing complexes as ribonucleoproteins (RNPs) without the risk of insertional mutagenesis or activation of the host immune response due to viral components or persistent transgene expression. Recent strategies rely on packaging the RNP editor via the Cas component, primarily by direct fusion to Gag,[17–21] which requires complex design considerations and optimization of the linker and the protease site depending on the editor protein of choice to enable efficient obligatory proteolytic cargo release.[22]

However, not only is a Cas9 apoenzyme less stable than a corresponding RNP complex,[23] the half-life of single guide RNAs (sgRNAs) is also orders of magnitude shorter than sgRNAs embedded into RNP complexes.[24–26] This characteristic leads to the conclusion that prime editing guide RNAs (pegRNAs), which carry a 3′-extended region encoding the desired edit as a reverse transcription template (RTT) followed by a primer binding site (PBS), are particularly prone to exonucleolytic degradation.[27,28]

We, therefore, opted for a recruitment mechanism based on RNA aptamers grafted onto (pe)gRNAs[29,30] to increase the likelihood of packaging functional RNPs. We further reasoned that such a VLP system could substantially benefit from the active transport of (pe)gRNAs from the nucleus to the cytosol, as (pe)gRNAs do not naturally reside in the cytosol where VLP cargo packaging occurs.

Thus, we have developed an optimized VLP system based on nucleocytosolic-shuttling vehicles that can load a Cas9 editor of choice via the (pe)gRNA, further stabilized by a dedicated 3′ protection mechanism. This design increases the fraction of functional RNP editors, which can be released in the target cell without proteolytic processing. We characterize the function of the individual features of this genetically engineered VLP-packaging system, which we call engineered nucleocytosolic vehicles for loading of programmable editors (ENVLPE). We benchmark ENVLPE's performance and demonstrate its utility in *ex vivo* and *in vivo* applications.

RESULTS

Gag-PCP shuttling enables efficient loading of (pe)gRNAs

To achieve packaging of the RNP editors via aptamer-tagged (pe)gRNAs, we inactivated the first zinc finger (ZF1) motif and installed the PP7 coat protein (PCP)[31] in lieu of the second zinc finger (ZF2) motif within the nucleocapsid (NC) domain of the HIV-1 Gag polyprotein (Figure 1A). We then introduced L21S into the matrix (MA) domain, which has been shown to enhance membrane trafficking,[32] as modifications within the NC domains

Figure 1. Development of nucleocytosolic shuttling vehicles to package editor-RNPs

(A) The top schematic diagram shows HIV-1-derived Gag-Pol$_{D64V}$, a lentiviral packaging vector encoding Gag (matrix [MA], capsid [CA], nucleocapsid [NC], and p6 domain), and the alternative reading frame encoding the enzymatic components, such as protease (PR), reverse transcriptase (RT), and an inactivated integrase (INT$_{D64V}$) as reference. The initial ENLVPE design is based on a codon-optimized Gag with L21S, which improves membrane-targeting, combined with the grafting of a PP7 coat protein (PCP) into the second zinc-finger motif within the NC domain to enable binding to PP7-aptamer-tagged guide RNAs. The first zinc-finger motif was inactivated by C>S mutations. The bottom illustration shows the additional insertions of a concatenation of nuclear localization (NLS) and export sequences (NES) to facilitate Gag shuttling between the nucleus and cytosol.

(B) Schematic of the RNP-packaging and budding mechanism. In the nucleus (gray shading), co-expression of PP7-aptamer-tagged (pe)gRNAs and Cas9 with an NLS (Cas9-NLS) leads to the formation of the RNP editor, which stabilizes the (pe)gRNA. The box on the right illustrates PP7-tagged (pe)gRNA used for prime editing (PE), with further 3′-protection by the evopreQ1 motif. Gag-PCP with nucleocytosolic shuttling functionality (NLS-NES) then relocates the RNP editor to the cytosol via the PP7 handle on the (pe)gRNA. At the plasma membrane, the RNP-editor is packaged into VLPs. Proteolytic cleavage of Gag can then lead to the structural maturation of the VLPs.

(C) The PE reporter system expresses a stably integrated mGreenLantern harboring two mutations in the chromophore (G65S, Y66H), resulting in a hypsochromic emission shift from green to blue fluorescence. Successful PE reverts the mutations to their original state, resulting in green fluorescence.

(D) The effect of the NLS-NES shuttling motif for the PE efficacies of ENVLPE delivering improved PE (iPE), quantified by fluorescence-activated cell sorting (FACS) of the blue mGL reporter HEK293T cell line. Bars represent mean ± SD (n = 3 biological replicates).

(E) Co-transduction of HEK293T with two separate ENVLPE preparations that deliver PP7-tagged pegRNA or mRNA coding for iPE (dual VLP), respectively, in comparison with delivery of all components in a single ENVLPE (single VLP). For each group, the pegRNA or the mRNA encoding iPE was either PP7-tagged or not. Bars represent mean ± SD (n = 3 biological replicates).

(F) Comparison of the initial pegRNA design with the PP7 aptamer inserted in the tetraloop (tetraloop$_{PP7}$) and a version with the PP7 aptamer moved toward the 3′-end to prevent packaging of 3′ truncated pegRNAs (3′$_{PP7}$). A variant with the NES shifted to the C terminus of Gag was also tested (C-NES). As a control (orange line), we compared a system with direct protein fusion of a prime editor to MMLV-gag (by switching the BE for a PE in v4 BE-eVLP [orange]). Experiments were performed on the blue mGL HEK293T line. Dots represent mean ± SD (n = 3 biological replicates). Log$_2$(V_{rel}SN): relative transduction volumes in 2× dilution steps. Editing rates of the lowest VLP titer were analyzed via Bonferroni multiple comparisons test (MCT) after one-way ANOVA ($p < 0.0001$; $^{**}p < 0.01$).

(G) PE performance of ENVLPE on human induced pluripotent stem cell (hiPSC)-derived cortical neurons carrying the blue mGL reporter. Bars represent mean ± SD (n = 3 biological replicates).

The results of two-tailed unpaired t tests are shown for (D) and (E) ($^{****}p < 0.0001$; $^{***}p < 0.001$; $^{**}p < 0.01$).

See also Figures S2, S3, and S17.

Please cite this article in press as: Geilenkeuser et al., Engineered nucleocytosolic vehicles for loading of programmable editors, Cell (2025), https://doi.org/10.1016/j.cell.2025.03.015

may negatively correlate with membrane recruitment and budding.[33] To enable packaging via PCP, a PP7 aptamer was grafted into the tetraloop of the SpCas9 gRNA/pegRNA scaffold (Figure 1B). In contrast to VLP-packaging mechanisms that use Gag-Cas fusions, this mode of gRNA recruitment binds the RNP complex at its least stable component to favor the packaging of fully assembled RNPs.

As a first characterization of the vesicular stomatitis virus G protein (VSV-G) pseudotyped VLP system, we confirmed proteolytic maturation of Gag-PCP, enhanced budding efficiency of the L21S mutation, and packaging of PP7-tagged mRNA (see design considerations in STAR methods; Figure S1). To assess the gene editing performance of the delivered prime editors, we generated a "blue" mGreenLantern fluorescent reporter HEK293T line (blue mGL) in which mutations in the chromophore of mGreenLantern (G65S and Y66H) can be reverted to shift the fluorescence profile from blue back to green (Figure 1C).

Since (pe)gRNAs are localized in the nucleus, we hypothesized that shuttling a Gag-PCP component between the nucleus and cytosol would allow active nuclear export of PP7-tagged (pe)gRNAs, which would otherwise rely on passive diffusion through the nuclear pore or nuclear envelope breakdown during mitosis. Therefore, we introduced an HIV-1 nuclear export sequence (NES) flanked by two nuclear localization sequences (NLSs) (MYC and a synthetic NLS) into the NC domain upstream of PCP to allow nucleocytosolic shuttling of the packaging component (Figure 1A).

For VLP production, we co-expressed the engineered Gag variants and wild-type (WT) Gag/Gag-Pol$_{D64V}$ to form mosaic VLPs and mitigate possible steric hindrance by PCP insertion. As prime editor, we used the "improved PE" (iPE) with C-terminal fusion of the Moloney murine leukemia virus (MMLV) pentamutant RT.[34] Indeed, the shuttling motif (NLS-NES-NLS) led to a substantial increase in PE activity when delivered to the blue mGL reporter cell line, suggesting that (pe)gRNA packaging was otherwise limited by low cytosolic concentration (Figure 1D). Immunofluorescence imaging revealed that the steady-state localization of the engineered shuttling Gag was in the cytosol as long as an NES motif was present (Figures S2A–S2C). Nuclear accumulation of Gag-PCP was evident as early as 1 h after the addition of leptomycin B, a nuclear export inhibitor. This observation suggests that Gag-PCP is continuously shuttled between the nucleus and cytosol (Figure S2C).

VLP delivery of prime editors as RNPs

Next, we sought to evaluate the potential contribution of mRNA recruitment to our delivery system. To this end, we tagged the 3′ UTR of the iPE mRNA with a single PP7. We then compared the prime editing (PE) efficacy in blue mGL HEK293T cells transduced with VLPs carrying the editor as RNP or as protein and pegRNA in separate particles (Figure 1E). Alternatively, only the mRNA or the pegRNA was delivered separately, while the other component was complemented by plasmid transfection (Figure S3A). Critically, we observed substantial editing only in those conditions where both the prime editor and the pegRNA were loaded into the same particle, independent of whether the mRNA encoding iPE was PP7-tagged (Figure 1E). In addition, we observed an increased editing efficacy for a non-tagged mRNA encoding iPE, compared with a PP7-tagged version, suggesting that more iPE proteins than mRNAs can be packaged into VLPs (Figure S3A). Jointly, these data indicate that the VLPs delivered the editors primarily as RNPs.

We transfected the blue mGL receiver cells with microRNAs (miRs)[35] targeting the 3′ UTR of the PP7-tagged prime editor mRNA prior to VLP delivery and observed no decrease in editing efficacy, documenting that there is no significant contribution of potentially co-packaged mRNA coding for iPE (Figure S3B). The functionality of the miR was validated by delivering a mGreenLantern mRNA with the same 3′ UTR. Transfection of the receiver cells with the miR prior to VLP transduction strongly suppressed mGreenLantern translation (Figure S1E).

ENVLPE design and pegRNA refinements

After completing additional validation experiments and optimizing the stoichiometry (Figures S3C–S3F), we also attempted to simplify the system to a single-component-packaging plasmid based on Gag-Pol$_{D64V}$, but the mosaic composition of Gag/Gag-Pol$_{D64V}$ and shuttling Gag-PCP was still superior (Figure S3G).

Despite using 3′ pseudoknot motifs such as evopreQ1 (Q1), packaged pegRNAs may be partially degraded. By moving the PP7 aptamer out of the gRNA scaffold to the 3′ end of the pegRNA between PBS and Q1, we limited packaging to only pegRNAs with intact 3′ ends (RTT and PBS), resulting in slightly increased editing efficacy, especially under low VLP doses. Both versions outperformed a Gag-PE fusion design, an architecture previously used for RNP delivery of Cas9, base-,[19,20] and prime-editors[17,18] (Figure 1F).

Moving the NES component of the shuttling domain to the Gag C terminus to improve cargo release was not beneficial (Figures 1F and S3H), indicating that cargo release was not limited by aptamer dissociation (see design considerations in STAR methods). Using this ENVLPE architecture, we achieved prime editing efficacies of up to 35% in human induced pluripotent stem cell (hiPSC)-derived cortical neurons carrying the blue mGL reporter system (Figure 1G).

Delivery of Cas9 effectors for KO and edits mediated by HDR

To utilize the high modularity of the guide-mediated packaging mechanism, we continued to test the capability of ENVLPE to deliver other Cas9-based effectors. Compared with pegRNAs, sgRNAs are bound with high affinity to *apo*-Cas9 (K_d ~5–20 nM[27] vs. ~10–300 pM[36,37]) and are more stable without a 3′ extension. Therefore, it appears that the loading capability of unaltered sgRNAs may be sufficient to enable efficient packaging in Gag-Cas9 fusion systems as well.

We thus conducted a comparison in HEK293T and hiPSCs, which revealed that Cas9 ENVLPE performed comparably to v4 Cas9 eVLPs[17] in a titration assay for targeted insertions and deletions (indels) at the *B2M* locus (Figure 2A). We then validated that Cas9 nuclease ENVLPEs were also effective in post-mitotic hiPSC-derived cortical neurons equipped with an "enhanced traffic-light reporter" (eTLR),[34] which reports all occurring mutagenic end-joining (mutEJ) indel events (Figure S4A).

Please cite this article in press as: Geilenkeuser et al., Engineered nucleocytosolic vehicles for loading of programmable editors, Cell (2025), https://doi.org/10.1016/j.cell.2025.03.015

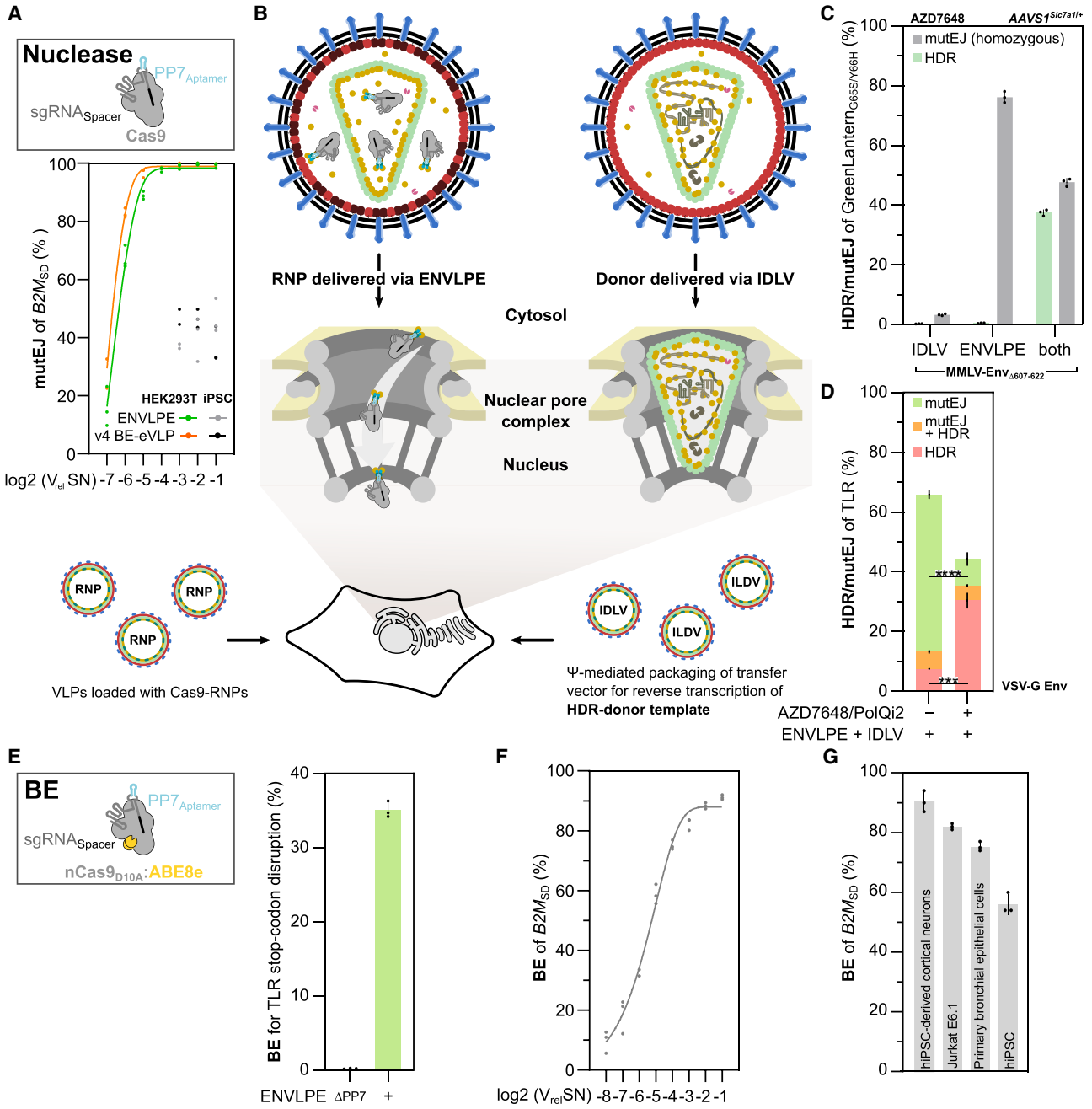

Figure 2. Delivery of various Cas9 effectors for mutEJ, HDR, and BE

(A) Cas9 ENVLPE was compared against v4 Cas9 eVLPs in targeting *B2M* in HEK293T cells and iPSCs. Indels were quantified via NGS, with points representing $n = 3$ biological replicates (except for HEK293T eVLP "−1" and "−2," iPSC ENVLPE "−3," and iPSC eVLP "−3," where $n = 2$). $Log_2(V_{rel}SN)$: relative transduction volumes in 2× dilution steps.

(B) To enable homology-directed repair (HDR), Cas9 ENVLPE was co-delivered with an HIV-1-based integrase-deficient lentivirus (IDLV) to revert the blue mGL reporter locus to its original green-fluorescent state. The IDLV delivers the reverse-transcribed donor template directly to the recipient cell's nucleus. The transfer plasmid contains the promoterless mGL HDR template, which includes homology arms to provide a DNA template for HDR.

(C) FACS-quantified percentages of HDR (green) and mutEJ (gray) events after transduction of the HEK293T blue mGL reporter cell line with Cas9 ENVLPE and HDR-donor IDLV in the presence of 0.5 μM AZD7648, a non-homologous end-joining (NHEJ) inhibitor. ENVLPE and IDLV were pseudotyped with ecotropic envelope proteins of the Moloney murine leukemia virus with deletion of the R-peptide (MMLV $Env_{\Delta 607-622}$); "blue mGL" reporter cells stably express the murine SLC7A1 receptor making them permissive for MMLV Env pseudotyped VLPs/IDLVs. Bars represent mean ± SD; $n = 3$ biological replicates.

(D) FACS-quantified percentages of HDR (red), mutEJ (green), or both (1st allele HDR, 2nd allele mutEJ, orange) of HEK293T eTLRv2 reporter cells after transduction with Cas9 ENVLPE and HDR-donor IDLV in the presence of 0.5 μM AZD7648 (NHEJ inhibitor) and 3 μM PolQi2 (MMEJ inhibitor) to promote HDR by

(legend continued on next page)

Please cite this article in press as: Geilenkeuser et al., Engineered nucleocytosolic vehicles for loading of programmable editors, Cell (2025), https://doi.org/10.1016/j.cell.2025.03.015

Nuclease-mediated editing is especially useful in stimulating homology-directed repair (HDR) to incorporate larger edits at a target site. In the context of HDR, VLPs have been used only in combination with other delivery modalities, such as co-precipitation of VLPs with dsDNA donors using polybrene or additionally electroporating the dsDNA donor into the recipient cells.[20] Many cell types, such as T lymphocytes, have sensitive innate immune responses toward cytosolic double-stranded DNA (dsDNA), resulting in massive cell death,[38,39] precluding direct delivery of dsDNA. Thus, *in vitro* generated single-stranded DNA (ssDNA)-based donors or AAVs (ssDNA genome) are common alternatives as HDR repair templates.

On the other hand, lentiviruses, such as HIV-1, can deliver their reverse-transcribed and capsid-shielded pseudo-genome directly to the nucleus without requiring the breakdown of the nuclear envelope,[40–42] thereby remaining undetected by cytosolic nucleic acid sensors.[38,39,43] Hence, we wondered whether Cas9 ENVLPEs could be combined with integrase-defective lentiviruses (IDLVs) that provide nuclear DNA templates after reverse transcription of the Ψ-tagged cargo RNA[44,45] (Figure 2B).

As a proof of concept, we provided IDLVs containing a promoterless mGreenLantern HDR template to repair the blue mGreenLantern back to its green-fluorescent state and co-delivered them with Cas9-ENVLPE into the recipient reporter cells. To show the flexibility of using fusogens other than VSV-G, we used the ecotropic MMLV envelope protein (MMLV-Env$_{\Delta 607\text{-}622}$)[46] to pseudotype both particles. Such pseudotyped particles cannot enter human cells unless the murine SLC7A1 receptor (mCAT1)[47] is heterologously expressed,[48] as in our modified blue mGreenLantern reporter HEK293T cell line. Upon co-delivery of Cas9 ENVLPEs together with the donor IDLVs in the presence of a non-homologous end-joining (NHEJ) inhibitor (0.5 μM AZD7648[49,50]), we observed chromophore repair in ∼40% of the population (Figure 2C), indicating highly efficient HDR. To raise the level of editing complexity, we increased the edit size from a 2 nt substitution in blue mGL to a 244 bp insertion to repair a truncated red fluorescent mScarlet-I protein in the eTLR reporter cell line, which reports mutEJ events as green fluorescence and successful HDR events as red fluorescence.[34] We observed 7% HDR, which could be increased to 30% in the presence of NHEJ/microhomology-mediated end-joining (MMEJ) inhibitors[51] (Figure 2D).

Delivery of Cas9 *trans*-activators and base editors

Next, we wondered whether functional CRISPR *trans*-activators, such as dCas9-miniVPR[52] RNPs, could be delivered using ENVLPE to induce *MAPT* expression in a HEK293T reporter cell line, which reports *MAPT* expression as a firefly luciferase (FLuc) activity.[53] We observed a significant 2-fold increase in reporter signal 48 h after CRISPRa-ENVLPE transduction, indicating successful gene activation (Figure S4B).

Lastly, we sought to extend ENVLPE to base editing (BE),[5–8] a double-strand-break-free and therapeutically promising gene editing technology. We first evaluated ENVLPE-mediated BE in our HEK293-TLR reporter cell line, which can also report the stop codon removal via a>g editing as green fluorescence, and observed that 35% of the cells were successfully edited (Figure 2E). We next tested BE ENVLPE on the *B2M* locus (Figures 2F and 2G) on multiple common cell types, where BE ENVLPE was able to facilitate BE with high efficacy at the *B2M* locus in all of the cell lines tested, reaching 90% in hiPSC-derived cortical neurons, and >55% in hiPSCs (Figure 2G). The latter cells are typically challenging to access with conventional techniques, such as lipofection or electroporation, which require tedious optimization.

3′ protection of pegRNA with Csy4 increases editing efficacy

Compared with gRNAs, pegRNAs particularly have a short half-life because of their degradation-prone 3′ extension.

Although our current design prioritizes packaging of PE RNPs with intact 3′ ends protected by the evopreQ1 pseudoknot,[27] we hypothesized that pegRNA stability may still limit the full potential of PE-ENVLPE. Accordingly, we used the CRISPR protein Csy4 (alias Cas6f) from *Pseudomonas aeruginosa*, which binds to a highly conserved 16 nt RNA motif (Csy4 motif, C4), wherein the nucleotides 2–16 form a hairpin with a 5 bp stem and a 5 nt loop. Csy4's processing activity has been used extensively in various CRISPR-Cas9 systems, e.g., to process arrays of gRNAs/crRNAs into individual gRNA/crRNAs for multiplexed gene editing,[54,55] or to enhance PE efficiency by preventing the pegRNA from folding back on itself due to the complementarity between the spacer and the PBS region.[56]

Importantly, the C4 RNA aptamer is bound by Csy4 with an exceptionally high affinity (K_d ∼50 pM[57]) that is ∼20-fold higher than the PCP-PP7 interaction (K_d ∼1 nM[58]). The C4 aptamer is precisely cleaved 3′ proximal to the hairpin without leaving any unpaired nucleotides as 3′-overhang. Csy4 remains bound with an unchanged affinity and thus may shield the 3′ end from a potential 3′ exonucleolytic attack.[57]

Although C4-modified pegRNAs showed no additional benefits in transient transfection experiments, in which pegRNA levels are naturally elevated (Figure S5A), we hypothesized that Csy4-mediated 3′ protection of the pegRNA could prove advantageous in conditions where RNA stability is limiting, such as during RNP delivery (Figure 3A). When Csy4 is co-expressed in the VLP-production cells, recruitment of the RNP complex is still

blocking NHEJ/MMEJ. Stacked bars represent mean ± SD; n = 3 biological replicates. Results from a two-tailed unpaired t test are shown (****$p < 0.0001$; ***$p < 0.001$); conditions were compared in the context of total indel rates (green + orange), as well as total editing rates (red + orange).

(E) ABE ENVLPE for disruption of the stop codon of an integrated eTLRv1 reporter in HEK293 cells, leading to green fluorescence by read-through. Editing was quantified via FACS; bars represent mean ± SD; n = 3 biological replicates.

(F and G) ABE ENVLPE for the disruption of a splice donor (SD) site of the first intron in the *B2M* gene was transduced into the indicated cell lines. Editing was quantified in HEK293T via NGS (F) or Sanger sequencing (G) 72 h after transduction. Points in (F) and bars in (G) represent n = 3 biological replicates. $Log_2(V_{rel}SN)$: relative transduction volumes in 2× dilution steps.

See also Figures S4 and S18.

Please cite this article in press as: Geilenkeuser et al., Engineered nucleocytosolic vehicles for loading of programmable editors, Cell (2025), https://doi.org/10.1016/j.cell.2025.03.015

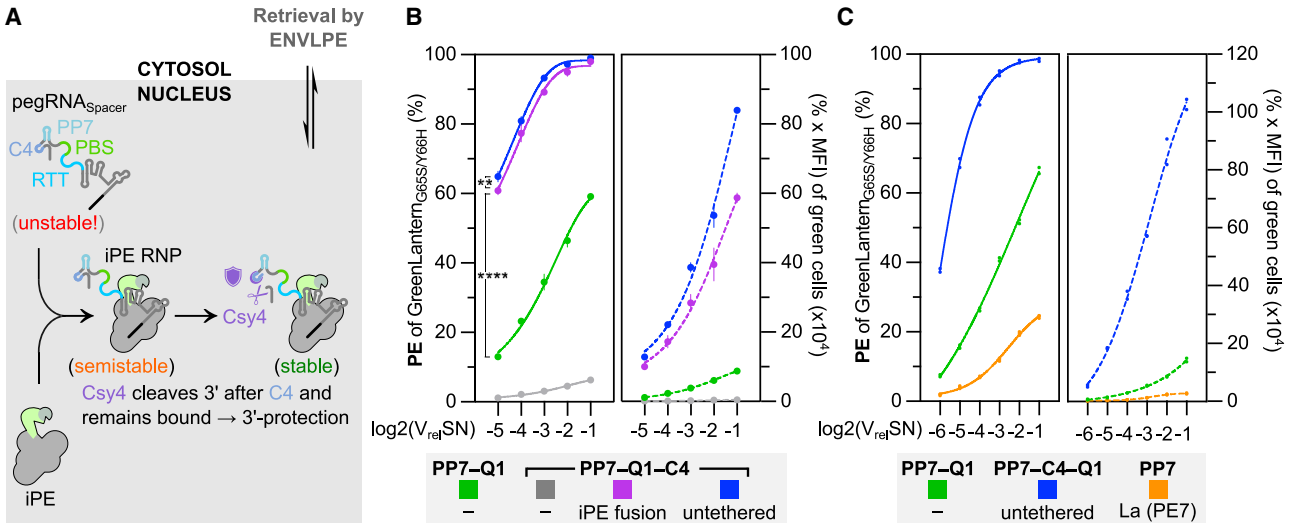

Figure 3. Implementation of Csy4 for improved PE pegRNA stability

(A) Schematic of Csy4-protected PE-RNP complex formation for packaging via ENVLPE. Csy4 cleaves off the 3′ overhanging nucleotides at the pegRNA's C4 aptamer and remains bound, thereby providing additional 3′-stabilization against exonucleolytic attack. The PE-RNP complex is then exported by the shuttling ENVLPE and combined with the budding module.

(B) Comparison of ENVLPE VLPs packaged with different 3′-stabilized PE-RNP complexes comprising the indicated 3′-modifications and covalent or non-covalent Csy4 tethers across a range of VLP doses. PE-mediated reversion of the blue mGL reporter in HEK293T cells is quantified via FACS and displayed as a percentage of green cells (left plot) or the percentage multiplied by the median fluorescence intensity (MFI) of green cells (right plot). PP7, PP7 aptamer bound by PP7 coat protein (PCP); Q1, evopreQ1 pseudoknot; C4, Csy4 aptamer hairpin bound and processed by Csy4; elements are described from 5′ to 3′ as they appear at the 3′-end of the respective pegRNA. Points represent mean ± SD (n = 3 biological replicates). $Log_2(V_{rel}SN)$: relative transduction volumes in 2× dilution steps. Editing rates of the lowest VLP titer were analyzed via Bonferroni multiple comparisons test (MCT) after one-way ANOVA (****$p < 0.0001$; **$p < 0.01$).

(C) Comparison of different VLP systems packaged with PE RNPs with different 3′-protection strategies applied to blue mGL HEK293T cells across a range of VLP doses. La indicates the fusion of the N-terminal fragment (amino acid [aa] 1–194) of La (SSB) used in PE7. The two plots represent the metrics as defined in (B). Points represent n = 3 individual replicates (orange) and n = 2 (green and blue). $Log_2(V_{rel}SN)$: relative transduction volumes in 2× dilution steps.

See also Figures S5–S10.

mediated by the PCP-PP7 system, and the 3′ end of the pegRNA in our initial setup contains an additional C4 motif downstream of the essential elements (RTT, PBS, and PP7). The editing efficacy in the recipient cells was strongly improved when Csy4 was co-expressed in the producer cells, either as a direct fusion to iPE or as an untethered module via a 2A peptide (iPE_{Csy4}) (Figure 3B), indicating that the increased efficacy is solely due to the 3′ protective effect of Csy4. Notably, the median fluorescence intensity (MFI) was strongly elevated for cells edited in the presence of Csy4, indicating either multi-allelic editing, faster editing kinetics, or a combination of both. We further observed that expressing Csy4 in an untethered fashion resulted in slightly higher % × MFI values than the fusion of Csy4 to iPE (Figure 3B). Interestingly, we observed an almost complete loss of editing activity in the control condition without Csy4, suggesting that unprocessed 3′-terminal nucleotides downstream of the C4 aptamer are highly susceptible to degradation (Figure 3B).

Evaluation of pegRNA 3′ end motifs

The effectiveness of PCP grafting into Gag was evaluated at different grafting positions to confirm that the observed improvement in protective Csy4 efficacy was not due to compensation for potentially suboptimal PCP grafting (Figure S5B). Alternative aptamer recruitment systems, such as Com (Figure S5C) or Csy4 alone, as a dual-purpose protection and recruitment module (Figure S6), did not provide additional benefits (see design considerations in STAR methods).

Therefore, we chose the 3′ configuration "PP7-C4-Q1" as the preferred mode for iPECsy4 because it can be used without Csy4 and thus provides the highest flexibility (Figure S7A).

We next compared iPE_{Csy4} with PE7, which utilizes the N-terminal fragment of the La protein fused to the prime editor to protect the 3′ ends of pegRNAs by binding to the 3′ poly(U) nucleotides, a scar left by RNA polymerase III termination.[28] With ENVLPE-mediated delivery, iPE_{Csy4} clearly outperformed PE7 in editing the blue mGL reporter line (Figure 3C). PE7-ENVLPE performance was increased by adding a tevopreQ1 motif to the pegRNA 3′ end but still displayed lower editing rates compared with iPE_{Csy4} ENVLPE (Figure S7B).

Evaluation of cell viability post-PE_{Csy4} delivery and potential application of Csy4 for canonical gRNAs

To evaluate the potential toxicity of Csy4 due to its RNA processing activity,[54] we investigated the effect of PE_{Csy4} transductions via ENVLPE on cellular fitness in recipient HEK293T and hiPSCs. However, we could not find relevant differences in cell viability compared with the non-VLP control condition and no difference in cytotoxicity compared with other VLP-transduced conditions lacking Csy4 (Figures S8A and S8B). We conclude that previous reports of Csy4's cytotoxic effect arise from circumstances

Please cite this article in press as: Geilenkeuser et al., Engineered nucleocytosolic vehicles for loading of programmable editors, Cell (2025), https://doi.org/10.1016/j.cell.2025.03.015

where Csy4 is excessively overexpressed in transient transfection settings.[54] Alternative strategies in which the protection and processing of the pegRNA 3′ end are separated into distinct processes did not prove to be beneficial (Figure S9; see design considerations in STAR methods).

We further tested whether Csy4-mediated 3′-stabilization of pegRNAs would also translate to conventional gRNA-based effectors that do not carry 3′-extensions. Likely due to the absence of 3′-vulnerable ends, gRNA-based nuclease and base-editing systems do not benefit from additional 3′-protection (Figure S10). In summary, Csy4 expressed via a 2A peptide with iPE (PE_{Csy4}), combined with PP7-C4-Q1 pegRNAs, substantially improves prime editing efficacy in ENVLPE-mediated RNP delivery.

Engineering of minimal, homomeric shuttling vehicles

Current VLP-delivery tools based on cargo fusion utilize co-assembly with virally derived Gag/Gag-Pol domains, as they are obligatorily dependent on the protease domain contained in the Pol frame for proteolytic cargo release.[14,17] We hypothesized that due to its aptamer recruitment and release mechanism, ENVLPE is not fundamentally dependent on protease-mediated release, even though it still utilizes mosaic assemblies with Gag/Gag-Pol domains composed of $Gag_{L21S,NLS\text{-}NES}$-PCP, Gag, and Gag-Pol.

Omitting Gag/Gag-Pol_{D64V} in the ENVLPE setup only resulted in a modest decrease in efficacy (Figure S11A), indicating that Gag/Gag-Pol_{D64V} was not essential. In contrast, omitting Csy4 led to a strong decrease in RNP transfer efficacy, indicating that RNP stability is a major bottleneck in aptamer-based RNP delivery systems (Figure S11A).

We identified the relatively mild impact of Gag/Gag-Pol_{D64V} omission as an opportunity to create a minimal VLP-like delivery system inspired by a previous publication.[59] We thus attempted to replace as many HIV-1 elements as possible with functional equivalents of non-viral elements (Figures 4A and 4B).

While preserving the nucleocytosolic shuttling motif and the aptamer-binding domain PCP, most of the MA/CA/NC regions were removed (ΔMA12–114, ΔCA133–277, ΔNC), except for the parts necessary to act as a spacer to induce membrane curvature during budding, as well as the budding domain p6 (Figure 4A). To compensate for Gag's eliminated oligomerization function, we incorporated GCN4 coiled coils, which form homomeric parallel dimers and trimers. Examining the functionality of this minimal design (miniENVLPE), we again found that the nucleocytosolic shuttling component is a key element in forming an efficient RNP packaging and delivery system (Figure 4C). Replacing the N-myristylation signal (MY) with a pleckstrin homology domain from phospholipase C-δ1 (PH)[60] that binds to phosphatidylinositol lipids, a component of the plasma membrane, further increased efficacy (Figure 4C). Remarkably, these miniature systems contained less than 13% of WT HIV-1 Gag sequences but were almost as active as full-length, homomeric $Gag_{L21S,NLS\text{-}NES}$-PCP setups (ENVLPE ΔGag/Gag-Pol_{D64V}; Figure 4D).

Since the minimal system is considerably decreased in size, which may shift its nucleocytosolic equilibrium, we re-tested several NES-NLS combinations on the miniENVLPE system. Still, we found no substantial improvement over the original nucleocytosolic shuttling sequence (Figure 4D).

Cryo-electron microscopy in our experiment revealed that HIV-1 Gag VLPs had a median radius of ∼55 nm, while ENVLPE and miniENVLPE had a smaller median radius of ∼31.5 nm (Figure S11B).

Mechanistic insights yield optimized ENVLPE$^+$

Further experiments on homomeric and minimal assemblies with different aptamers for recruitment provided additional evidence for our mechanistic insights on the ENVLPE system for PE (see design considerations in STAR methods). First, the PE efficacy improvement of PE_{Csy4} is also compatible with homomeric and minimal ENVLPE variants (Figures 4E and S11A). Second, cargo release is sufficient without proteolytic activity but is restricted to aptamer systems with intermediate affinities (nM range) since ultra-high-affinity aptamer systems (pM range) limit cargo release in the recipient cells (Figures 4F, S5C, and S11C). Last, Gag/Gag-Pol is not essential for particle assembly but is still generally beneficial (Figures 4F, S11A, S11C, and S11D).

Since GCN4 coiled coils were successfully applied in miniENVLPE, we also introduced them into ENVLPE (Figure 5A). Remarkably, this led to another significant increase in efficacy (Figure 5A), probably by enhancing productive PCP-PCP homodimerization. We termed this GCN4-enhanced final configuration ENVLPE$^+$.

Characterization of cargo loading efficiency

We next combined ENVLPE$^+$ with PE_{Csy4} as the optimal configuration for PE and conducted comparisons with v3 and v3b PE-eVLPs. As they are based on distinct packaging mechanisms compared with ENVLPE$^+$ (Figure S12), we chose to compare the amount of pegRNA and Cas9 effector protein per VLP. We found that one ENVLPE$^+$ particle was loaded with an average of 78 Cas9 molecules and 77 pegRNAs (ratio 0.99). In contrast, similar Cas9 levels were observed for v3 and v3b PE-eVLPs but distributed in a higher number of VLPs per volume and with a Cas9:pegRNA ratio of 0.58 and 0.61 for v3 and v3b PE-eVLPs, respectively (Figures S13A and S13B). This result aligns with our hypothesis that ENVLPE favors packaging of pegRNA:Cas9 complexes, while packaging of pegRNAs or Cas9 apoenzymes alone is improbable due to instability or absence of a recruitment handle. This observation is additionally supported by the findings of An et al., which suggested that improved RNP packaging could be a result of the additional introduction of Gag-aptamer-binding-proteins in v3 and v3b PE-eVLP.[18]

Benchmarking ENVLPE$^+$ against eVLP on endogenous targets

We proceeded to benchmark the editing efficacy and precision of ENVLPE$^+$ in base- and prime-editing modes on established endogenous loci against the MMLV-based v4 BE-eVLP and v3b PE-eVLP systems (see Figure S12 for the mechanistic differences). Because eVLP production is driven by CMV promoters, which are considered to be one of the strongest promoters in HEK293T cells,[61] we also switched ENVLPE$^+$ to CMV promoter-driven expression and optimized the plasmid stoichiometries again (Figure S13C). We wondered whether v3 or v3b

Please cite this article in press as: Geilenkeuser et al., Engineered nucleocytosolic vehicles for loading of programmable editors, Cell (2025), https://doi.org/10.1016/j.cell.2025.03.015

CellPress
OPEN ACCESS

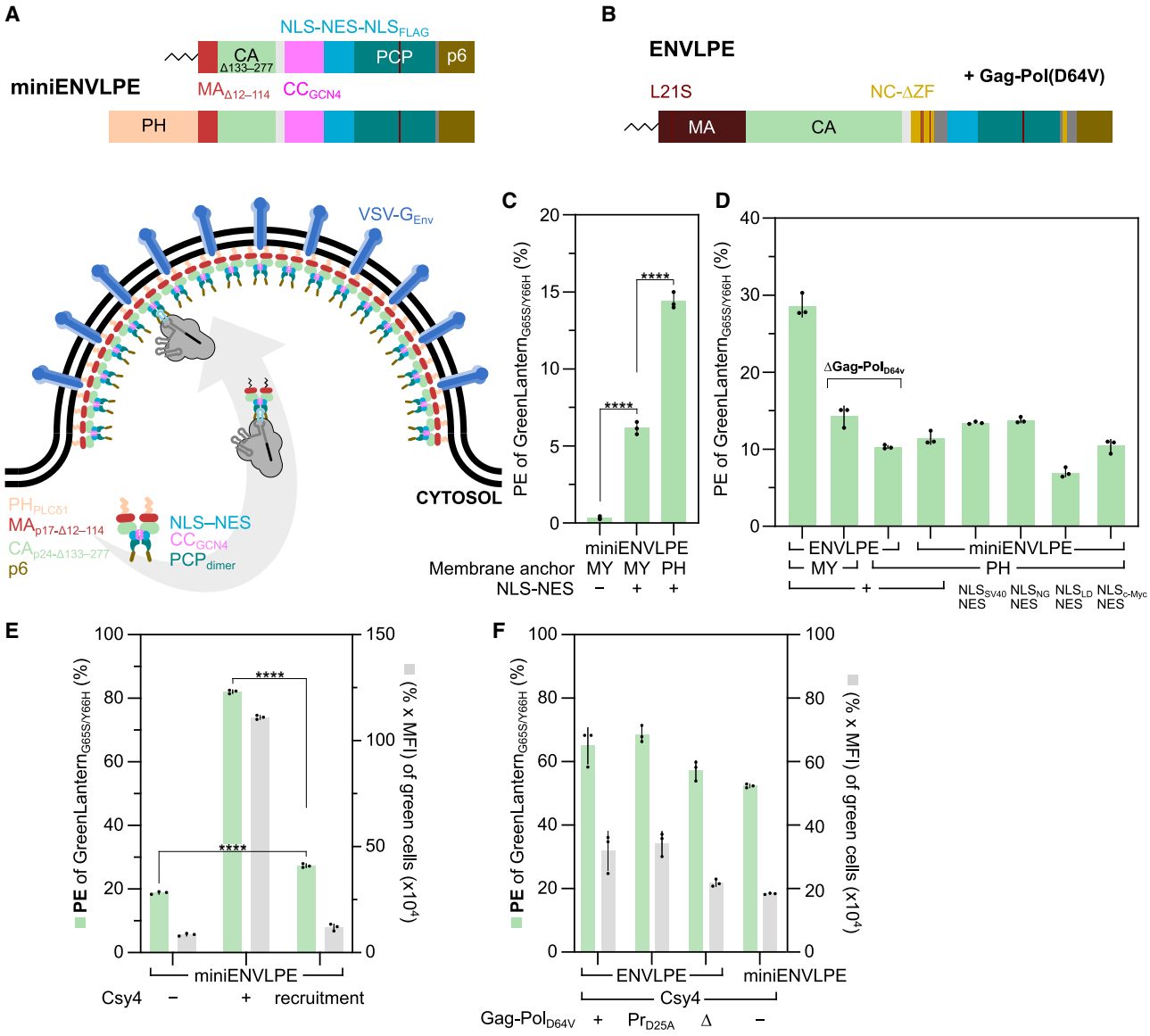

Figure 4. Engineering of a minimal Gag variant for delivery of functional RNPs

(A) Schematic representation of engineered minimal Gag versions with a majority of MA and CA deleted as indicated. The shuttling motif and PCP replace the complete NC domain, which also ablates the function of Gag to homo-oligomerize. Homo-oligomerization is restored by the introduction of GCN4 coiled coils (CC_{GCN4}). A PH was fused to the N terminus to replace the native N-myristoylation site. The resulting particles are formed from homomeric assemblies.

(B) Schematic representation of full-length Gag-PCP as used in ENVLPE for reference.

(C) Quantification of PE events in the blue mGL HEK293T reporter cell line via flow cytometry 72 h after transduction. Respective ENVLPE variants, shuttling domain variants, and membrane anchors (MY, HIV-1 N-myristoylation; PH, phospholipase C-δ1 pleckstrin homology domain) are indicated. Bars represent mean ± SD (n = 3 biological replicates).

(D) Comparison of the original ENVLPE (left) with variants without Gag/Gag-Pol_{D64V} and the addition of PH to full-length Gag-PCP as in (A, top) to miniENVLPE versions with different engineered nucleocytosolic shuttling motifs. PE was quantified in the blue mGL reporter HEK293T cell line via flow cytometry 72 h after transduction with VLPs. Bars represent mean ± SD (n = 3 biological replicates).

(E) Validation of the Csy4-C4 3′-protection module in the untethered or direct recruitment mode (see Figure S6) in the context of miniENVLPE. Experiments were conducted in the blue mGL HEK293T cell line. Bars represent mean ± SD (n = 3 biological replicates).

(F) The influence of proteolytic activity on PE efficacy in the blue mGL HEK293T reporter cell line in the context of the ENVLPE/Gag-Pol_{D64V} mosaic setup and the homomeric miniENVLPE. Bars represent mean ± SD (n = 3 biological replicates).

Selected results of Bonferroni MCT after one-way ANOVA analysis are shown for (C) and (E) (****$p < 0.0001$).

See also Figure S11.

Please cite this article in press as: Geilenkeuser et al., Engineered nucleocytosolic vehicles for loading of programmable editors, Cell (2025), https://doi.org/10.1016/j.cell.2025.03.015

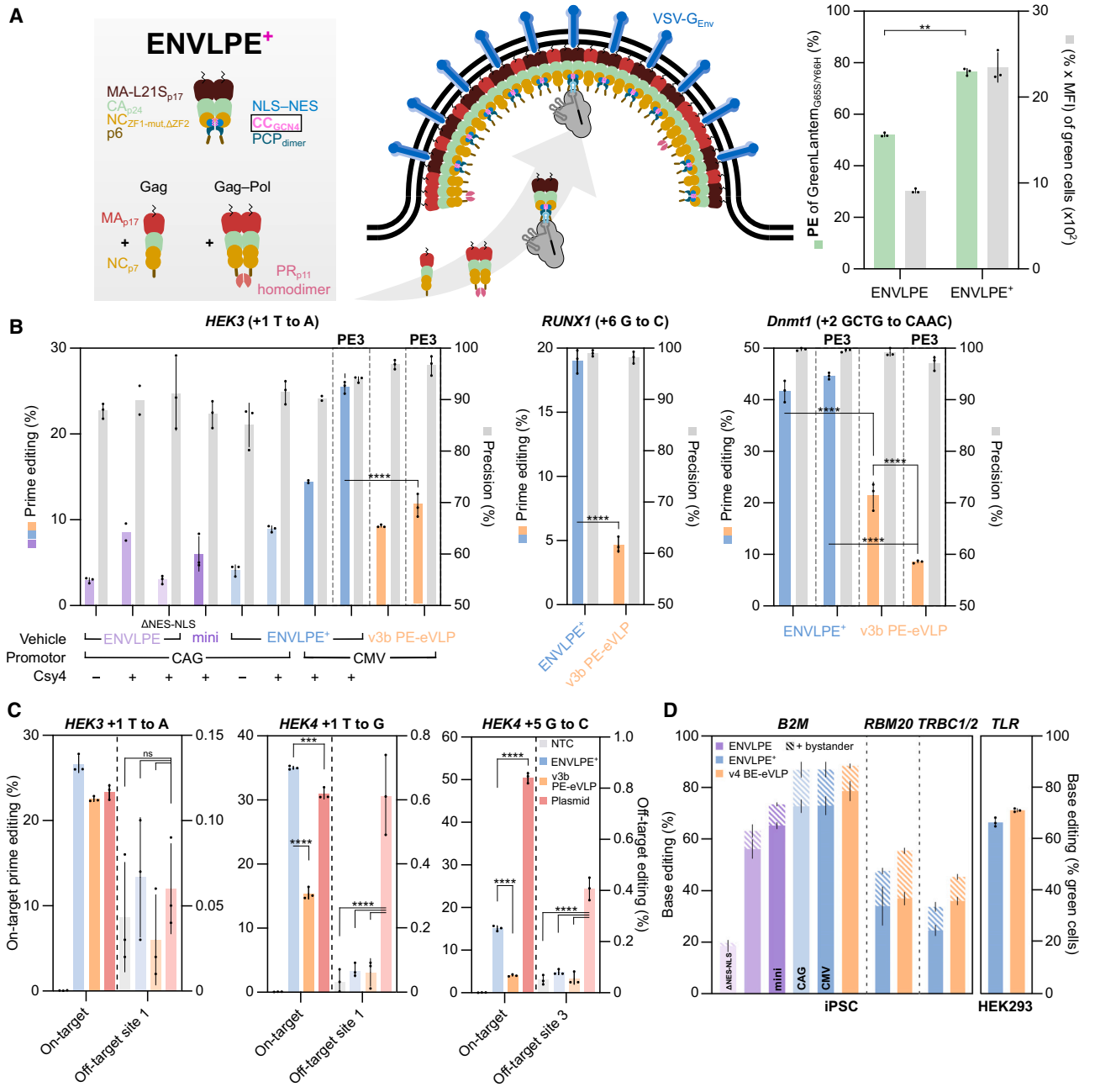

Figure 5. Optimized ENVLPE⁺ benchmarked for PE and BE at several endogenous sites

(A) Depiction of the improved module with an additional GCN4 domain (ENVLPE⁺) to assist Gag oligomerization (left). Editing performance of ENVLPE⁺ compared with ENVLPE (right). Experiments were performed on the blue mGL HEK293T line. Bars represent mean ± SD (n = 3 biological replicates). Results from a paired t test are indicated (**p < 0.01).

(B) Evaluation of ENVLPE, miniENVLPE, ENVLPE⁺, and v3b PE-eVLP delivery on several endogenous loci in HEK293T cells (*HEK3* and *RUNX1*) and in Neuro-2a cells (*Dnmt1*) using either the PE2 (default) or PE3 (indicated on top) strategy. Editing efficacy was analyzed via targeted amplicon sequencing, and precision was calculated by the ratio of intended edits divided by the total number of all non-WT reads × 100%. Bars represent mean ± SD (n = 3 biological replicates, except in *HEK3* PE$_{Csy4}$ ENVLPE [CAG] and PE$_{Csy4}$ ENVLPE⁺ [CMV] where n = 2). *HEK3* and *Dnmt1* data were analyzed using two-way ANOVA with Bonferroni MCT (****p < 0.0001). The conditions of *RUNX1* editing were analyzed by an unpaired two-tailed t test (****p < 0.0001).

(C) Additional assessment of on- and off-target editing in HEK293T of the respective VLP systems in HEK293T cells compared with plasmid-transfection of PE components targeting the respective targets. The same non-targeting control (NTC) of *HEK4* on-target editing is shown for both edit types. The off-target % is

(legend continued on next page)

Please cite this article in press as: Geilenkeuser et al., Engineered nucleocytosolic vehicles for loading of programmable editors, Cell (2025), https://doi.org/10.1016/j.cell.2025.03.015

PE-eVLP systems would benefit from Csy4 protection as well, and while both v3 and v3b PE-eVLP showed improvements with the additional 3′-protection to varying extents, ENVLPE$^+$ still achieved the highest prime-editing efficacy of all tested conditions (Figure S13D).

We then performed a detailed comparison of the endogenous *HEK3* locus (+1 t>a editing), including additional controls and comparisons with individual features of the ENVLPE system in HEK293T cells (NLS-NES, PE$_{Csy4}$, miniENVLPE, GCN4 coiled coils, CMV promoter). Evaluation of the editing performance at endogenous loci again demonstrated the functional relevance of the features built into ENVLPE$^+$ and reaffirmed CMV-driven PE$_{Csy4}$ ENVLPE$^+$ as the optimal configuration. This configuration also outperformed the state-of-the-art v3b PE-eVLP system[18] in both prime editing modes, "PE2" and "PE3" (Figure 5B).

We continued to benchmark our system across three additional loci and further editing types (t>a, g>c, t>g, +2 gctg>cacc), which showed that iPE$_{Csy4}$ ENVLPE$^+$ displayed consistently higher editing than v3b PE-eVLP across multiple endogenous sites in HEK293T and in Neuro-2a cells (Figures 5B and 5C). No significant increase in off-targets[62] compared with v3b PE-eVLP was found despite higher on-target efficacy (Figure 5C). On the other hand, plasmid-transfection of prime-editing components led to elevated off-target rates (Figure 5C). As expected for PE, editing precision (proportion of correct edits within all edited reads) was consistently high across all systems, mostly above 90%.

We extended ENVLPE$^+$ benchmarking against eVLPs to include BE and found similar rates for editing of multiple endogenous sites as observed with v4 BE-eVLPs in HEK293T and hiPSCs, with miniENVLPE also mediating comparable editing efficacies (Figure 5D).

BE with ENVLPE$^+$ for *ex vivo* T cell engineering

We next sought to assess the use of ENVLPE for generating hypo-immunogenic T cells suitable for cell-based therapeutic interventions. To achieve sufficient titers, we scaled up ENVLPE$^+$ particle production and transitioned to ultracentrifuge precipitation for enrichment.

We then administered ENVLPE$^+$ to primary T lymphocytes, facilitating a base edit in splice donor sites of the *B2M* and *TRBC1/2* loci to knock out major histocompatibility complex (MHC) class I and T cell receptor (TCR), two common knockout (KO) targets to generate hypoimmunogenic CAR-T cells[63] (Figure 6A). ENVLPE$^+$ facilitated both base edits at high efficacy and in a dose-dependent fashion (Figures 6B and 6C).

For *B2M* modification, we observed a direct correlation between editing efficacy and surface protein expression that is consistent with the requirement for biallelic modification to achieve complete KO (Figure 6B). This relation was less clear for *TRBC1/2*, where the KO of CD3 more closely follows editing (Figure 6C). It is likely that this pattern is caused by only one TRBC locus being transcriptionally active at a time,[64] resulting in a bias in both editing and expression toward the same allele.

We then proceeded to compare the efficacy of a simultaneous gene KO with a single transduction of either ENVLPE$^+$ or v4 BE-eVLPs. Our findings revealed comparable performance for both systems, albeit at a remarkably 40-fold higher titer of v4 BE-eVLPs (5.43×10^{11} v4 BE-eVLP particles and 1.34×10^{10} ENVLPE$^+$ particles per 50,000 cells; Figure 6D).

Distribution of ENVLPE *in vivo* after subretinal injection

We next set out to evaluate ENVLPE's editing performance in an *in vivo* setting and chose an ophthalmology context, since the eye has been used as a potent testbed for precision genome editing.[65] Multiple BE and PE strategies have been demonstrated in a diverse set of inherited retinal degeneration models, though virally delivered BE and PE limit the clinical applicability of the studies.[66–68]

To first test ENVLPE's transduction efficacy and local distribution of ENVLPE upon subretinal injection, we applied VSV-G-pseudotyped ENVLPE loaded with Cre$_{NLS}$ mRNA$_{PP7}$ to mT/mG mice (Figure 7A), which report Cre-recombinase activity as a conversion from red to green fluorescence. We injected 1.0, 1.5, and 2.0 μL of an ENVLPE solution (2.53×10^8 particles μL^{-1} in PBS) and observed broad and homogeneous green fluorescence-reporter activation across the retinal pigment epithelium (RPE) in 17/18 injected eyes 1 week after injection (Figures 7B and S14A). More importantly, no gross change of the compact RPE layer's pentagonal and hexagonal cell morphology was evident, suggesting ENVLPE was well tolerated. Consistent with these results, ENVLPE also performed well as an mRNA-delivery tool in a titration experiment in a Cre-dependent green-to-red-reporter HEK293 line (Figure S14B).

Prime editing of inherited retinal degeneration mouse models with PE$_{csy4}$ ENVLPE$^+$

Encouraged by the results from mRNA delivery, we sought to benchmark the performance of VLP-mediated PE in our optimized configuration iPE$_{Csy4}$ ENVLPE$^+$. To this end, we chose mouse models of retinitis pigmentosa (*rd6*) and of Leber congenital amaurosis (*rd12*), which have recently been used to measure the editing performance of v3 PE-eVLPs after subretinal injection.[18]

The loss-of-function phenotype in the *rd6* mouse model is caused by a 4 bp deletion in the splice donor region of *Mfrp* intron 4, abolishing protein expression (Figure 7C). To enable a direct head-to-head comparison with the recently published v3 PE-eVLP systems *in vivo*,[18] we employed the identical PE3b strategy for ENVLPE$^+$ (including identical spacers and 3′ extensions of the pegRNA but adapted to our scaffold and with 3′-modifications required for the Csy4/C4 protection; Figure 7C). We then produced both VLP systems in parallel from 15 cm dishes with 12.5×10^6 HEK293T cells/dish using original

calculated by subtracting the number of WT reads from the total reads of the indicated off-target loci. Bars represent mean ± SD (n = 3 biological replicates). Selected results of Bonferroni MCT after one-way ANOVA are indicated (****$p < 0.0001$; ***$p < 0.001$; ns $p > 0.05$).

(D) Evaluation of VLP-mediated BE in the HEK293 traffic-light reporter (TLR) cell line and other endogenous sites and cell lines. Editing efficacy was analyzed via targeted amplicon sequencing; bars represent mean ± SD (n = 3 biological replicates).

See also Figures S12 and S13.

Please cite this article in press as: Geilenkeuser et al., Engineered nucleocytosolic vehicles for loading of programmable editors, Cell (2025), https://doi.org/10.1016/j.cell.2025.03.015

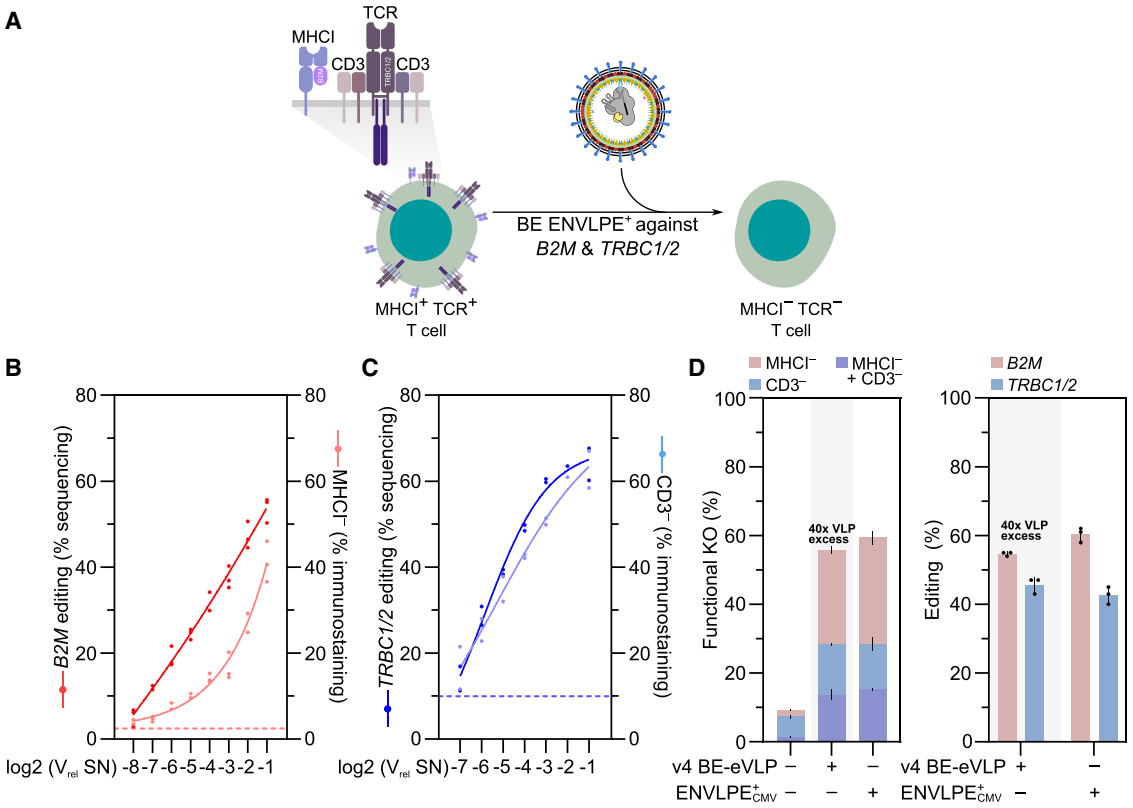

Figure 6. Using ENVLPE⁺ to generate hypoimmunogenic T cells *ex vivo*

(A) Schematic illustration of T cell receptor (TCR)/CD3 and MHC class I knockout (KO) by targeting *B2M* and *TRBC1/2* in primary T lymphocytes.

(B) *Ex vivo* delivery of adenine BE RNPs via $_{CAG}$ENVLPE⁺ to primary T lymphocytes. Quantification of *B2M* KO and the effect on MHC class I surface expression were analyzed 72 h after VLP delivery via NGS or flow cytometry (FC) after MHC class I immunostaining, respectively. $Log_2(V_{rel}SN)$, relative transduction volumes in 2× dilution steps.

(C) *Ex vivo* delivery of adenine BE RNPs via $_{CAG}$ENVLPE⁺ to primary T lymphocytes. Quantification of *TRBC1/2* KO and the effect on TCR surface expression were analyzed 72 h after VLP delivery via NGS or FC after CD3 immunostaining, respectively.

(D) Analysis of functional MHC class I⁻/CD3⁻ double KO in primary T lymphocytes by BE ENVLPE⁺ vs. v4 BE-eVLPs. KO efficiency was quantified via FC (functional) and NGS 72 h after delivery of the indicated VLP systems. Bars represent mean ± SD ($n = 3$). Titers of the respective VLP systems were measured via ELISA (5.43×10^{11} v4 BE-eVLP particles per 50,000 cells; 1.34×10^{10} ENVLPE⁺ particles per 50,000 cells; Figure S15). For dual targeting, 46 μL of VLPs containing either *B2M*-targeting sgRNAs or *TRBC1/2*-targeting sgRNAs were used for the eVLP or ENVLPE system, respectively.

See also Figures S12, S13, and S15.

plasmids for v3 PE-eVLPs[18] (from Addgene; see STAR Methods for details), concentrated the VLPs by ultracentrifuge precipitation using a sucrose cushion, and quantified the titers by ELISA against the capsid proteins in ENVLPE⁺ (HIV-1 p24) or v3 PE-eVLP (MMLV p30), respectively (Figure S15). 5- to 7-week-old *rd6* mice were injected with equal doses of $PE3b_{Csy4}$ ENVLPE⁺ or v3 PE3b-eVLP (1.6×10^9 particles μL^{-1} in 1 μL PBS). 3 weeks post-injection, we analyzed the protein expression of *Mfrp* in the eye cup via immunoblot and assessed the editing outcomes via targeted amplicon sequencing. Only ENVLPE⁺-treated eyes showed visibly restored MFRP protein expression (Figure 7D), mediated by the restoration of the splice donor site (median 8.6%; Figure 7E) with no detectable indels (Figure 7F), while samples from v3 PE3b-eVLP-treated mice exhibited MFRP levels beyond detection limit.

We repeated our head-to-head comparison on a second mouse model, *rd12*, which displays a more severe loss-of-function phenotype caused by a nonsense mutation in exon 3 of *Rpe65*, which abolishes the canonical visual cycle leading to visual impairment (Figure 7G). 3 weeks after subretinal injection of equal doses (1×10^9 particles μL^{-1} in 1 μL PBS) of both preparations into the RPE of 5- to 7-week-old *rd12* mice, immunoblot analysis of RPE homogenates revealed that the restored RPE65 protein could only be detected in eyes treated with $PE3b_{Csy4}$ ENVLPE⁺, whereas protein levels in eyes treated with v3 PE3b-eVLP remained below the detection limit (Figure 7H).

Comparable results were found by analyzing *Rpe65* exon 3 via targeted amplicon sequencing, which revealed substantial successful prime editing events with a median of 6.3% for $PE3b_{Csy4}$ ENVLPE⁺ (Figure 7I) without detectable indels (Figure 7J). In comparison, editing levels in the v3 PE3b-eVLP condition were below the detection threshold. The electroretinography (ERG) response correlated with the observed editing results across all samples from ENVLPE⁺ (Figure S16).

rd12 mice display a virtually absent light-dependent retinal activity that can be quantified via ERG (Figures 7K and 7L).

Please cite this article in press as: Geilenkeuser et al., Engineered nucleocytosolic vehicles for loading of programmable editors, Cell (2025), https://doi.org/10.1016/j.cell.2025.03.015

CellPress
OPEN ACCESS

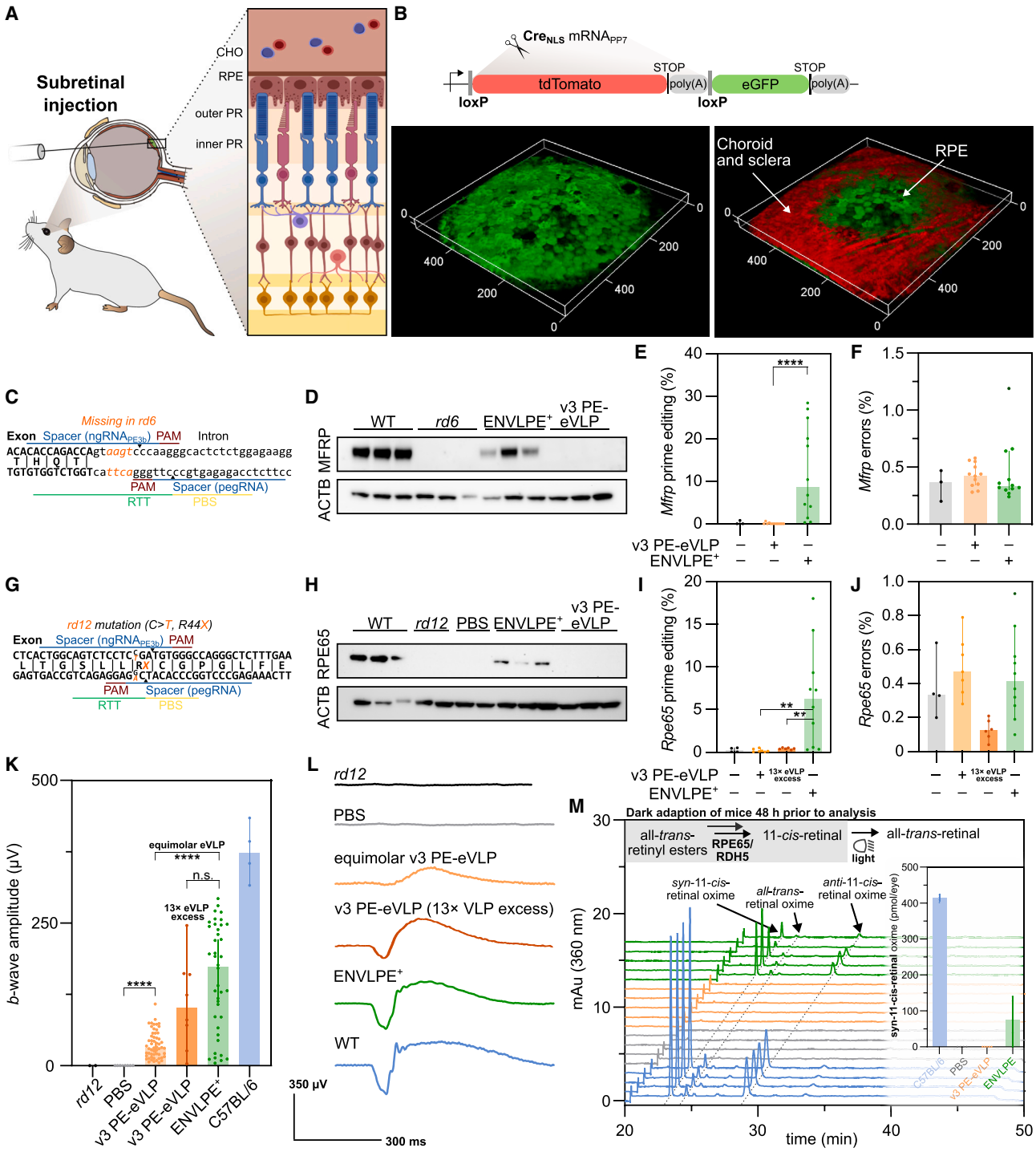

Figure 7. Subretinal injection of ENVLPE particles for mRNA delivery into Cre-reporter mice and for PE-RNP delivery to mouse models for inherited retinal degeneration

(A) Depiction of subretinal injection of VLPs into mouse retina. CHO, choroid; RPE, retinal pigment epithelium; PR, photoreceptor.

(B) Genetic construct of the reporter mouse indicating delivery of mRNA-encoded Cre activity with a red-green switch of fluorescent proteins expressed in RPE. Example 3D rendering of an imaging volume of the posterior portion of the intact eye acquired by two-photon imaging after subretinal injection of 1.5 μL sample (containing 3.63×10^8 ENVLPE particles). Left: green channel only; Right: green-red overlay. The units on the axes are in micrometers. Green fluorescence was observed in 17 out of 18 eyes; additional images are shown in Figure S14.

(C) Schematic diagram of 4 bp deletion in the SD region of exon 4 of *Mfrp* in *rd6* mice.

(legend continued on next page)

Please cite this article in press as: Geilenkeuser et al., Engineered nucleocytosolic vehicles for loading of programmable editors, Cell (2025), https://doi.org/10.1016/j.cell.2025.03.015

Treatment with ENVLPE$^+$ evoked ~5.5-fold higher *b*-wave signal (median 173.5 μV) compared with an equal dose of v3 PE-eVLPs (median 31.52 μV). A response of the comparable magnitude (median 102.2 μV) was evoked only after injecting a dose of v3 PE-eVLP that was approximately one order of magnitude higher (13.7×10^9 particles μL^{-1}; Figures 7K and 7L).

In *rd12* mice, the absence of RPE65 disrupts the visual cycle, leading to a deficiency of 11-*cis*-retinal. High-performance liquid chromatography (HPLC) analysis of retinoids in PE3b$_{Csy4}$ ENVLPE$^+$-treated *rd12* mouse eyes revealed significant restoration of 11-*cis*-retinal after dark adaptation, reaching ~20% of WT levels, suggesting a partially restored visual cycle (Figure 7M). Instead, 11-*cis*-retinal levels in v3-PE3b-eVLP-treated samples were below the detection limit, though some restoration must have occurred due to the recordable *b*-wave signals (Figures 7K and 7L).

DISCUSSION

We have introduced a highly effective and versatile tool for delivering all major classes of RNA-guided gene editors into a variety of cell types. Ultimately, we demonstrated its applicability for *in vivo* studies by restoring visual function in *rd12* mice and correcting the *rd6* mutation.

By systematically analyzing VLP methods for the delivery of gene editing RNP complexes, we identified three interrelated bottlenecks that limit their performance. First, the formation of guide RNA/Cas complexes in the nucleus is spatially separated from the budding process at the plasma membrane. Second, unbound guide RNAs, especially pegRNAs, are the least stable RNP components in the packaging cells. Third, the transport and packaging of RNP editors via protein fusions of an adapter to Gag protein instead of RNA aptamers limits the efficiency and modularity of the resulting VLPs.

Therefore, we have incorporated both NLS and NES and adjusted their relative strengths to enable an active nucleocytosolic export of editor-RNP complexes via an aptamer tag attached to the guide RNAs. This is in distinction to v3 and v3b PE-eVLP systems where multiple NES were added to the NLS motifs already contained in Gag-PE (v3) or P4-PE (v3b) but not inserted into the respective fusions of Gag and aptamer-binding proteins (Gag-MCP-Pol, v3; Gag-COM-Pol, v3b).[18] Thus, the purpose of the NES was to override the NLS on the Cas-containing fusion proteins to facilitate cytoplasmic packaging at the plasma membrane. Moreover, VLP-packaging mechanisms that recruit the RNP editor via the Cas protein component, either as direct fusions to Gag[17,19–21] or via coiled-coil adapters,[18] can result in empty *apo*-Cas packaging directly after cytosolic translation. Instead, ENVLPE ensures that the PP7-tagged stabilized RNP complex is directly picked up by the shuttling Gag-PCP component and then actively exported out of the nucleus for packaging at the plasma membrane. The Cas-effector concentration can be adjusted independently to maximize the transport of fully functional RNP editors, such that the dominant transport form is a fully assembled RNP.

Moreover, the aptamer-based recruitment mechanism of ENVLPE provides a high level of modularity, as the aptamer-tagged guide RNA serves as a universal interface to essentially any Cas effector of choice, which can be replaced without the need to re-optimize the editing performance. This also opens up the possibility of recruiting other RNA-guided effector proteins, given that their incorporation of an aptamer-tagged RNA is sufficiently stable. In the context of Cas9 effectors, this design enables seamless transitions between PE, nuclease + HDR, and BE functionalities without altering core components or stoichiometries of ENVLPE.

For PE-ENVLPE, we found that the pegRNA benefits from additional protection via Csy4/Cas6f beyond the evopreQ1 pseudoknot. While Csy4/Cas6f has been used in the past to enable multiplexed (pe)gRNA expression,[54,55] we found that Csy4/Cas6f resulted in at least an order of magnitude increase in PE efficacy.

Although this increased PE performance was also observed when Csy4 was used as a full replacement for PCP as an adapter (ENVLPE$_{Csy4}$), we suggest using Csy4 protection together with PCP-PP7-mediated recruitment strategy for maximum flexibility. In this mode, pegRNAs comprising a unified handle (3′-PP7-C4-Q1) can be used with or without Csy4. Csy4 can then be co-expressed as an untethered

(D) Immunoblot analysis of MFRP protein levels in *rd6* mouse eyes, 3 weeks after prime editing.
(E and F) Analysis of gDNA-editing efficacy and indel rate. Bars represent median with 95% CI ($n = 12$ biological replicates, except for "untreated" where $n = 3$). Selected statistical comparisons using the Kolmogorov-Smirnov test are shown (****$p < 0.0001$).
(G) Schematic diagram of the nonsense-mutation in exon 3 of *Rpe65* in *rd12* mice.
(H) Immunoblot analysis of RPE65 protein levels in *rd12* mice after prime editing.
(I and J) Analysis of the corresponding editing efficacy and error rate, including indels. Bars represent median with 95% CI ($n = 4$ [untreated]; $n = 7$ [eVLP]; $n = 6$ [eVLP 13× excess]; $n = 10$ [ENVLPE$^+$] biological replicates). Selected statistical comparisons using the Kolmogorov-Smirnov test are shown (**$p < 0.01$).
(K) Scotopic electroretinogram (ERG) *b*-wave amplitudes upon the light stimulus of −0.3 log[cd s m^{-2}] flash 3 weeks after injection of the different VLP systems or controls. Bars represent median with 95% CI ($n = 2$ [*rd12*]; $n = 9$ [PBS]; $n = 56$ [v3 PE-eVLP light orange]; $n = 8$ [v3 PE-eVLP dark orange], $n = 40$ [ENVLPE$^+$]; $n = 10$ [C57BL/6] biological replicates). Mice were dark-adapted overnight prior to analysis. Selected statistical comparisons using the Kolmogorov-Smirnov test are shown (****$p < 0.0001$; ns $p > 0.05$).
(L) Representative ERG traces from (K). Traces are represented as plots of potential (μV) versus time (ms).
(M) Schematic diagram of a portion of the visual cycle. Extracted whole-eye retinoids were analyzed by HPLC to quantify *syn*-11-*cis*-retinal. The mobile phase for retinal oxime elution was 90% hexanes and 10% ethyl acetate; the mobile phase for the earlier all-*trans*-retinyl ester elution (not shown in figure) was 99.4% hexanes and 0.6% ethyl acetate. Retinoid levels were determined using a standard curve. Results on the right show median and 95% CI for $n = 4$ control samples and $n = 5$ ENVLPE$^+$ and eVLP samples.
In (D)–(M), injection volumes were adjusted to equalize the injected VLP titers from v3 PE-eVLP and ENVLPE$^+$ particles per eye. VLP titers were quantified via ELISA (Figure S15).
See also Figures S12–S16.

Please cite this article in press as: Geilenkeuser et al., Engineered nucleocytosolic vehicles for loading of programmable editors, Cell (2025), https://doi.org/10.1016/j.cell.2025.03.015

protective module during VLP production. In this configuration, Csy4 protection is decoupled from the recruitment mechanism and can, therefore, be applied to other delivery systems that might benefit from pegRNA stabilization, as we have demonstrated exemplary for PE-eVLP.

We further found that the combination of HDR-donor IDLVs, Cas9 ENVLPEs, and DNA repair pathway modulators efficiently promotes knockins, useful for targeted integration of larger cassettes into safe-harbor loci or tagging of endogenous loci by homologous recombination. One important advantage of using our HIV-1-based ENVLPE + IDLV as dsDNA carriers is that the IDLV capsid acts as a molecular "Trojan horse" to deliver reverse-transcribed dsDNA donor directly into the nucleus, therefore likely circumventing the host's innate immune system (cGAS-STING).[43] Of note, MMLV or FMLV-based integrase-defective retroviruses (IDRV) rely on the dissolution of the nuclear envelope during mitosis, which is followed by the G1 phase. Homologous recombination, however, is restricted to the late G2/S phase, making MMLV/FMLV-based IDRVs a suboptimal choice as donor carriers for HDR. It remains to be seen whether an "all-in-one" VLP, encompassing both the RNP and the HDR template, is a viable option.

In ENVLPE, the RNP can dissociate from the aptamer interface without proteolytic Gag maturation, unlike direct fusions of Gag to CRISPR effectors. A non-maturing homomeric ENVLPE formulation still achieved 50% editing efficacy compared with the mosaic ENVLPE system. Understanding the mechanisms of efficient budding led us to the further improved ENVLPE^{+} by facilitating Gag-PCP oligomerization via coiled coils. It also allowed us to create a minimal variant (miniENVLPE) with ~13% of the original HIV-1 Gag/Gag-Pol sequence, achieving comparable editing efficacies. Given its independence from proteolytic maturation and co-expression of unmodified Gag/Gag-Pol, miniENVLPE can serve as a blueprint for future Gag-independent budding modules, e.g., by incorporating *de novo* cages or bacterial encapsulins.

For the *ex vivo* generation of T cells, we observed editing efficiencies comparable to v4 BE-eVLPs but at much lower titers, which is particularly relevant when injection volumes are limited.

The *in vivo* comparisons in several ophthalmologic mouse models showed potent mRNA delivery and superior "per VLP" editing efficacies with increased RNP loading compared with PE-eVLPs. Although we observed a higher per VLP editing efficacy of ENVLPE^{+} compared with PE-eVLPs, the titer (1×10^{9} particles per μL) we obtained for our equimolar comparison was 26-and 40-fold lower than in the referenced study for PE-eVLPs in the *rd6* or *rd12* models, respectively.[18] Moreover, we observed a higher variability of the protein levels, most likely because we did not control the selection of the tissue via a co-expressed fluorescent protein, as was done previously via AAV1-eGFP co-transductions.[18]

In summary, our characterization and application of the ENVLPE mechanism revealed that an optimized (pe)gRNA-mediated VLP packaging of gene editors as RNPs substantially improves editing efficacy per particle. This makes ENVLPE a potent delivery tool for base- and prime-editing, as well as HDR-based insertions or transactivation.

Limitations of the study

While extensive PE and BE data highlight the modularity of ENVLPE, experiments for CRISPRa and HDR were not carried out beyond proof of principle. Such future applications of ENVLPE could also include other Cas effectors, such as CRISPRi or CRISPRoff, and other RNA-targeting Cas enzymes, which were not explicitly considered here.

The transient nature of VLP-based delivery vehicles, as reported before,[17,19–21,29] decreases the risk of off-target edits due to prolonged expression of the editor complex. VLP systems may further attenuate potential immune responses, observed for traditional AAV-based gene therapy vectors that can continuously express their cargo for months to years in non-dividing cells. However, to deliver the desired genetic edits during the limited time window of transient expression, the VLP system must be highly optimized. In any case, the immunogenicity of different VLP systems should be closely examined in follow-up studies to compare their immunogenic potential. Additionally, immunogenic epitopes should be eliminated to minimize immune responses triggered by multiple VLP administrations. In this regard, our efforts to construct minimal packaging modules can serve as a blueprint for developing such low-immunogenic variants.

A key benefit of VLP strategies over LNP formulations is that tropism can be modified more easily via pseudotyping. We have demonstrated that ENVLPE can be pseudotyped with ecotropic glycoproteins, and it will be interesting to explore recent advancements in glycoprotein engineering to further refine and restrict VLP tropism to specific cell types.[13,14]

Our study also found a clear benefit of Csy4 for the efficacy of VLP-delivered prime editors across all experiments. Nevertheless, additional investigations into its generalizability across a broader range of targets and with other delivery systems would be advantageous.

Please note that despite our best efforts to prepare v4 BE-eVLPs and v3/v3b PE-eVLPs using original plasmids deposited at Addgene and the methods for VLP preparation described in the original documentation,[17,18] we cannot rule out the possibility that minor discrepancies in the protocol may have resulted in a slight reduction in the efficacy of the eVLPs compared with those used in previous studies. Moreover, in the rapidly evolving field of VLP development, the fifth version of the BE-eVLPs has recently been published. It is thus likely that an updated PE-eVLP will prove more effective than the current v3/v3b version. Nevertheless, we consider the per-particle editing efficacy to be an important metric for further optimization of VLP technology for *in vivo* applications.

RESOURCE AVAILABILITY

Lead contact

Requests for further information and resources should be directed to the lead contact, Dong-Jiunn Jeffery Truong (jeffery.truong@helmholtz-munich.de).

Materials availability

Plasmids generated in this study have been deposited to Addgene (details are provided in the key resources table).

Data and code availability

Source data are provided in this paper. All other data reported will be shared by the lead contact upon request.

ACKNOWLEDGMENTS

We thank Janna Nawroth and Tankut G. Güney for kindly providing primary bronchial epithelial cells (hBECs). We acknowledge the technical support of Flow Cytometry Core Facility at Helmholtz Munich. We would like to thank Dr. Carsten Peters and the TUM Electron Microscopy Facility for conducting sample preparation and image acquisition in automated cryo-EM. We also appreciate the assistance of Dr. Zhiqian Dong and Dr. Aleksander Tworak with mouse colony maintenance. We thank the members of the Center for Translational Vision Research and the Gavin Herbert Eye Institute for their comments and insights into this manuscript.

We acknowledge the support of the German Federal Ministry of Education and Research (BMBF) and the Free State of Bavaria within the framework of the Excellence Strategy of the Federal Government and the Länder through the ONE MUNICH project Munich Multiscale Biofabrication (J.G. and G.G.W.). G.G.W. acknowledges support from the European Research Council (ERC-CoG 865710 and ERC-PoC 101138939). J.G., N.A., G.G.W., and D.-J.J.T. acknowledge support from the European Innovation Council (EIC Pathfinder 101115574). This work was also supported in part by grants from the National Institutes of Health (NIH), including R01EY009339 (K.P.), R01EY034501 (K.P.), R01EY036994 (K.P.), T32GM008620 (S.W.D.), F30EY033642 (S.W.D.), and F31EY034027 (Z.J.E.). We acknowledge support frrom the Department of Ophthalmology, Gavin Herbert Eye Institute at the University of California, Irvine, from an unrestricted Research to Prevent Blindness award, from NIH core grant P30EY034070, and from a University of California, Irvine School of Medicine Dean's Office grant.

AUTHOR CONTRIBUTIONS

N.A. and J.G. contributed equally to this study. The exact order of the co-first authors was decided by a coin flip. J.G. and N.A. performed all experiments with the help of E.S., E.M.H.B., Y.L., N.W.W., S.V.W., F.v.d.L., E.M.S., X.N., L.S., T.H.S., K.N., C.G., and D.-J.J.T. D.-J.J.T. conceptualized and coordinated the study and oversaw the construct designs. S.S. and T.O. generated and differentiated the hiPSC reporter lines. C.G. provided the EPN-24-PCP construct for benchmarking. N.K. and A.S. performed the experiments with T lymphocytes. S.W.D. and K.P. designed the *rd6* and *rd12* study. S.W.D., G.P., C.R.M., E.R., and Z.J.E. performed *in vivo* injection experiments and their downstream analysis. S.W.D., G.P., C.R.M., E.R., and Z.J.E. analyzed data associated with *rd6* and *rd12*. K.P. analyzed data associated with *rd6* and *rd12* and supervised the *rd6* and *rd12* mouse experiments. A.G. produced the recombinant LgBiT, which was used for the quality control assays of the VLPs. O.B. performed the cryo-EM measurements to determine the size of the VLPs. D.-J.J.T. generated the sketches with modifications from J.G. and N.A. J.G., N.A., E.S., and D.-J.J.T. analyzed and visualized the data. J.G., N.A., D.-J.J.T., and G.G.W. wrote the manuscript. D.-J.J.T. and G.G.W. supervised the research.

DECLARATION OF INTERESTS

D.-J.J.T., J.G., N.A., and G.G.W. are inventors of the described technology and have filed patent applications through Helmholtz Munich and the Technical University of Munich (TUM). K.P. is a consultant for Polgenix Inc. and serves on the Scientific Advisory Board at Hyperion Eye Ltd. This work does not pertain to the above activities.

STAR★METHODS

Detailed methods are provided in the online version of this paper and include the following:

- KEY RESOURCES TABLE
- EXPERIMENTAL MODEL AND STUDY PARTICIPANT DETAILS
  - Animals
  - Cell lines and cultivation
- METHOD DETAILS
  - Molecular cloning and DNA analysis
  - Mammalian cell culture
  - Quality control of edited hiPSCs
  - Generation of hiPSC-derived cortical neurons
  - VLP production
  - IDLV production and transduction
  - Anti-FLAG staining
  - Delivery of VLPs in primary T lymphocytes
  - Viability and toxicity assays
  - Flow cytometry
  - Bioluminescence quantification
  - Cryo-electron microscopy
  - p24 (HIV-1) and p30 (MMLV) quantification
  - Cas9 protein quantification
  - pegRNA quantification
  - Subretinal injection
  - Electroretinography (ERG)
  - Retinoid analysis
  - Western blotting
  - Two-photon imaging
  - Design considerations
- QUANTIFICATION AND STATISTICAL ANALYSIS

SUPPLEMENTAL INFORMATION

Supplemental information can be found online at https://doi.org/10.1016/j.cell.2025.03.015.

Received: February 16, 2024
Revised: January 3, 2025
Accepted: March 7, 2025
Published: April 9, 2025

REFERENCES

1. Richter, M.F., Zhao, K.T., Eton, E., Lapinaite, A., Newby, G.A., Thuronyi, B.W., Wilson, C., Koblan, L.W., Zeng, J., Bauer, D.E., et al. (2020). Phage-assisted evolution of an adenine base editor with improved Cas domain compatibility and activity. Nat. Biotechnol. *38*, 883–891. https://doi.org/10.1038/s41587-020-0453-z.
2. Neugebauer, M.E., Hsu, A., Arbab, M., Krasnow, N.A., McElroy, A.N., Pandey, S., Doman, J.L., Huang, T.P., Raguram, A., Banskota, S., et al. (2023). Evolution of an adenine base editor into a small, efficient cytosine base editor with low off-target activity. Nat. Biotechnol. *41*, 673–685. https://doi.org/10.1038/s41587-022-01533-6.
3. Lam, D.K., Feliciano, P.R., Arif, A., Bohnuud, T., Fernandez, T.P., Gehrke, J.M., Grayson, P., Lee, K.D., Ortega, M.A., Sawyer, C., et al. (2023). Improved cytosine base editors generated from TadA variants. Nat. Biotechnol. *41*, 686–697. https://doi.org/10.1038/s41587-022-01611-9.
4. Chen, L., Zhu, B., Ru, G., Meng, H., Yan, Y., Hong, M., Zhang, D., Luan, C., Zhang, S., Wu, H., et al. (2023). Re-engineering the adenine deaminase TadA-8e for efficient and specific CRISPR-based cytosine base editing. Nat. Biotechnol. *41*, 663–672. https://doi.org/10.1038/s41587-022-01532-7.
5. Kurt, I.C., Zhou, R., Iyer, S., Garcia, S.P., Miller, B.R., Langner, L.M., Grünewald, J., and Joung, J.K. (2020). CRISPR C-to-G base editors for inducing targeted DNA transversions in human cells. Nat. Biotechnol. *39*, 41–46.
6. Komor, A.C., Kim, Y.B., Packer, M.S., Zuris, J.A., and Liu, D.R. (2016). Programmable editing of a target base in genomic DNA without double-stranded DNA cleavage. Nature *533*, 420–424. https://doi.org/10.1038/nature17946.

7. Gaudelli, N.M., Komor, A.C., Rees, H.A., Packer, M.S., Badran, A.H., Bryson, D.I., and Liu, D.R. (2017). Programmable base editing of A•T to G•C in genomic DNA without DNA cleavage. Nature *551*, 464–471. https://doi.org/10.1038/nature24644.

8. Tong, H., Wang, X., Liu, Y., Liu, N., Li, Y., Luo, J., Ma, Q., Wu, D., Li, J., Xu, C., et al. (2023). Programmable A-to-Y base editing by fusing an adenine base editor with an N-methylpurine DNA glycosylase. Nat. Biotechnol. *41*, 1080–1084. https://doi.org/10.1038/s41587-022-01595-6.

9. Anzalone, A.V., Randolph, P.B., Davis, J.R., Sousa, A.A., Koblan, L.W., Levy, J.M., Chen, P.J., Wilson, C., Newby, G.A., Raguram, A., et al. (2019). Search-and-replace genome editing without double-strand breaks or donor DNA. Nature *576*, 149–157. https://doi.org/10.1038/s41586-019-1711-4.

10. Anzalone, A.V., Gao, X.D., Podracky, C.J., Nelson, A.T., Koblan, L.W., Raguram, A., Levy, J.M., Mercer, J.A.M., and Liu, D.R. (2022). Programmable deletion, replacement, integration and inversion of large DNA sequences with twin prime editing. Nat. Biotechnol. *40*, 731–740. https://doi.org/10.1038/s41587-021-01133-w.

11. Yarnall, M.T.N., Ioannidi, E.I., Schmitt-Ulms, C., Krajeski, R.N., Lim, J., Villiger, L., Zhou, W., Jiang, K., Garushyants, S.K., Roberts, N., et al. (2023). Drag-and-drop genome insertion of large sequences without double-strand DNA cleavage using CRISPR-directed integrases. Nat. Biotechnol. *41*, 500–512. https://doi.org/10.1038/s41587-022-01527-4.

12. Raguram, A., Banskota, S., and Liu, D.R. (2022). Therapeutic in vivo delivery of gene editing agents. Cell *185*, 2806–2827. https://doi.org/10.1016/j.cell.2022.03.045.

13. Strebinger, D., Frangieh, C.J., Friedrich, M.J., Faure, G., Macrae, R.K., and Zhang, F. (2023). Cell type-specific delivery by modular envelope design. Nat. Commun. *14*, 5141. https://doi.org/10.1038/s41467-023-40788-8.

14. Hamilton, J.R., Chen, E., Perez, B.S., Sandoval Espinoza, C.R., Kang, M.H., Trinidad, M., Ngo, W., and Doudna, J.A. (2024). In vivo human T cell engineering with enveloped delivery vehicles. Nat. Biotechnol. *42*, 1684–1692. https://doi.org/10.1038/s41587-023-02085-z.

15. Höfig, I., Barth, S., Salomon, M., Jagusch, V., Atkinson, M.J., Anastasov, N., and Thirion, C. (2014). Systematic improvement of lentivirus transduction protocols by antibody fragments fused to VSV-G as envelope glycoprotein. Biomaterials *35*, 4204–4212. https://doi.org/10.1016/j.biomaterials.2014.01.051.

16. Dobson, C.S., Reich, A.N., Gaglione, S., Smith, B.E., Kim, E.J., Dong, J., Ronsard, L., Okonkwo, V., Lingwood, D., Dougan, M., et al. (2022). Antigen identification and high-throughput interaction mapping by reprogramming viral entry. Nat. Methods *19*, 449–460. https://doi.org/10.1038/s41592-022-01436-z.

17. Banskota, S., Raguram, A., Suh, S., Du, S.W., Davis, J.R., Choi, E.H., Wang, X., Nielsen, S.C., Newby, G.A., Randolph, P.B., et al. (2022). Engineered virus-like particles for efficient in vivo delivery of therapeutic proteins. Cell *185*, 250–265.e16. https://doi.org/10.1016/j.cell.2021.12.021.

18. An, M., Raguram, A., Du, S.W., Banskota, S., Davis, J.R., Newby, G.A., Chen, P.Z., Palczewski, K., and Liu, D.R. (2024). Engineered virus-like particles for transient delivery of prime editor ribonucleoprotein complexes in vivo. Nat. Biotechnol. *42*, 1526–1537. https://doi.org/10.1038/s41587-023-02078-y.

19. Hamilton, J.R., Tsuchida, C.A., Nguyen, D.N., Shy, B.R., McGarrigle, E.R., Sandoval Espinoza, C.R., Carr, D., Blaeschke, F., Marson, A., and Doudna, J.A. (2021). Targeted delivery of CRISPR-Cas9 and transgenes enables complex immune cell engineering. Cell Rep. *35*, 109207. https://doi.org/10.1016/j.celrep.2021.109207.

20. Mangeot, P.E., Risson, V., Fusil, F., Marnef, A., Laurent, E., Blin, J., Mournetas, V., Massouridès, E., Sohier, T.J.M., Corbin, A., et al. (2019). Genome editing in primary cells and in vivo using viral-derived Nanoblades loaded with Cas9-sgRNA ribonucleoproteins. Nat. Commun. *10*, 45. https://doi.org/10.1038/s41467-018-07845-z.

21. Haldrup, J., Andersen, S., Labial, A.R.L., Wolff, J.H., Frandsen, F.P., Skov, T.W., Rovsing, A.B., Nielsen, I., Jakobsen, T.S., Askou, A.L., et al. (2023). Engineered lentivirus-derived nanoparticles (LVNPs) for delivery of CRISPR/Cas ribonucleoprotein complexes supporting base editing, prime editing and *in vivo* gene modification. Nucleic Acids Res. *51*, 10059–10074. https://doi.org/10.1093/nar/gkad676.

22. Kaczmarczyk, S.J., Sitaraman, K., Young, H.A., Hughes, S.H., and Chatterjee, D.K. (2011). Protein delivery using engineered virus-like particles. Proc. Natl. Acad. Sci. USA *108*, 16998–17003. https://doi.org/10.1073/pnas.1101874108.

23. Jiang, F., Taylor, D.W., Chen, J.S., Kornfeld, J.E., Zhou, K., Thompson, A.J., Nogales, E., and Doudna, J.A. (2016). Structures of a CRISPR-Cas9 R-loop complex primed for DNA cleavage. Science *351*, 867–871. https://doi.org/10.1126/science.aad8282.

24. Wang, H., Nakamura, M., Abbott, T.R., Zhao, D., Luo, K., Yu, C., Nguyen, C.M., Lo, A., Daley, T.P., La Russa, M., et al. (2019). CRISPR-mediated live imaging of genome editing and transcription. Science *365*, 1301–1305. https://doi.org/10.1126/science.aax7852.

25. Hendel, A., Bak, R.O., Clark, J.T., Kennedy, A.B., Ryan, D.E., Roy, S., Steinfeld, I., Lunstad, B.D., Kaiser, R.J., Wilkens, A.B., et al. (2015). Chemically modified guide RNAs enhance CRISPR-Cas genome editing in human primary cells. Nat. Biotechnol. *33*, 985–989. https://doi.org/10.1038/nbt.3290.

26. Ma, H., Tu, L.-C., Naseri, A., Huisman, M., Zhang, S., Grunwald, D., and Pederson, T. (2016). CRISPR-Cas9 nuclear dynamics and target recognition in living cells. J. Cell Biol. *214*, 529–537. https://doi.org/10.1083/jcb.201604115.

27. Nelson, J.W., Randolph, P.B., Shen, S.P., Everette, K.A., Chen, P.J., Anzalone, A.V., An, M., Newby, G.A., Chen, J.C., Hsu, A., et al. (2022). Engineered pegRNAs improve prime editing efficiency. Nat. Biotechnol. *40*, 402–410. https://doi.org/10.1038/s41587-021-01039-7.

28. Yan, J., Oyler-Castrillo, P., Ravisankar, P., Ward, C.C., Levesque, S., Jing, Y., Simpson, D., Zhao, A., Li, H., Yan, W., et al. (2024). Improving prime editing with an endogenous small RNA-binding protein. Nature *628*, 639–647. https://doi.org/10.1038/s41586-024-07259-6.

29. Lyu, P., Javidi-Parsijani, P., Atala, A., and Lu, B. (2019). Delivering Cas9/sgRNA ribonucleoprotein (RNP) by lentiviral capsid-based bionanoparticles for efficient "hit-and-run" genome editing. Nucleic Acids Res. *47*, e99. https://doi.org/10.1093/nar/gkz605.

30. Lyu, P., Lu, Z., Cho, S.-I., Yadav, M., Yoo, K.W., Atala, A., Kim, J.-S., and Lu, B. (2021). Adenine base editor ribonucleoproteins delivered by Lentivirus-like particles show high on-target base editing and undetectable RNA off-target activities. CRISPR J. *4*, 69–81. https://doi.org/10.1089/crispr.2020.0095.

31. Prel, A., Caval, V., Gayon, R., Ravassard, P., Duthoit, C., Payen, E., Maouche-Chretien, L., Creneguy, A., Nguyen, T.H., and Martin, N. (2015). Highly efficient in vitro and in vivo delivery of functional RNAs using new versatile MS2-chi- meric retrovirus-like particles. Mol. Ther. Methods Clin. Dev. *2*, 15039.

32. Paillart, J.C., and Göttlinger, H.G. (1999). Opposing effects of human immunodeficiency virus type 1 matrix mutations support a myristyl switch model of gag membrane targeting. J. Virol. *73*, 2604–2612. https://doi.org/10.1128/JVI.73.4.2604-2612.1999.

33. Grigorov, B., Décimo, D., Smagulova, F., Péchoux, C., Mougel, M., Muriaux, D., and Darlix, J.L. (2007). Intracellular HIV-1 Gag localization is impaired by mutations in the nucle- ocapsid zinc fingers. Retrovirology *4*, 54.

34. Truong, D.-J.J., Geilenkeuser, J., Wendel, S.V., Wilming, J.C.H., Armbrust, N., Binder, E.M.H., Santl, T.H., Siebenhaar, A., Gruber, C., Phlairaharn, T., et al. (2024). Exonuclease-enhanced prime editors. Nat. Methods *21*, 455–464. https://doi.org/10.1038/s41592-023-02162-w.

35. Fellmann, C., Hoffmann, T., Sridhar, V., Hopfgartner, B., Muhar, M., Roth, M., Lai, D.Y., Barbosa, I.A.M., Kwon, J.S., Guan, Y., et al. (2013). An optimized microRNA backbone for effective single-copy RNAi. Cell Rep. *5*, 1704–1713. https://doi.org/10.1016/j.celrep.2013.11.020.

36. Wright, A.V., Sternberg, S.H., Taylor, D.W., Staahl, B.T., Bardales, J.A., Kornfeld, J.E., and Doudna, J.A. (2015). Rational design of a split-Cas9 enzyme complex. Proc. Natl. Acad. Sci. USA *112*, 2984–2989. https://doi.org/10.1073/pnas.1501698112.

37. Yourik, P., Fuchs, R.T., Mabuchi, M., Curcuru, J.L., and Robb, G.B. (2019). *Staphylococcus aureus* Cas9 is a multiple-turnover enzyme. RNA *25*, 35–44. https://doi.org/10.1261/rna.067355.118.

38. Motwani, M., Pesiridis, S., and Fitzgerald, K.A. (2019). DNA sensing by the cGAS–STING pathway in health and disease. Nat. Rev. Genet. *20*, 657–674. https://doi.org/10.1038/s41576-019-0151-1.

39. An, J., Zhang, C.-P., Qiu, H.-Y., Zhang, H.-X., Chen, Q.-B., Zhang, Y.-M., Lei, X.-L., Zhang, C.-X., Yin, H., and Zhang, Y. (2024). Enhancement of the viability of T cells electroporated with DNA via osmotic dampening of the DNA-sensing cGAS–STING pathway. Nat. Biomed. Eng. *8*, 149–164. https://doi.org/10.1038/s41551-023-01073-7.

40. Zila, V., Margiotta, E., Turoňová, B., Müller, T.G., Zimmerli, C.E., Mattei, S., Allegretti, M., Börner, K., Rada, J., Müller, B., et al. (2021). Cone-shaped HIV-1 capsids are transported through intact nuclear pores. Cell *184*, 1032–1046.e18. https://doi.org/10.1016/j.cell.2021.01.025.

41. Dickson, C.F., Hertel, S., Tuckwell, A.J., Li, N., Ruan, J., Al-Izzi, S.C., Ariotti, N., Sierecki, E., Gambin, Y., Morris, R.G., et al. (2024). The HIV capsid mimics karyopherin engagement of FG-nucleoporins. Nature *626*, 836–842. https://doi.org/10.1038/s41586-023-06969-7.

42. Fu, L., Weiskopf, E.N., Akkermans, O., Swanson, N.A., Cheng, S., Schwartz, T.U., and Görlich, D. (2024). HIV-1 capsids enter the FG phase of nuclear pores like a transport receptor. Nature *626*, 843–851. https://doi.org/10.1038/s41586-023-06966-w.

43. Papa, G., Albecka, A., Mallery, D., Vaysburd, M., Renner, N., and James, L.C. (2023). IP6-stabilised HIV capsids evade cGAS/STING-mediated host immune sensing. EMBO Rep. *24*, e56275. https://doi.org/10.15252/embr.202256275.

44. Cornu, T.I., and Cathomen, T. (2007). Targeted genome modifications using integrase-deficient lentiviral vectors. Mol. Ther. *15*, 2107–2113. https://doi.org/10.1038/sj.mt.6300345.

45. Lombardo, A., Genovese, P., Beausejour, C.M., Colleoni, S., Lee, Y.-L., Kim, K.A., Ando, D., Urnov, F.D., Galli, C., Gregory, P.D., et al. (2007). Gene editing in human stem cells using zinc finger nucleases and integrase-defective lentiviral vector delivery. Nat. Biotechnol. *25*, 1298–1306. https://doi.org/10.1038/nbt1353.

46. Tschorn, N., Söhngen, C., Berg, K., and Stitz, J. (2022). Ecotropic HIV-1 vectors pseudotyped with R-peptide-deleted envelope protein variants reveal improved gene transfer efficiencies. Virology *577*, 124–130. https://doi.org/10.1016/j.virol.2022.09.008.

47. Albritton, L.M., Tseng, L., Scadden, D., and Cunningham, J.M. (1989). A putative murine ecotropic retrovirus receptor gene encodes a multiple membrane-spanning protein and confers susceptibility to virus infection. Cell *57*, 659–666. https://doi.org/10.1016/0092-8674(89)90134-7.

48. Mangeot, P.-E., Dollet, S., Girard, M., Ciancia, C., Joly, S., Peschanski, M., and Lotteau, V. (2011). Protein transfer into human cells by VSV-G-induced nanovesicles. Mol. Ther. *19*, 1656–1666. https://doi.org/10.1038/mt.2011.138.

49. Fok, J.H.L., Ramos-Montoya, A., Vazquez-Chantada, M., Wijnhoven, P.W.G., Follia, V., James, N., Farrington, P.M., Karmokar, A., Willis, S.E., Cairns, J., et al. (2019). AZD7648 is a potent and selective DNA-PK inhibitor that enhances radiation, chemotherapy and olaparib activity. Nat. Commun. *10*, 5065. https://doi.org/10.1038/s41467-019-12836-9.

50. Truong, D.-J.J., Armbrust, N., Geilenkeuser, J., Lederer, E.-M., Santl, T.H., Beyer, M., Ittermann, S., Steinmaßl, E., Dyka, M., Raffl, G., et al. (2022). Intron-encoded cistronic transcripts for minimally invasive monitoring of coding and non-coding RNAs. Nat. Cell Biol. *24*, 1666–1676. https://doi.org/10.1038/s41556-022-00998-6.

51. Wimberger, S., Akrap, N., Firth, M., Brengdahl, J., Engberg, S., Schwinn, M.K., Slater, M.R., Lundin, A., Hsieh, P.-P., Li, S., et al. (2023). Simultaneous inhibition of DNA-PK and Polθ improves integration efficiency and precision of genome editing. Nat. Commun. *14*, 4761. https://doi.org/10.1038/s41467-023-40344-4.

52. Vora, S., Cheng, J., Xiao, R., VanDusen, N.J., Quintino, L., Pu, W.T., Vandenberghe, L.H., Chavez, A., and Church, G. (2018). Rational design of a compact CRISPR-Cas9 activator for AAV-mediated delivery. Preprint at bioRxiv. https://doi.org/10.1101/298620.

53. Truong, D.-J.J., Phlairaharn, T., Eßwein, B., Gruber, C., Tümen, D., Baligács, E., Armbrust, N., Vaccaro, F.L., Lederer, E.-M., Beck, E.M., et al. (2021). Non-invasive and high-throughput interrogation of exon-specific isoform expression. Nat. Cell Biol. *23*, 652–663. https://doi.org/10.1038/s41556-021-00678-x.

54. Nissim, L., Perli, S.D., Fridkin, A., Perez-Pinera, P., and Lu, T.K. (2014). Multiplexed and programmable regulation of gene networks with an integrated RNA and CRISPR/Cas toolkit in human cells. Mol. Cell *54*, 698–710. https://doi.org/10.1016/j.molcel.2014.04.022.

55. Kurata, M., Wolf, N.K., Lahr, W.S., Weg, M.T., Kluesner, M.G., Lee, S., Hui, K., Shiraiwa, M., Webber, B.R., and Moriarity, B.S. (2018). Highly multiplexed genome engineering using CRISPR/Cas9 gRNA arrays. PLoS One *13*, e0198714. https://doi.org/10.1371/journal.pone.0198714.

56. Liu, Y., Yang, G., Huang, S., Li, X., Wang, X., Li, G., Chi, T., Chen, Y., Huang, X., and Wang, X. (2021). Enhancing prime editing by Csy4-mediated processing of pegRNA. Cell Res. *31*, 1134–1136. https://doi.org/10.1038/s41422-021-00520-x.

57. Sternberg, S.H., Haurwitz, R.E., and Doudna, J.A. (2012). Mechanism of substrate selection by a highly specific CRISPR endoribonuclease. RNA *18*, 661–672. https://doi.org/10.1261/rna.030882.111.

58. Lim, F., Downey, T.P., and Peabody, D.S. (2001). Translational Repression and Specific RNA Binding by the Coat Protein of the Pseudomonas Phage PP7. J. Biol. Chem. *276*, 22507–22513. https://doi.org/10.1074/jbc.M102411200.

59. Accola, M.A., Strack, B., and Göttlinger, H.G. (2000). Efficient Particle Production by Minimal Gag Constructs Which Retain the Carboxy-Terminal Domain of Human Immunodeficiency Virus Type 1 Capsid-p2 and a Late Assembly Domain. J. Virol. *74*, 5395–5402. https://doi.org/10.1128/jvi.74.12.5395-5402.2000.

60. Urano, E., Aoki, T., Futahashi, Y., Murakami, T., Morikawa, Y., Yamamoto, N., and Komano, J. (2008). Substitution of the myristoylation signal of human immunodeficiency virus type 1 Pr55Gag with the phospholipase C-δ1 pleckstrin homology domain results in infectious pseudovirion production. J. Gen. Virol. *89*, 3144–3149. https://doi.org/10.1099/vir.0.2008/004820-0.

61. Qin, J.Y., Zhang, L., Clift, K.L., Hulur, I., Xiang, A.P., Ren, B.-Z., and Lahn, B.T. (2010). Systematic comparison of constitutive promoters and the doxycycline-inducible promoter. PLoS One *5*, e10611. https://doi.org/10.1371/journal.pone.0010611.

62. Malinin, N.L., Lee, G., Lazzarotto, C.R., Li, Y., Zheng, Z., Nguyen, N.T., Liebers, M., Topkar, V.V., Iafrate, A.J., Le, L.P., et al. (2021). Defining genome-wide CRISPR-Cas genome-editing nuclease activity with GUIDE-seq. Nat. Protoc. *16*, 5592–5615. https://doi.org/10.1038/s41596-021-00626-x.

63. Madison, B.B., Patil, D., Richter, M., Li, X., Tong, M., Cranert, S., Wang, X., Martin, R., Xi, H., Tan, Y., et al. (2022). Cas-CLOVER is a novel high-fidelity nuclease for safe and robust generation of TSCM-enriched allogeneic CAR-T cells. Mol. Ther. Nucleic Acids *29*, 979–995. https://doi.org/10.1016/j.omtn.2022.06.003.

64. Horna, P., Weybright, M.J., Ferrari, M., Jungherz, D., Peng, Y., Akbar, Z., Tudor Ilca, F., Otteson, G.E., Seheult, J.N., Ortmann, J., et al. (2024). Dual T-cell constant β chain (TRBC)1 and TRBC2 staining for the identification of T-cell neoplasms by flow cytometry. Blood Cancer J. *14*, 34. https://doi.org/10.1038/s41408-024-01002-0.

65. Suh, S., Choi, E.H., Raguram, A., Liu, D.R., and Palczewski, K. (2022). Precision genome editing in the eye. Proc. Natl. Acad. Sci. USA *119*, e2210104119. https://doi.org/10.1073/pnas.2210104119.

66. Du, S.W., Newby, G.A., Salom, D., Gao, F., Menezes, C.R., Suh, S., Choi, E.H., Chen, P.Z., Liu, D.R., and Palczewski, K. (2024). In vivo photoreceptor base editing ameliorates rhodopsin-E150K autosomal-recessive retinitis pigmentosa in mice. Proc. Natl. Acad. Sci. USA *121*, e2416827121. https://doi.org/10.1073/pnas.2416827121.

67. Suh, S., Choi, E.H., Leinonen, H., Foik, A.T., Newby, G.A., Yeh, W.-H., Dong, Z., Kiser, P.D., Lyon, D.C., Liu, D.R., et al. (2021). Restoration of visual function in adult mice with an inherited retinal disease via adenine base editing. Nat. Biomed. Eng. *5*, 169–178. https://doi.org/10.1038/s41551-020-00632-6.

68. Choi, E.H., Suh, S., Foik, A.T., Leinonen, H., Newby, G.A., Gao, X.D., Banskota, S., Hoang, T., Du, S.W., Dong, Z., et al. (2022). In vivo base editing rescues cone photoreceptors in a mouse model of early-onset inherited retinal degeneration. Nat. Commun. *13*, 1830. https://doi.org/10.1038/s41467-022-29490-3.

69. Shi, Y., Kirwan, P., and Livesey, F.J. (2012). Directed differentiation of human pluripotent stem cells to cerebral cortex neurons and neural networks. Nat. Protoc. *7*, 1836–1846. https://doi.org/10.1038/nprot.2012.116.

70. Votteler, J., Ogohara, C., Yi, S., Hsia, Y., Nattermann, U., Belnap, D.M., King, N.P., and Sundquist, W.I. (2016). Designed proteins induce the formation of nanocage-containing extracellular vesicles. Nature *540*, 292–295. https://doi.org/10.1038/nature20607.

71. Horns, F., Martinez, J.A., Fan, C., Haque, M., Linton, J.M., Tobin, V., Santat, L., Maggiolo, A.O., Bjorkman, P.J., Lois, C., et al. (2023). Engineering RNA export for measurement and manipulation of living cells. Cell *186*, 3642–3658.e32. https://doi.org/10.1016/j.cell.2023.06.013.

Please cite this article in press as: Geilenkeuser et al., Engineered nucleocytosolic vehicles for loading of programmable editors, Cell (2025), https://doi.org/10.1016/j.cell.2025.03.015

STAR★METHODS

KEY RESOURCES TABLE

REAGENT or RESOURCE	SOURCE	IDENTIFIER
Antibodies		
anti-RPE65 clone KPSA1	UC Irvine	N/A
anti-beta-actin clone 13E5	Cell Signaling Tech-nologies	4970; RRID:AB_2223172
anti-MFRP	R&D Systems	AF3445; RRID:AB_2142759
donkey anti-goat IgG HRP	Thermo Thermo Fisher Scientific	A16005; RRID:AB_2534679
anti-mouse IgG HRP	Cell Signaling Technologies	7076; RRID:AB_330924
anti-rabbit IgG HRP	Cell Signaling Technologies	7074S; RRID:AB_2099233
PE anti-human HLA-A,B,C Antibody	Biolegend	311406; RRID:AB_314875
APC anti-human CD3 Antibody	Biolegend	317318; RRID:AB_1937212
Bacterial and virus strains		
NEB Stable Competent *E. coli*	New England BioLabs	C3040H
Chemicals, peptides, and recombinant proteins		
Poly-L-lysine solution	Sigma-Aldrich, Merck	P4832
Advanced DMEM	Gibco, Thermo Thermo Fisher Scientific	12491015
RPMI 1640 Medium	Gibco, Thermo Thermo Fisher Scientific	11875093
Essential 8 Flex Medium Kit	Gibco, Thermo Thermo Fisher Scientific	A2858501
Geltrex LDEV-Free Reduced Growth Factor Basement Membrane Matrix	Gibco, Thermo Thermo Fisher Scientific	A1413201
Fetal Bovine Serum	Gibco, Thermo Thermo Fisher Scientific	A5256701
Penicillin-Streptomycin	Sigma-Aldrich, Merck	P4333
Accutase - Enzyme Cell Detachment Medium	Invitrogen, Thermo Fisher Scientific	00-4555-56
DPBS, calcium, magnesium	Gibco, Thermo Thermo Fisher Scientific	14190144
D(+)-Saccharose	ROTH	9097
anti-CD3/CD28 Dynabeads	Gibco, Thermo Thermo Fisher Scientific	40203D
recombinant human IL-2	Peprotech	200-02
jetOPTIMUS® transfection reagent	Polyplus	101000006
Critical commercial assays		
Plasmid Maxi Kit	QIAGEN	12165
Nano-Glo® HiBiT Lytic Detection System	Promega	N3030
Lenti-X p24 Rapid Titer Kit	Takara Bio	631476
QuickTiter MuLV p30 Core Antigen ELISA Kit	Cell Biolabs	VPK-156
Quick-DNA 96 Kit	Zymo Research	D3011
Experimental models: Cell lines		
HEK293T as producer cell line	ECACC	12022001; RRID:CVCL_0063
HEK293	ECACC	85120602; RRID:CVCL_0045
Jurkat E6.1	ECACC	88042803; RRID:CVCL_0367
Neuro-2a	ECACC	89121404; RRID:CVCL_0470
hiPSCs	Helmholtz Zentrum München (HMGU)	ISFi001-A; RRID:CVCL_YT30
primary human T cells	Technical University Munich	N/A
Small airway epithelial cells	Cell Systems	FC-0106
Experimental models: Organisms/strains		
C57BL/6J mice	Jackson Laboratory	RRID:IMSR_JAX:000664
rd6 mice	Jackson Laboratory	RRID:IMSR_JAX:003684

(*Continued on next page*)

Please cite this article in press as: Geilenkeuser et al., Engineered nucleocytosolic vehicles for loading of programmable editors, Cell (2025), https://doi.org/10.1016/j.cell.2025.03.015

Continued

REAGENT or RESOURCE	SOURCE	IDENTIFIER
rd12 mice	Jackson Laboratory	RRID:IMSR_JAX:005379
Oligonucleotides		
NGS_B2M_fw	CGGTCTCACAAGCATGGATGC TTGTTGGGAAGGTGGAAGCTC	N/A
NGS_B2M_rv	CACAATCGAGCTCCATCTGTGG ACCAGTCCTTGCTGAAAGACAAG	N/A
NGS_TRBC1/2_fw	CGGTCTCACAAGCATGGATGCT CAATGACTCCAGATACTGCCTG	N/A
NGS_TRBC1/2_rv	CACAATCGAGCTCCATCTGTGGC TACCTGGATCTTTCCATTTTCC	N/A
rd6_genomic_HTS_F	ACACTCTTTCCCTACACGACGCTCTTCCG ATCTNNNNAAGAACCCACTGCTCACCCGA	N/A
rd6_genomic_HTS_R	TGGAGTTCAGACGTGTGCTCTTCCGATC TAGAGGTCTTCCCCAACCTGCAA	N/A
rd12_genomic_HTS_F	ACACTCTTTCCCTACACGACGCTCTTCCG ATCTNNNNTGATATCTCACTTTGCTGCAGG	N/A
rd12_genomic_HTS_R	TGGAGTTCAGACGTGTGCTCTTCCGATCTA TGGCTAGACCATGAAGAAAGAAG	N/A
Recombinant DNA		
pCMV-VSV-G	Addgene	8454
pRSV-REV	Addgene	12253
psPAX2-D64V	Addgene	63586
pCMV_ENVLPE^{+}	This study	232427
pCMV_iPE-C_P2A_Csy4	This study	232428
pCMV_ABE8e	This study	232429
pCMV_Cas9	This study	232430
pCMV_miniENVLPE	This study	232431
pU6_empty-sgRNA(PP7)	This study	232432
pU6_rd6_pegRNA_(PP7-C4-Q1)	This study	232433
pU6_rd6_nsgRNA(PP7)	This study	232434
pU6_rd12_pegRNA_(PP7-C4-Q1)	This study	232435
pU6_rd12_nsgRNA(PP7)	This study	232436
pU6_HEK3+1T>A_(PP7-C4-Q1)	This study	232437
pU6_HEK3_nsgRNA(PP7)	This study	232444
pU6_B2M_sgRNA(PP7)	This study	232438
pCMV_CreNLS_PP7	This study	232439
pCMV_mGL_PP7	This study	232440
Software and algorithms		
Geneious Prime 2022/2023/2024	Biomatters (https://www.geneious.com/)	N/A
Prism 9/10	GraphPad (https://www.graphpad.com)	N/A
FlowJo v10	BD Biosciences (https://www.flowjo.com/solutions/flowjo)	N/A
Other		
38.5 mL, Open-Top Thinwall Ultra-Clear Tube, 25 x 89 mm	Beckman Coulter	344058
Millex®-HV Filter Unit (Sterile)	Merck Millipore	SLHV033RS
BD Plastipak™ Plastic Concentric Luer-Lock Syringe	BD	300865
Injekt® Solo Luer, disposable syringes 5 mL	Braun	4606051V
Sterican needle 0.80 x 120 mm	Braun	4665643
Swinging-bucket centrifuge rotor	Beckman Coulter	SW 28

(*Continued on next page*)

Please cite this article in press as: Geilenkeuser et al., Engineered nucleocytosolic vehicles for loading of programmable editors, Cell (2025), https://doi.org/10.1016/j.cell.2025.03.015

Continued

REAGENT or RESOURCE	SOURCE	IDENTIFIER
Cotton Swabs 2,2/145 mm	Greiner Bio-One	421084
Ultrafree-CL Centrifugal Filter	Merck Millipore	UFC40GV0S
Amicon® Ultra-4 Centrifugal Filter Unit	Merck Millipore	UFC810024

EXPERIMENTAL MODEL AND STUDY PARTICIPANT DETAILS

Animals

Mouse experiments and procedures were approved by the Institutional Animal Care and Use Committee at the University of California, Irvine and conform to the Association for Research in Vision and Ophthalmology Statement for the Use of Animals in Ophthalmic and Vision Research. Breeding colonies of wild-type C57BL/6J (000664), *rd6* (003684), and *rd12* (005379) mice were established by purchase from the Jackson Laboratory (Bar Harbor, ME). Mice were housed in the specific pathogen-free vivarium of the University of California, Irvine on a 12 h/12 h light/dark cycle and fed *ad libitum*. 5–7 weeks old homozygous mouse littermates were randomly assigned to experimental groups. Both male and female mice were used equally. No mice were involved in previous procedures.

Cell lines and cultivation

Cells were cultured at 37 °C, 5% CO_2, and an H_2O-saturated atmosphere.

HEK293T (ECACC: 12022001, Sigma-Aldrich) and HEK293 (ECACC 85120602) cells were maintained in advanced DMEM (Gibco, Thermo Fisher Scientific) supplemented with 10% FBS (Gibco, Thermo Fisher Scientific), GlutaMAX (Gibco, Thermo Fisher Scientific), 100 μg/ml Penicillin-Streptomycin (Gibco, Thermo Fisher Scientific), 10 μg/ml Piperacillin (Sigma-Aldrich), and 10 μg/ml Ciprofloxacin (Sigma-Aldrich). Cells were passaged at 90% confluence by removing the medium, washing with DPBS (Gibco, Thermo Fisher Scientific) and detaching the cells with Accutase solution (Gibco, Thermo Fisher Scientific). Cells were then incubated for 5–10 min at room temperature until a visible detachment of the cells was observed. Accutase was subsequently inactivated by addition of pre-warmed DMEM including 10% FBS and all supplements. Cells were then transferred into a new flask at an appropriate density, or counted and distributed on 96-well or 6-well plates for plasmid transfection or VLP transduction.

Jurkat E6.1 cells (ECACC 88042803) were maintained in RPMI media 1640 (Gibco, Thermo Fisher Scientific) with GlutaMAX (Gibco, Thermo Fisher Scientific) and 100 μg/ml Penicillin-Streptomycin (Gibco, Thermo Fisher Scientific). For transduction, they were seeded into 96-well plates at 25,000 cells/well. The proper density was achieved by centrifugation at 200 relative centrifugal force (rcf) for 2 min and subsequent dilution with RPMI 1640 to the desired density.

Human induced pluripotent stem cells (hiPSCs (ISFi001-A) were incubated in Essential 8 (E8) Flex medium (Thermo Fisher Scientific, A2858501) at 37 °C under 5% CO2 saturation on (v/v) Vitronectin-coated (A31804, Thermo Fisher Scientific) plates. At 70% confluency, the cells were subcultivated using StemMACS Passaging Solution XF (Miltenyi Biotec) by incubating the cells for 6 min at room temperature. Subsequently, StemMACS Passaging Solution XF was removed by aspiration, and hiPSC colonies were harvested in E8 flex medium and chopped using a 1000 μl pipette tip. Collected cells were seeded on 96-, 48-, 24-, or 6-well plates at the appropriate cell densities.

Small airway epithelial cells (donor 08938, purchased from Cell systems) were thawed in a 37 °C water bath and seeded onto a 10 cm^2 petri dish containing 15 ml warm medium (airway epithelial growth medium (Promocell) supplemented with bovine pituitary extract, hydrocortisone, human epidermal growth factor (hEGF), epinephrine, transferrin, insulin, retinoic acid, and triiodothyronine (Promocell) according to the company's instructions, further supplemented with Primocin (Invivogen) at 100 $\mu g\ ml^{-1}$). The medium was changed every 2 days until the culture was 80% confluent, before being detached using Accutase (Sigma) and seeded into 96-well plates at 25k cells/well in 200 μl of airway-epithelial growth medium, 24 hours before transduction.

METHOD DETAILS

Molecular cloning and DNA analysis

Genetic constructs

The ENVLPE packaging plasmid is based on $psPAX2_{D64V}$ encoding CAG-driven Gag/Gag–Pol with a D64V mutation in the HIV-1-integrase domain. During optimization, Gag/Gag–Pol ($psPAX2_{D64V}$) and shuttling Gag-PCP variants were co-expressed on separate plasmids. Later, we grafted the optimized CAG-driven shuttling Gag-PCP/Gag–Csy4 expression cassettes to yield equimolar expression of Gag/Gag–Pol and Gag-PCP/Gag–Csy4 into $psPAX2_{D64V}$. For CMV-driven $ENVLPE^+$, the CAG promoters were exchanged for CMV promoters taken from pCMV-VSV-G. All core plasmids will be deposited on Addgene. (pe)gRNA sequences are listed in Table S1.

Please cite this article in press as: Geilenkeuser et al., Engineered nucleocytosolic vehicles for loading of programmable editors, Cell (2025), https://doi.org/10.1016/j.cell.2025.03.015

PCR

Single-stranded primer deoxyribonucleotides (Integrated DNA Technologies (IDT)) were resolubilized (100 μM) in nuclease-free water. PCR reactions with plasmid and genomic DNA templates were performed with Platinum SuperFi II PCR Master Mix (Thermo Fisher Scientific) according to the manufacturer's protocol. PCR reactions were purified by DNA agarose gel electrophoresis and subsequent DNA extraction using a Monarch DNA Gel Extraction Kit (New England Biolabs (NEB)).

DNA digestion with restriction endonucleases

Samples were digested with NEB restriction enzymes according to the manufacturer's protocol in a total volume of 40 μl with 1–3 μg of plasmid DNA. Afterwards, DNA fragments were purified by agarose gel-electrophoresis and subsequent purification using Monarch DNA Gel Extraction Kit (NEB).

Ligation and Gibson assembly

Concentrations of agarose-gel purified DNA fragments were determined by a spectrophotometer (NanoDrop 1000, Thermo Fisher Scientific). Ligations were carried out at room temperature for 5–10 min, with 50–100 ng backbone-DNA (DNA fragment containing the ori) in a 20 μl volume, with molar backbone:insert ratios of 1:1–3, using T4 DNA ligase (Quick Ligation Kit, NEB). Gibson assemblies were performed with 75 ng of backbone DNA in a 15 μl reaction volume and molar backbone:insert ratios of 1:1–5, using NEBuilder HiFi DNA Assembly Master Mix (2×) (NEB) for 20–60 min at 50 °C.

DNA agarose gel-electrophoresis

1% (m/m) agarose (Agarose Standard, Carl Roth) gels were prepared in 1× TAE buffer and 1:10,000 SYBR Safe stain (Thermo Fisher Scientific). Gel electrophoreses were carried out for 20–40 min at 100 V. For size determination, 1 kb Plus DNA Ladder (NEB) was used. DNA samples were mixed prior to loading with Gel Loading Dye (Purple, 6×) (NEB).

Bacterial strains (E. coli) for molecular cloning

Chemically competent *E. coli* K12 cells (NEB Stable) were used for transformation of circular plasmid DNA. For plasmid amplification, carbenicillin (Carl Roth) was used as a selection agent at a final concentration of 100 μg/ml. All bacterial cells were incubated in Lysogeny Broth (LB) medium or on LB agar plates, including the respective antibiotics.

Bacterial transformation with plasmid DNA

Transformation was performed by mixing 1-5 μl of ligation- or Gibson-reaction mixture with 50 μl of thawed, chemically competent cells, which were incubated on ice for 30 min before heat shocking at 42 °C for 30 s. Afterward, cells were incubated on ice for 5 min and mixed with 450 μl of SOC-medium (NEB). Transformed cells were then plated on agar plates containing an appropriate type and concentration of antibiotics according to the supplier's information. Plates were incubated overnight at 37 °C.

Plasmid DNA purification and Sanger sequencing

E. coli colonies with correct potential constructs were inoculated from agar plates in 2 ml LB medium at 37 °C with the respective antibiotics, and incubated for at least 6 h or overnight. Plasmid DNA was extracted with a Monarch Plasmid Miniprep Kit (NEB) according to the manufacturer's protocol, and sent out for Sanger sequencing (GENEWIZ, Azenta Life Sciences). Sanger-sequencing-validated clones were inoculated in 100 ml LB medium overnight at 37 °C containing the respective antibiotic selection agent. Plasmid DNA was extracted using a Plasmid Maxi Kit (QIAGEN).

Genomic DNA isolation

72 hours after transfection or transduction in 96-well format, genomic DNA was isolated with a Quick-DNA 96 Kit (Zymo Research) according to the manufacturer's protocol, with an elution volume of 30 μl.

For animal experiments, after the mice were euthanized, the anterior segment (iris, lens, cornea, ciliary body) was removed by dissection, and the neural retina was peeled from the posterior eyecup (RPE, choroid, and sclera). The eyecup was then immediately immersed in buffer RLT Plus with 1% beta-mercaptoethanol (Qiagen # 1053393), and the RPE was disassociated from the eyecup by pipetting before homogenization by QiaShredder (Qiagen # 79654). DNA was then isolated with the AllPrep DNA/RNA Micro kit according to manufacturer instructions (Qiagen # 80284).

Amplicon PCR and purification

Primer sequences are provided in Table S1. PCR was performed as described above using ~50 ng of gDNA and appropriate primers for each target. Amplicon lengths were designed to approach 250 bp for sequencing. PCR purification was performed using the DNA Clean & Concentrator-5 Kit (Zymo Research) according to the manufacturer's protocol with an elution volume of 30 μl.

For analysis of animal experiments, PCR was performed with Phusion Plus green mastermix (Thermo # F632S) and PCR products were checked by electrophoresis on a 1% agarose TAE gel. PCR products were then purified with a QiaQuick MinElute PCR kit (Qiagen # 28004) and quantified spectrophotometrically with a NanoDrop 1000 spectrophotometer.

Amplicon sequencing and analysis

Genomic DNA was used as a template for PCR on the locus of interest (40 cycles). For pooled analysis of multiple samples, a second outer PCR using barcoded primers was performed and the samples were subsequently pooled. PCR products were gel-purified as described above, normalized to 20 ng/μl and submitted for Amp-EZ sequencing (GENEWIZ, Azenta Life Sciences). For samples from animal experiments, next-generation sequencing was performed commercially by Quintara Biosciences (Hayward, CA) by Illumina MiSeq utilizing 2 × 250 bp chemistry.

The resulting fastq files containing paired reads were analyzed with Geneious (including barcode separation for pooled samples), trimming all merged reads shorter than 200 bp and using an analysis window spanning at least 50 bp around the nicking site.

Please cite this article in press as: Geilenkeuser et al., Engineered nucleocytosolic vehicles for loading of programmable editors, Cell (2025), https://doi.org/10.1016/j.cell.2025.03.015

Alternatively, PCR amplicons were analyzed *via* Sanger sequencing followed by chromatogram quantification with interference of CRISPR edits (ICE, Synthego).

Mammalian cell culture

HEK293T 'blue' mGreenLantern reporter generation

Cell lines were created by cloning the reporter coding for the blue-shifted mGreenlantern mutant (G65S, Y66H) with a CAG-promoter, a bovine growth hormone (bGH) polyadenylation signal (pA) flanked by homology arms for a safe-harbor locus of choice. To create a HEK293T reporter cell line, cells were transfected with the CRISPR donor plasmid and a second plasmid encoding Cas9 and the corresponding gRNA. Cells were transfected according to the manufacturer's protocol (jetOPTIMUS, Polyplus) 24 hours post-seeding on a 6-well plate (600k cells in 3 ml per well) in the presence of 0.5 μM AZD7648 (HY-111783; MedChemExpress), a DNA-PKcs inhibitor, and a CAG-promoter-driven i53, a 53BP1 inhibitor, to inhibit NHEJ and thereby shifting the DNA repair towards HDR. The surviving polyclonal population was monoclonalized using limiting dilution in 96-well plates, and selected clones were genotyped to determine homozygosity.

hiPSC reporter lines generation

The hiPSC reporter cell lines were generated by integrating the blue-shifted mGreenlantern mutant (G65S, Y66H) (Figure S17A) or the enhanced traffic light reporter v2 (eTLRv2) (Figure S18A) version 2 into the human safe-harbor locus *AAVS1*.

hiPSCs (ISFi001-A (RRID:CVCL_YT30)) were passaged using Accutase (Sigma, A6964-500ML) for 10 min at 37 °C, counted using a Neubauer improved cell-counting chamber (Carl Roth, PK361), and electroporated as single cells in a 100 μl cuvette using the CB-156 program with the P3 Primary Cell 4D-Nucleofector X Kit (Lonza Group Ltd) and the 4D Nucleofector (Lonza Group Ltd) according to the manufacturer's instructions (2×10^6 hiPSCs, 1 μg Cas9-gRNA plasmid, 2 μg integration plasmid). After nucleofection, hiPSCs were seeded on one well of a Vitronectin-coated 6-well plate, and incubated in E8 flex medium supplemented with 10 μM Y27632 (Enzo Life Sciences, ALX-270333-M005) and 0.5 μM AZD7648 (HY-111783; MedChemExpress) for 24 h. Cells were allowed to recover to ~70 % confluency in E8 flex medium. Gene-edited hiPSCs were selected with puromycin (A1113803, Thermo Fisher Scientific) at a concentration of 0.5μg/ml in E8 flex medium for 3 days; then at 1 μg ml^{-1} puromycin for 4 additional days. Subsequently, hiPSC colonies were clonalized and expanded. For characterization, genomic DNA was isolated using the QIAamp DNA Mini Kit (Qiagen) according to the manufacturer's instructions for cultured cells. A correct integration was verified by genotyping PCRs and Sanger sequencing of amplicons reaching over the 5' homology arm into the CAG promoter (P1: CCACTCTGTGCTGACCACTC; P2: AGGCGGGCCATTTACCGTAAG), over the 3' homology arm into the puromycin resistance gene (P3: GAGTTTGCCAAGC AGTCACC; P4: CCTGAGGGCCCTAGAACCT), and within the knock-in from the CAG promoter to the pA

(P5: TTCGGCTTCTGGCGTGTG; P6: CGAGGCTGATCAGCGAGCTC). Heterozygosity was confirmed by a genotyping PCR amplifying the region of the homology arms (P1; P3). The expression and functionality of the integrated reporter were verified by FACS analysis. In total, 2 clones per reporter cell line ('blue' mGreenLantern reporter or eTLR) were selected and further quality controlled.

Quality control of edited hiPSCs

Karyotyping

Single-nucleotide polymorphism (SNP) array-based karyotyping was performed as described previously. The genomic DNA of the hiPSCs was extracted using the QIAamp DNA Mini Kit (Qiagen) according to the manufacturer's instructions. The DNA concentration was measured using Quant-iT PicoGreen (Invitrogen, Thermo Fisher Scientific) according to the Infinium HTS Assay Protocol Guide (Illumina). SNPs were identified using an Infinium Global Screening Array-24 v3.0 Kit (Illumina) and an iScan system (Illumina) according to the Infinium HTS Assay Protocol Guide.

The assay was performed by the Genomics Core Facility of Helmholtz Munich. Clustering, quality control, and SNP calling were done using GenomeStudio 2.0.5 (Illumina) as described. Copy number variations (CNVs) on autosomes were determined using the cnvPartition v3.2.1 (Illumina) plugin with default settings, including a confidence threshold of 50. No CNVs exceeding 1 kbp could be identified for the 'blue' mGreenLantern reporter (Figure S17B), nor the eTLRv2 (Figure S18B) hiPSC lines.

Pluripotency staining

hiPSC were cultured on Vitronectin-coated glass coverslips for 5 days. Cells were fixed with 10% Formalin (Sigma, F5554) for 20 min at 37 °C, washed twice with PBS (Thermo Fisher Scientific), and permeabilized/blocked using a blocking solution (PBS containing 1 % BSA (Sigma-Aldrich, A7906-500G) and 0.3% Triton X-100 (Sigma-Aldrich, T9284)) for 15 min at room temperature. Primary antibodies were diluted in a blocking solution, and antibody incubation was performed at 4 °C overnight. Cells were washed twice with PBS and incubated in a blocking solution containing secondary antibodies for 2 h at room temperature. Nuclei were stained with PBS containing 0.1 μg/ml DAPI (Thermo Fisher Scientific, 62248) for 10 min at room temperature. Cells were washed twice with PBS and coverslips were mounted using Aqua-Poly/Mount (Polysciences Inc., 18606-20). Primary antibodies were diluted as follows: NANOG (AF1997, R&D Systems; 1:200), POU5F1 (2840 S, Cell Signaling; 1:500), SOX2 (sc-365823, Santa Cruz; 1:500). Secondary antibodies were diluted as follows: donkey-anti-mouse IgG Alexa 488 (A21202, Thermo Fisher Scientific; 1:500), donkey-anti-goat IgG Alexa 594 (A11058, Thermo Fisher Scientific; 1:500), donkey-anti-rabbit IgG Alexa 594 (A21207, Thermo Fisher Scientific; 1:500). Fluorescence images were acquired using an EVOS FL Auto Imaging System (Thermo Fisher Scientific) (Figures S17C and S18C).

Please cite this article in press as: Geilenkeuser et al., Engineered nucleocytosolic vehicles for loading of programmable editors, Cell (2025), https://doi.org/10.1016/j.cell.2025.03.015

Trilineage differentiation

The differentiation potential of edited cells was verified by trilineage differentiation into the ectoderm, mesoderm, and endoderm lineage. hiPSCs were maintained on Vitronectin-coated 6-well plates. At 70% confluency, hiPSCs were passaged using Accutase for 10 min at 37 °C, sheared to single cells by pipetting using a 1,000 μl tip, and diluted in E8 flex medium containing 10 μM ROCK inhibitor Y27632. hiPSCs were harvested at 200 rcf for 5 min and resuspended in E8 flex medium containing 10 μM ROCK inhibitor Y27632. Cell number was determined using a Neubauer improved cell counting chamber, and 50,000 cells per well with 9 replicates per cell line were seeded in E8 flex medium containing 10 μM ROCK inhibitor Y27632 on Vitronectin-coated 96-well plates. Trilineage differentiation was performed in triplicates using the STEMdiff Trilineage Differentiation Kit (StemCell Technologies) according to the manufacturer's instructions. Subsequently, cells were fixed with 10% Formalin (Sigma, F5554) for 20 min at 37 °C. Differentiation efficiency was quantified by immunostainings as described above for the pluripotency staining. Primary antibodies were diluted as follows: SOX2 (sc-365823, Santa Cruz; 1:500), NES (Ma1110, Thermo Fisher Scientific; 1:250), AFP (MAB1368, R&D; 1:500), SOX17 (AF1924, R&D Systems; 1:500), NCAM1 (Sc-106, Santa Cruz; 1:500), TBXT (ab209665, Abcam; 1:500). Secondary antibodies were diluted as follows: donkey-anti-mouse IgG Alexa 488 (A21202, Thermo Fisher Scientific; 1:500), donkey-anti-goat IgG Alexa 594 (A11058, Thermo Fisher Scientific; 1:500), donkey-anti-rabbit IgG Alexa 594 (A21207, Thermo Fisher Scientific; 1:500). Fluorescence images were acquired using an EVOS FL Auto Imaging System (Thermo Fisher Scientific) (Figures S17D and S18D).

Generation of hiPSC-derived cortical neurons

hiPSCs were differentiated into neuronal precursor cells and further into cortical neurons by using a dual SMAD-signaling inhibition strategy as described.[69] At 70% confluency, hiPSCs were passaged using Accutase for 10 min at 37 °C, sheared to single cells by pipetting using a 1000 μl tip and diluted in E8 flex medium containing 10 μM ROCK inhibitor Y27632. hiPSCs were harvested at 200f rcf for 5 min and resuspended in E8 flex medium containing 10 μM ROCK inhibitor Y27632. Cell number was determined using a Neubauer improved cell-counting chamber, and hiPSC were seeded on Vitronectin-coated 6-well plates at a density of 30,000 cells/cm^2. The next day (day 0), differentiation was started by replacing the E8 flex medium with neural-induction medium (50% DMEM/F12-GlutaMAX (Thermo Fisher Scientific, 31331093), 50% Neurobasal medium (Thermo Fisher Scientific, 21103049) supplemented with 1% B27 (Thermo Fisher Scientific, 17504044), 0.5% N2 (Thermo Fisher Scientific, 17502048), 0.5% GlutaMAX (Thermo Fisher Scientific, 35050061), 0.5% non-essential amino acids (Thermo Fisher Scientific, 11140035), 1% Penicillin-Streptomycin (Thermo Fisher Scientific, 15070063), 2.5 g/ml Insulin (Sigma, I3536-100MG), 10 μM SB431542 (Miltenyi Biotec, 130-106-275), 100 nM LDN193189 (Tocris Bioscience, 6053), and 0.02 % beta-mercaptoethanol (Thermo Fisher Scientific, 31350010)). The medium was replaced daily until day 21. On day 14, cells were reseeded on a 15 μg/ml poly-L-ornithine and 10 μg/ml laminin-coated 6-well plate at a ratio of 1:2. The neuroepithelial sheet was collected using a StemPro EZPassage tool (Thermo Fisher Scientific, 23181010) and transferred using a 1,000 μl tip. On day 21, neuronal precursor cells were reseeded and expanded. The medium was removed by aspiration, cells were washed once with PBS, and detached using Accutase for 10 min at 37 °C. Dissociated cells were diluted in neural-induction medium, centrifuged at 200 rcf for 5 min, and resuspended in neural-induction medium containing 10 μM ROCK inhibitor Y27632. Cell number was determined using a Neubauer improved cell-counting chamber, and neuronal precursor cells were seeded on poly-L-ornithine-laminin-coated 6-well plates at a density of 200,000 cells cm^2. On day 22, the medium was changed to neural-maintenance medium (50% DMEM/F12-GlutaMAX, 50% Neurobasal supplemented with 1% B27, 0.5% N2, 0.5% GlutaMAX, 0.5% non-essential amino acids, 1% penicillin-streptomycin, 2.5 g ml^{-1} insulin, 0.02 % beta-mercaptoethanol, 200 μM ascorbic acid 2-phosphate (Sigma, A8960-5G), and 20 ng/ml human BDNF (Miltenyi Biotec, 130-093-811)). The medium was replaced daily until day 50. On day 50, cortical neurons were reseeded on poly-L-ornithine-laminin-coated glass coverslips, and 96-, 48-, 24-, or 6-well plates for direct use. The medium was removed by aspiration, the cells were washed once with PBS, and detached using Accutase for 10 min at 37 °C. Dissociated cortical neurons were diluted in neural-maintenance medium, centrifuged at 200 rcf for 5 min, and resuspended in neural-maintenance medium containing 10 μM ROCK inhibitor Y27632. Cell number was determined using a Neubauer improved cell-counting chamber and cortical neurons were seeded on the desired vessels at a density of 200,000 cells/cm^2. Before use, cortical neurons were maintained at 37 °C under 5% CO2 saturation for 14 additional days, with medium changes every second day. Differentiation efficiency was verified by immunostainings as described above for the pluripotency staining. Cortical neurons grown on glass coverslips were fixed with 10% Formalin (Sigma, F5554) for 20 min at 37 °C. Primary antibodies were diluted as follows: BCL11B (Abcam, ab18465; 1:500), CUX1 (Sigma Aldrich, SAB1405681; 1:500), TUBB3 (T5076, Sigma-Aldrich; 1:1000), MAP2 (Sigma Aldrich, AB5622-I; 1:500). Secondary antibodies were diluted as follows: donkey-anti-mouse IgG Alexa 488 (A21202, Thermo Fisher Scientific; 1:500), donkey-anti-mouse IgG Alexa 594 (A21203, Thermo Fisher Scientific; 1:500), donkey-anti-rat IgG Alexa 488 (A21208, Thermo Fisher Scientific; 1:500), donkey-anti-rabbit IgG Alexa 594 (A21207, Thermo Fisher Scientific; 1:500). Fluorescence images were acquired using an EVOS FL Auto Imaging System (Thermo Fisher Scientific) (Figures S17E and S18E).

VLP production

A general schematic depiction of the VLP production process can be found in Figure S19.

Plasmid transfection for VLP production

For production on 6-well plates (poly-D-lysine-coated), 750,000 cells were seeded at 3 ml per well in full DMEM with 10% FBS 24 h prior to transfection. The cells were transfected (jetOPTIMUS, Polyplus) with a total of 1.2 μg plasmid DNA using JetOPTIMUS

Please cite this article in press as: Geilenkeuser et al., Engineered nucleocytosolic vehicles for loading of programmable editors, Cell (2025), https://doi.org/10.1016/j.cell.2025.03.015

transfection reagent. The reagent volume to DNA mass ratio (V/m) was 1:1 in a total volume of 120 μl (fill-up with JetOPTIMUS Buffer, 10 min incubation at room temperature for complex formation). The detailed plasmid stoichiometries of the different systems are shown in Table S1.

For production on 15 cm dishes (poly-D-lysine-coated), 12.5×10^6 cells were seeded in 50 ml per well in full DMEM with 10% FBS 24 h prior to transfection. The cells were transfected (jetOPTIMUS, Polyplus) with a total of 19.2 μg plasmid DNA using JetOPTIMUS transfection reagent. The reagent volume to DNA mass ratio (V/m) was 1:1 in a total volume of 1.92 ml (fill-up with JetOPTIMUS Buffer, 10 min incubation at room temperature for complex formation). The detailed plasmid stoichiometries of the different systems are shown in Table S1.

Concentration and transduction of VLPs

The supernatant (SN) containing the VLPs was sterile-filtered to remove cell debris and remaining lipofection reagents. Subsequently, the filtered SN was concentrated to approximately 1/30 of the original volume using a 100 kDa molecular weight cutoff filter (Amicon Ultra-4, UFC810024 (Merck)). For transduction (TD), the respective reporter cell line was seeded on a 96-well plate (25,000 cells in 200 μl advanced DMEM). 6 h post-seeding, the supernatant of one 6-well production (or a corresponding dilution in 2-fold steps) was applied to a triplicate of receiver cells on the 96-well plate without exceeding 20% of the total volume of the receiver cell's original growth medium. For optimizing the VLP system, cells were analyzed at 72 h post-TD when delivering an RNP complex, and 24 h post-TD when delivering mRNA.

Storage capabilities of the ENVLPE VLPs vary depending on pseudotyping. VSV-G pseudotyped VLPs can be stored at 4 °C for at least three days without significant loss of infectivity. For other pseudotyped VLPs it is recommended to quick-freeze the VLPs using liquid nitrogen and avoid repeated freeze-thaw cycles.

Ultracentrifugation of VLPs

For experiments with primary T lymphocytes and all animal studies, VLPs were purified by ultracentrifugation. After 72 hours of expression in a 15 cm dish (12,500,000 cells in 50 ml advanced DMEM), the supernatant was harvested and sterile-filtered (0.45 μm). 35 ml of the filtrate was transferred into a Beckman Coulter Ultra-Clear Tube, and 3 ml of a 20% sucrose PBS solution was layered below the supernatant. The supernatants were spun for two hours at 26,000 rpm in a Beckman LE-70 ultracentrifuge. The SW28 swinging-bucket rotor was cooled to 4 °C. After removing the supernatant, the rim of the centrifugation tubes were dried with cotton swabs and pellets were resuspended in 1/1000 of the original volume using PBS supplemented with 10% sucrose and 1× PenStrep.

IDLV production and transduction

For the production of ecotropic integrase-defective lentiviruses (IDLV) to facilitate editing of the 'blue' mGL reporter locus, HEK293T cells were seeded 1 day prior transfection on a 6-well plate in 3 ml advanced DMEM with a concentration of 200,000–250,000 cells/ml. The cells were transfected according to the manufacturer's protocol (jetOPTIMUS, Polyplus) with the following components: 400 ng psPAX2$_{D64V}$ (a gift from David Rawlings & Andrew Scharenberg (Addgene # 63586)), 600 ng lentiviral transfer vector encoding the HDR-donor, and 200 ng of the CMV promoter-driven ecotropic MMLV envelope protein (MMLV-Env$_{\Delta607\text{-}622}$). The IDLVs were purified as described for VLPs and then co-transduced with Cas9-ENVLPE. 4 days after transduction, green fluorescence was measured *via* FACS to quantify HDR events. Additionally, the decrease of blue fluorescence indicated the indel rate.

To facilitate the larger edit of the TLR locus, we produced VSV-G-pseudotyped IDLVs. For lipofection, 12,500,000 HEK293T cells were seeded on a 15 cm dish (poly-L-lysine coated) in 50 ml DMEM. 5376 ng psPAX2$_{D64V}$ (Addgene # 63586), 8064 ng lentiviral transfer vector encoding the HDR-donor, 2688 ng pRSV-REV (Addgene #12253) and 3072 ng of pCMV-VSV-G (Addgene #8454) were co-transfected according to the manufacturer's protocol (jetOPTIMUS, Polyplus). The Cas9-ENVLPE was also produced in a 15 cm dish. Both ENVLPE and IDLV were purified *via* ultracentrifugation and resuspended in PBS at 1/1000 of the original volume.

Cas9-ENVLPE and IDLVs were co-transduced in a 1:1 ratio.

Anti-FLAG staining

HEK293T cells were seeded (80,000 cells in 300 μl advanced DMEM) one day before transfection in 8-well μ-Slides (Ibidi). 48 hours post-TF, half of the medium was removed, and cells were pre-fixed with 10% neutral-buffered formalin (Sigma-Aldrich) for 5 minutes at room temperature, followed by fixation with 10% neutral buffered formalin for 10 min at room temperature. Afterward, cells were washed three times with DPBS before incubation for 2 h at room temperature with 1:1000 Monoclonal ANTI-FLAG M2 antibody from mouse (Sigma-Aldrich, 1 mg/ml) in DPBS containing 1% BSA (Sigma-Aldrich) and 1% Triton X-100 (Sigma-Aldrich) for permeabilization. Following three additional washing steps with DPBS, cells were treated with Cy3-conjugated goat anti-mouse IgG (2 mg/ml stock), diluted 1:100 in DPBS with 1% BSA, and incubated for 45 min at room temperature. The next washing step included Hoechst 33342 stain (10 mg/ml stock diluted 1:10,000 in DPBS), followed by two additional washing steps with DPBS. Confocal microscopy was performed using a Leica SP5 system (Leica Microsystems) under identical conditions for all samples across all experimental conditions.

Delivery of VLPs in primary T lymphocytes

Cryopreserved primary human T cells, isolated in-house (# 19661; Stem Cell Technologies) from anonymous healthy donors under an institutional review board-approved protocol, were thawed on day 0 and activated with anti-CD3/CD28 Dynabeads (#40203D; Gibco)

Please cite this article in press as: Geilenkeuser et al., Engineered nucleocytosolic vehicles for loading of programmable editors, Cell (2025), https://doi.org/10.1016/j.cell.2025.03.015

in RPMI medium (10% FBS and 1% P/S), supplemented with 20 IU/ml recombinant human IL-2 (#200-02; Peprotech). 50,000 T cells/well were plated in a 96-well U-bottom plate. One day afterward, the activated T cells were treated with VLPs, prepared *via* ultracentrifugation, targeting B2M and/or TRBC1/2 in duplicates or triplicates per condition. On the third day after T cell activation, cells were split in half, and fresh RPMI medium with recombinant IL-2 was added. On the fifth day following T cell activation, anti-CD3/CD28 beads were removed magnetically, and MHCI (#311406; Biolegend) and CD3 (#317318; Biolegend) surface presentation was analyzed by flow cytometry, while the respective *TRBC1/2* and *B2M* loci were analyzed *via* NGS following gDNA isolation and PCR.

For flow cytometry, cells were washed with FC buffer (PBS + 2% FBS), stained with the indicated antibodies (1:100 dilution) for 30 min at 4 °C in the dark, washed twice to remove unbound antibodies, and resuspended in FC buffer with DAPI (Thermo Fisher, #62247). Samples were acquired on a BD LSRFortessa and analyzed using FlowJo software (v10).

Viability and toxicity assays

To assess viability and cytotoxicity in receiver cells, HEK293T cells were seeded in a 96-well format (25,000 cells in 200 μl advanced DMEM) and transduced six hours post-seeding with the equivalent of half the supernatant of one 6-well production distributed across a triplicate. Additionally, hiPSCs cells were seeded as single cells (25,000 cells) on a Geltrex-coated 96-well plate in 100 μl E8 flex media supplemented with 10 μM Y27632 (Enzo Life Sciences, ALX-270333-M005). One day post-seeding, cells were washed with DPBS, 100 μl new E8 flex media was added and transduced with the equivalent of half the supernatant of one 6-well production distributed across a triplicate. One day post-TD, receiver cells were washed with DPBS, new pre-warmed media was added, and puromycin (2 μg/ml) was administrated in triplicate as a control. The CellTiter-Glo 2.0 Cell Viability Assay (Promega, G9241), as well as LDH-Glo Cytotoxicity Assay (Promega, J2380) were performed according to the manufacturer's protocol, 48 hours post-TD for HEK293T, and 24 hours post-TD for hiPSCs. Measurements were taken on a Varioskan LUX microplate reader (Thermo Fisher Scientific).

Flow cytometry

72 h post-transduction, cells were gently detached in a suitable volume of Accutase, pelleted (200 rcf, 5 min), and resuspended in ice-cold 0.4% formalin for 10 min. Fixed cells were pelleted again (200 rcf, 5 min) and resuspended in 200 μl ice-cold DPBS. Analysis was performed on the BD FACSaria II or the BD FACSymphony A3 Cell Analyzer (BD Biosciences). Data were analyzed with FlowJo (10.10.0, BD BioSciences). Briefly, the main population of the cells was gated according to their FSC-A and SSC-A. Secondly, single cells were gated using FSC-A and FSC-W (FACSAria II) or FSC-H (FACSymphony A3). The final gate (green fluorescence plotted against red fluorescence to compensate for autofluorescence artefacts) was used to determine the proportion of successfully edited or transduced cells, as well as their median fluorescence intensity.

Bioluminescence quantification

For dual-luciferase readout using the Nano-Glo Dual-Luciferase Reporter Assay System (Promega), NLuc and FLuc signals were read on-plate 48 hours post-transfection. Measurements were taken on a Centro LB 960 plate reader (Berthold Technologies) with 0.5 s acquisition time 10 min after the addition of Reagent 1 (ONE-Glo EX Luciferase) for FLuc, and 10 min after the addition of Reagent 2 (NanoDLR Stop & Glo) for NLuc. Reagent 2 contains a FLuc inhibitor.

Cryo-electron microscopy

After production of VLPs in HEK293T, the supernatant was sterile filtered and the VLPs purified *via* ultracentrifugation. VLPs were resuspended in 1/1000th of the original volume. 4 μL of the ultracentrifuged material for each of the samples was applied onto carbon-coated 200 mesh copper grids R2/1 (Quantifoil Micro Tools), blotted, and immediately plunged frozen in liquid ethane, using Vitrabot Mark 4 (Thermo Scientific). The grids were loaded into the autoloader of a 200 kV Glacios cryo-TEM, equipped with a Falcon4i direct electron detector camera (Thermo Scientific). EPU software (Thermo Scientific) was used for automatic image acquisition in different grid squares to streamline data generation. Acquired data was manually checked for the ice quality and the particles' presence. Selected sets of foil hole images with a pixel size of 0.246 nm were passed for downstream image analysis. Images were grouped by the sample origin. The contrast of the images was enhanced in Fiji image software through the application of the Contrast Limited Adaptive Histogram Equalization (CLAHE) plugin (block size 127, histogram bins 256, maximum slope 1.5). The visibility of the particles was further enhanced by 2× application of Despeckle (median filter) operation in Fiji image software. Vesicle lipid envelopes were manually segmented, avoiding damaged or distorted particles. The segmented areas were used to create the binary masks and the binary masks were quantified in Fiji to acquire area per particle with subsequent conversion of circular area to a radius individually for each of the particles.

p24 (HIV-1) and p30 (MMLV) quantification

VLP titers after ultracentrifugation were determined using commercial ELISA kits. For HIV-1-derived ENVLPE, the Lenti-X p24 Rapid Titer Kit (Takara Bio, 631476) was used according to the manufacturer's protocol.

The MMLV-derived eVLPs were quantified using the QuickTiter MuLV p30 Core Antigen ELISA Kit (Cell Biolabs, VPK-156) according to the manufacturer's protocol.

Please cite this article in press as: Geilenkeuser et al., Engineered nucleocytosolic vehicles for loading of programmable editors, Cell (2025), https://doi.org/10.1016/j.cell.2025.03.015

In both ELISAs, titers were calculated by using the recommended dilution series of recombinant antigens and at least two different dilutions of the VLP solution in PBS. For calculations, we assumed that one particle contains, on average, 2500 HIV-1-Gag monomers or 1800 MMLV-Gag monomers.

Cas9 protein quantification

Samples were concentrated *via* ultracentrifugation and the concentration of editor protein was determined using the Cas9 ELISA Kit (Cell Biolabs, PRB-5079) according to the manufacturer's protocol. For VLP lysis, 25 μl of Triton-X100 was added to 225 μl of the sample (experimental or standard) and incubated for 30 min at 37 °C before application to the anti-Cas9 antibody-coated plate. The concentration was calculated using the recommended dilution series of recombinant *S. pyogenes* Cas9 and at least two different dilutions of the VLP solution in PBS.

pegRNA quantification

For pegRNA quantification, RNA was extracted from the purified VLPs, which were also used for Cas9 quantification by the Quick-RNA Viral 96 Kit, following the manufacturer's protocol. Purified RNA was stored at −80 °C. RNA samples were subjected to DNase digestion with DNase I (NEB) with the following protocol changes: the DNase concentration was doubled, and the incubation time was extended to 15 min.

For standard curve generation, plasmids encoding pegRNAs were *in vitro* transcribed using the Quick T7 High Yield RNA Synthesis Kit (NEB #E2050), following the manufacturer's protocol, which was adjusted for sgRNA synthesis as instructed by the manufacturer. Transcribed RNA was purified using the Monarch RNA Cleanup Kit (50 μg) (NEB #T2040), and subsequently subjected to DNase digestion as described above. The RNA concentration was quantified using the Qubit RNA High Sensitivity (HS) assay kit (Thermo Fisher) according to the manufacturer's protocol.

Standard and experimental samples were serially diluted in nuclease-free water. Reverse transcription was performed using SuperScript IV Reverse Transcriptase (Invitrogen, 18090010) following the manufacturer's protocol. Sequence-specific primers (Table S1) were annealed at 65 °C for 5 min ramping down, followed by reverse transcription at 65 °C for 20 min and heat inactivation at 80 °C for 10 min.

For qPCR, Power SYBR Green Master Mix (Applied Biosystems, 4368577) was used according to the manufacturer's protocol, with a primer mix containing 900 nM of each forward and reverse primer (Table S1). Reactions were run in 384-well plates (11 μl per well) in technical duplicates for 45 cycles. Control amplification reactions without reverse transcriptase were carried out as a reference for each RT-qPCR run. The reactions were performed and monitored in an Applied Biosystems QuantStudio 12K Flex Real-Time PCR system.

Subretinal injection

Prior to injection, VLPs were clarified by centrifugation at 17,000 rcf for 1 min at room temperature. Mice were prepared for injection by sequential dilation with 1% tropicamide solution (Somerset Therapeutics #119758) and 2.5% phenylephrine solution (Akorn #118050). Mice were anesthetized with a ketamine-/xylazine cocktail and GenTeal Severe 0.3% hypromellose gel (Alcon #0065806401) was applied to the corneas. Under a surgical microscope (Zeiss), a corneal incision was made with a disposable 27G beveled needle before a 34G blunt injection needle connected to Silflex tubing (World Precision Instruments # RPE-KIT) was advanced through the incision and into the subretinal space. 1 μl of VLPs were injected at 70 nl s-1, controlled by a UMP3 pump (World Precision Instruments #UMP3-3). Anesthesia was reversed with atipamezole (Zoetis #10000449) and the mice recovered on a heating pad prior to return to their cage.

Electroretinography (ERG)

Mice were dark adapted for 24 hours preceding the ERG recordings. Under a safety light, mice were dilated with topical administration of 1% tropicamide ophthalmic solution (Akorn #17478-102-12) followed by 10% phenylephrine ophthalmic solution (MWI Animal Health #054243) and underwent anesthesia by isoflurane inhalation. The mice were placed on a Diagnosys Celeris rodent-ERG device (Diagnosys LCC, Lowell, MA, USA) equipped with a heating pad and hypromellose administration (Akorn #9050-1) for hydration. Ocular stimulator electrodes were placed on the corneas, a ground electrode was placed subdermally in the rear leg and the reference electrode was placed subdermally between the ears. Green-light stimulation (peak emission 544 nm, bandwidth ~160 nm) of -0.3 log (cd s m-2) was recorded from each eye. The responses for 10 stimuli with an inter-stimulus interval of 10 s were averaged, and the a- and *b*-wave amplitudes were acquired from the averaged ERG waveform. Data were analyzed with Espion V6 software (Diagnosys LLC).

Retinoid analysis

Mice were dark adapted for 48 hours prior to sacrifice. Single, whole eyes were enucleated under dim red light and frozen on dry ice before wrapping in aluminum foil and storing for a short-term at −80 °C. The whole eyes were unwrapped and allowed to thaw on ice prior to Dounce homogenization in 1 ml of a chilled, sodium-phosphate-based buffer containing hydroxylamine and methanol (10 mM sodium phosphate, 100 mM hydroxylamine hydrochloride, and 50% methanol by volume). Following incubation of the homogenates at room temperature for 25 min, 2 ml of 3M NaCl and 3 ml of ethyl acetate were added to each homogenate. The tubes were

Please cite this article in press as: Geilenkeuser et al., Engineered nucleocytosolic vehicles for loading of programmable editors, Cell (2025), https://doi.org/10.1016/j.cell.2025.03.015

vigorously shaken for 2 min to partition the retinoids into the ethyl acetate layer, then centrifuged at 3,220 rcf in a tabletop centrifuge for 15 min at 20 °C. The top ethyl acetate layer was collected in separate tubes, and an additional 3 ml of ethyl acetate was added to each tube. The shaking and centrifugation steps were then repeated, and the ethyl acetate fractions were consolidated for each sample. Following consolidation, each fraction was dried under vacuum at approximately 32 °C. The dried retinoids were resuspended in 400 μl of hexanes and centrifuged in a tabletop centrifuge at 16,100 rcf for 15 min at 4 °C to pellet undissolved material. All steps prior to loading onto the HPLC were done in darkroom conditions with dim red illumination. The top 350 μl of each sample were placed into amber HPLC vials and loaded into a normal-phase Agilent 1260 Infinity II high-performance liquid chromatograph (Agilent, Santa Clara, CA) equipped with an Agilent Rx-SIL HPLC column (Neta Scientific, Hainesport NJ, cat #: 880975-901). The elution protocol consisted of two steps; one less-polar elution step (99.4% hexanes: 0.6% ethyl acetate) for 20 min followed by a more polar elution step (90% hexanes: 10% ethyl acetate) for 25 min, followed by a brief shift to the less-polar elution step for 5 min. Eluted retinoids were detected spectrophotometrically by monitoring changes in absorbance at 325 nm and 360 nm. Retinoids were identified by their elution times and spectra. To quantify individual retinoids in terms of pmol/eye, areas under each retinoid peak were multiplied by conversion factors derived from standard curves that were generated for all-*trans*-retinyl esters, *syn*-11-*cis*-retinal oxime (derivative of *syn*-11-*cis*-retinal), or all-*trans*-retinal oxime (derivative of all-*trans*-retinal). These retinoid standards were dissolved in hexanes.

Western blotting

After eyecups were isolated as described above for nucleic acid extraction, eyecups were immersed into 1×c RIPA buffer with protease inhibitors (Roche # 04693132001). The eyecups were homogenized mechanically with a pestle before incubation for 20 min on ice. The homogenates were then spun at 4 °C at 21,300 rcf for 20 min and supernatants were collected. Homogenates were then cleared of mouse immunoglobulins *via* incubation for 15 min at 4 °C with Protein G Dynabeads (Invitrogen # 10003D). Protein lysates were separated on a 4-12% Bis-Tris gel (Invitrogen # NP0323BOX) in 1× MOPS running buffer before fast wet transfer (GenScript eBlot L1 # L00686) to PVDF membranes (Millipore # IPFL00010). The membranes were blocked with 5% non-fat milk in phosphate buffered saline, pH 7.4 with 0.1% Tween-20 (PBS-T) for 1 h at room temperature with constant agitation before incubation with primary antibodies in PBS-T with 1% non-fat milk overnight at 4 °C with constant agitation. Primary antibodies in this study include anti-RPE65 (1:1,000, clone KPSA1, produced in-house), anti-beta-actin (1:2,000, clone 13E5, Cell Signaling Technologies # 4970S), anti-Cas9 (1:5,000, clone 7A9, Biolegend # 844301), and anti-MFRP (1:1,000, R&D Systems # AF3445). The following day, the membranes were washed 3 times for 10 min each with PBS-T before incubation with secondary antibodies in PBS-T with 1% non-fat milk for 1 h at room temperature with constant agitation. Secondary antibodies in this study include donkey anti-goat IgG HRP (1:5,000, Thermo #A16005), anti-mouse IgG HRP (1:5,000, Cell Signaling Technologies # 7076S), and anti-rabbit IgG HRP (1:5,000, Cell Signaling Technologies # 7074S). The membranes were washed 3 times again for 10 min each with PBS-T before HRP detection with Clarity Max substrate (Bio-Rad # 1705062)and then imaged on a Bio-Rad ChemiDoc.

Two-photon imaging

Two-photon excitation imaging was accomplished using our custom TP-imaging system based on a Leica TCSSP8 and equipped with a 1.0 NA 20× water immersion objective and a Vision S (Coherent) Ti:sapphire laser delivering 950 nm 80 MHz pulsing light. To image and spectrally separate GFP and tdTomato, two internal spectral detectors were used with their detection bandwidths set to 490–545 nm for GFP, and 590–680 nm for tdTomato. Intact mouse eyes were imaged *ex vivo* after euthanasia and enucleation. Leica ASX 4.7.0.28176 and image J were used for the reconstruction of 3D stacks and quantification of transduced cells.

Design considerations

ENVLPE engineering

ENVLPE is based on the human immunodeficiency virus type 1 (HIV-1) gag protein. The first zinc finger motif within the NC domain was modified by mutation of all cysteine residues to serines to prevent unspecific RNA binding, and the second zinc finger motif was replaced with the aptamer-binding domain PP7 coat protein (PCP) to enable the binding and recruitment of mRNA molecules tagged with the PP7 aptamer (Figures 1A and S1A). VLPs containing mRNA information can be delivered to other cells when equipped with a suitable surface glycoprotein such as VSV-G. VSV-G and mGreenLantern (mGL) with a PP7 aptamer in its 3' UTR were co-expressed to determine essential elements required for efficient cargo delivery. Since proteolytic processing of VLPs is thought to be both critical and tightly regulated for VLP transduction efficacy, the most efficient VLP delivery systems are found to rely on mosaic constructs wherein protease activity is provided by lentiviral Gag/Gag-Pol plasmids, such as psPAX2 with an inactivated integrase domain ($psPAX_{D64V}$). It was observed that HIV-1 protease was essential for the delivery of PP7-tagged mRNAs encoding mGL (mGL_{PP7}), as efficient delivery was abolished when the HIV-1 protease inhibitor darunavir was added during production (Figure S1B).

L21S was introduced in the MA domain of Gag, which had previously been demonstrated to increase budding efficacy (Figure S1C). Budding efficiency was enhanced by the L21S mutation, particularly when it was present in only half of the particle-forming Gag proteins (Figure S1C). When PCP was grafted directly into the NC domain of Gag/Gag–PolD64V in an attempt to simplify the system, the capability for efficient mRNA delivery was abolished (Figure S1D). The fraction of green fluorescence that could be attributed to mRNA or protein delivery in transduced cells was subsequently investigated. When the CS1 aptamer was used to control for unspecific packaging of mGL mRNA, green fluorescence was still exhibited by almost all recipient cells, although the mean fluorescence

Please cite this article in press as: Geilenkeuser et al., Engineered nucleocytosolic vehicles for loading of programmable editors, Cell (2025), https://doi.org/10.1016/j.cell.2025.03.015

intensity (MFI) was drastically reduced. Co-transfection of microRNA (miR) targeting mGL mRNA reduced the MFI to the level of unspecific controls. This suggests that although most of the green fluorescence was a result of successful mRNA delivery, a substantial amount of mGL protein was non-specifically co-packaged into VLPs and co-transferred into recipient cells (Figure S1E).

To provide a calibration for the performance of the mosaic Gag/Gag–PolD64V + Gag-PCP system compared to recently published experiments with *de novo* protein cages,[70] EPN-24-PCP nanocages with a C-terminal fusion of PCP or single-chain tandem-PCP were compared and found its MFI to be on the same level as the Gag-PCP without Gag/Gag–Pol, but 8-fold lower than Gag-PCP co-expressed with Gag/Gag–PolD64V and the integrase-deficient Gag–Pol (Figure S1F).

Notably, observations from mRNA delivery did not translate seamlessly to RNP delivery. For example, while the unsuccessful attempts to omit Gag/Gag–PolD64V indicated that certain factors of Gag–Pol are crucial for efficient mRNA delivery, the cost of omitting Gag–PolD64V was much smaller when delivering RNPs (Figures S1F and S3C). Remarkably, while RNP delivery is apparently less dependent on Gag/Gag–PolD64V, no signal from non-specific packaging could be detected (Figure 1E), even though a substantial amount with mRNA delivery was observed (Figures S1C and S1E). This effect could be attributed to the fact that the (digital) editing reporter is less sensitive to non-specifically packaged amounts of protein, especially since this is one way that 'empty' Cas9 moieties can be packaged with VLPs.

Incorporation of the PP7 aptamer into the 3' UTR could additionally allow iPE mRNA to be packaged into the functional RNP, but instead led to a decrease in editing efficacy (Figure 1E), suggesting a potential interference of mRNA cargo recruitment/loading with transcription. Competition between mRNA and (pe)gRNA for PCP binding sites could be eliminated as the cause for this effect by including PP7-tagged decoy mRNAs with unrelated functions, which are not expected to affect editing activity. When the individual components unique to Gag/Gag–PolD64V were examined more closely, small effects were found for each, which may have the potential to add up. Interestingly, the negative effect of protease inhibition by darunavir or knockout on VLP production and/or RNP delivery was rather small compared to mRNA delivery and occurred even when darunavir was added during transduction (Figures S1B and S3D). Beyond the protease, it remains unclear how the effects of the respective KO variants in Figure S3D are mechanistically related to VLP assembly or RNP packaging or why RNA delivery was more affected by the absence of Gag/Gag–PolD64V. While this could be related to cargo size (as RNPs are much more spatially compact than mRNAs), it is conceivable that HIV-1 Gag/Gag–Pol is also mechanistically involved in mRNA cargo loading, *e.g.*, by providing a properly matured nucleocapsid (NC) structure and thus mediating mRNA condensation.

Next, the stoichiometry of all ENVLPE components was optimized (Figures S3E and S3F). Optimal results were obtained when a slight excess (2:1) of cargo over VLP was used. Regarding the ratio of each budding component, Gag/Gag–PolD64V gave ideal results when supplied in slight deficit in relation to engineered Gag-PCP. As a ratio of 1:1 was already close to optimal, a combined plasmid was constructed where both components are expressed at identical strength (Gag/Gag–PolD64V & GagNLS-NES_ΔZF2+L21S-PCP, both driven by a separate hybrid CAG promoter on the same plasmid). The optimal ratio for RNP formation appeared to be a 3-fold excess of pegRNA over the prime editor, which should be transferrable to other Cas9 effector strategies as well.

The cargo release mechanism was investigated and optimized in the next step. If the RNP remained tethered to the NC domain in the recipient cell after maturation, the NES of the shuttling domain would likely prevent the nuclear import of the genome editing RNP complex. However, no additional benefit was observed when the NES was repositioned to the C-terminus downstream of the budding domain (p6) (Figures 1H and S3H), indicating that the non-covalent interaction of PCP–PP7 is sufficiently amenable to a local concentration decrease in the recipient cell to shift the equilibrium and facilitate cargo release.

Csy4 increases PE efficacy by 3' protection

To ensure that the improved efficacy of protective Csy4 did not just compensate for potential suboptimal PCP grafting into Gag, the PCP–PP7 system (PCP grafting in NC) was benchmarked to variants with alternative grafting positions (grafting downstream of the p6 domain), which has been previously reported to be a viable option.[71] Since PCP binds as a homodimer to the PP7 aptamer, variants encoding tandem copies of PCP (tdPCP) were compared. Indeed, the previous PCP–PP7-based setup was already the best performing compared to alternative graft positions and tandem variants (Figure S5B, PCP_{ZF2} > $tdPCP_{C\text{-}terminus}$ > $tdPCP_{ZF2}$ > $PCP_{C\text{-}terminus}$).

Harnessing the COM–Com aptamer system as an alternative for PCP–PP7 was also evaluated by introducing Com into either the scaffold or the 3' end of the pegRNA while fusing the Com-binding protein COM to the C-terminus of Gag (Figure S5C). While COM-based ENVLPE worked in general, its performance was reduced compared to the PCP-based ENVLPE setup, which could be explained either by the lower affinity of the COM-Com system or suboptimal RNA-folding of the *com* aptamer. This result still emphasizes the modularity of an aptamer-based recruitment mechanism that can be quickly adapted to other aptamer systems of choice.

Csy4 for 3'-protection and cargo recruitment

After discovering that the recruitment functionality in ENVLPE can be quickly adapted to other aptamer systems beyond PCP–PP7 (Figure S5C), the possibility of Csy4 fulfilling both functions simultaneously was investigated: 3' protective function and cargo loading, harnessing its exceptionally high affinity for the C4 aptamer. For that experiment, the PCP domain was replaced with a C-terminally fused Csy4 domain (Figure S6A), which would be responsible for both recruiting and stabilizing the RNP complex (Figure S6B). Remarkably, this mode of packaging ($ENVLPE_{Csy4}$) also drastically improved prime editing efficacy (Figure S6C), similar to the combination of PCP–PP7 recruitment and untethered Csy4-mediated stabilization. Initially, a fusion of Csy4 to the C-terminus of Gag was tested since Csy4, in contrast to PCP, is monomeric, so the assumption was made that interference with the budding process is less likely. Indeed, no differences were evident in whether Csy4 was C-terminally fused or, as PCP previously, grafted into the NC domain

Please cite this article in press as: Geilenkeuser et al., Engineered nucleocytosolic vehicles for loading of programmable editors, Cell (2025), https://doi.org/10.1016/j.cell.2025.03.015

of Gag (Figure S6D). In this instance, the effect of the omission of PP7 and evopreQ1 was investigated, as Csy4 now covered both functions, recruitment and protection. PP7 could be eliminated without consequence if the C4 aptamer was moved downstream of evopreQ1 to the 3' of the pegRNA, suggesting that a linker sequence separating C4 from the PBS is required for optimal ENVLPE$_{Csy4}$ performance (Figure S6D).

Alternative strategies for 3' protection

Alternative strategies were explored in which the protection and processing of the pegRNA 3' end are performed in separate steps. For this experiment, a cleavage-inactive dCsy4 (Csy4$_{H29A}$) mutant of Csy4 was tested, which supposedly fully retains its high affinity for the C4 aptamer, and combined with the self-cleaving HDV ribozyme motif added to the 3' end of the pegRNA (Figure S9A). While this strategy should, in theory, lead to the same protected 3' end as with active Csy4, it could not provide any additional benefit over evopreQ1 alone (Figure S9B). Placing an HDV ribozyme between evopreQ1 (Q1) and the polyU motif with varied spacer nucleotides between Q1 and HDV led to a significant improvement over Q1 alone (Figure S9B), indicating that precise processing by HDV ribozyme to remove 3'-unpaired nucleotides provided additional protection against 3'-exonucleolytic attack, but still was outperformed by the dedicated Csy4/C4 protection module. Attempts using alternative structured motifs were also proven unsuccessful when compared to evopreQ1 alone (Figure S9C).

Evaluation of 3' protection in BE and Cas9 mode

Next, it was investigated whether the improvements of Csy4 protection can be transferred to conventional gRNA-based effectors. Since 3' extensions are usually accompanied by a major decrease in Cas9 activity (while loop modifications are generally better tolerated), both PP7 aptamer engraftments were examined (Figure S10A) but no benefits of Csy4/C4 protection in Cas9 ENVLPE (Figure S10B) or BE ENVLPEs (Figure S10C) were found.

Engineering minimal, homomeric shuttling vehicles

In-depth investigations into the necessary functionalities in a minimal budding and RNP transfer system resulted in miniENVLPE that also benefits from the dedicated untethered Csy4/C4 protection; however, functional replacement of PCP by Csy4 for direct recruitment of the cargo in miniENVLPE (miniENVLPE$_{Csy4}$) performed very poorly in a direct comparison (Figure 4E).

When the protease (Pr$_{D25A}$) in ENVLPE$_{Csy4}$ and PCP-based ENLVPE was inactivated, it only caused a significant 20% decrease in efficacy for ENVLPE$_{Csy4}$ (Figure S11C) but not in PCP-based ENVLPE (Figure 4F), indicating that ENVLPE$_{Csy4}$ is more dependent on proteolytic release. Also, the omission of Gag/Gag–Pol$_{D64V}$ (containing the protease domain in the Pol frame) is much more detrimental for ENVLPE$_{Csy4}$ (Figure S11D) than for PCP–PP7-based ENVLPE (Figure S11A). This result supports the proposed aptamer-mediated release mechanism for the PCP–PP7 pair since the more stable Csy4–C4 interaction presumably adds a constraint to cargo release, which can then be alleviated again by additional proteolytic activity.

Importantly, ENVLPE$_{Csy4}$ with ΔGag/Gag–Pol$_{D64V}$ was almost completely inactive as a homomeric formulation (Figure S11D), beyond what was to be expected from the data on miniENVLPE$_{Csy4}$ (Figure 4E). It is, therefore, possible that the dimerization of PCP could have contributed to particle assembly, while Csy4 lacks such a property but was compensated for in miniENVLPE with GCN4.

QUANTIFICATION AND STATISTICAL ANALYSIS

Statistics were calculated as specified in each figure using Prism (v.10, GraphPad). Mean and standard deviation (SD) were calculated across biological replicates.

For next-generation sequencing experiments, precision was calculated as the proportion of correct editing events among all editing events (correct/(correct + error) × 100).

We made an effort to reduce any biases introduced during the sample preparation by using master mixes and multichannel pipettes.

No data were excluded from the analyses except for some FACS analyses where replicates were lost during sample processing, and some next-generation sequencing analyses for which certain replicates had to be excluded from calculating the mean value due to obvious technical errors (no reads).

Details on all performed statistical tests are provided in Table S2.

CellPress
OPEN ACCESS

Supplemental figures

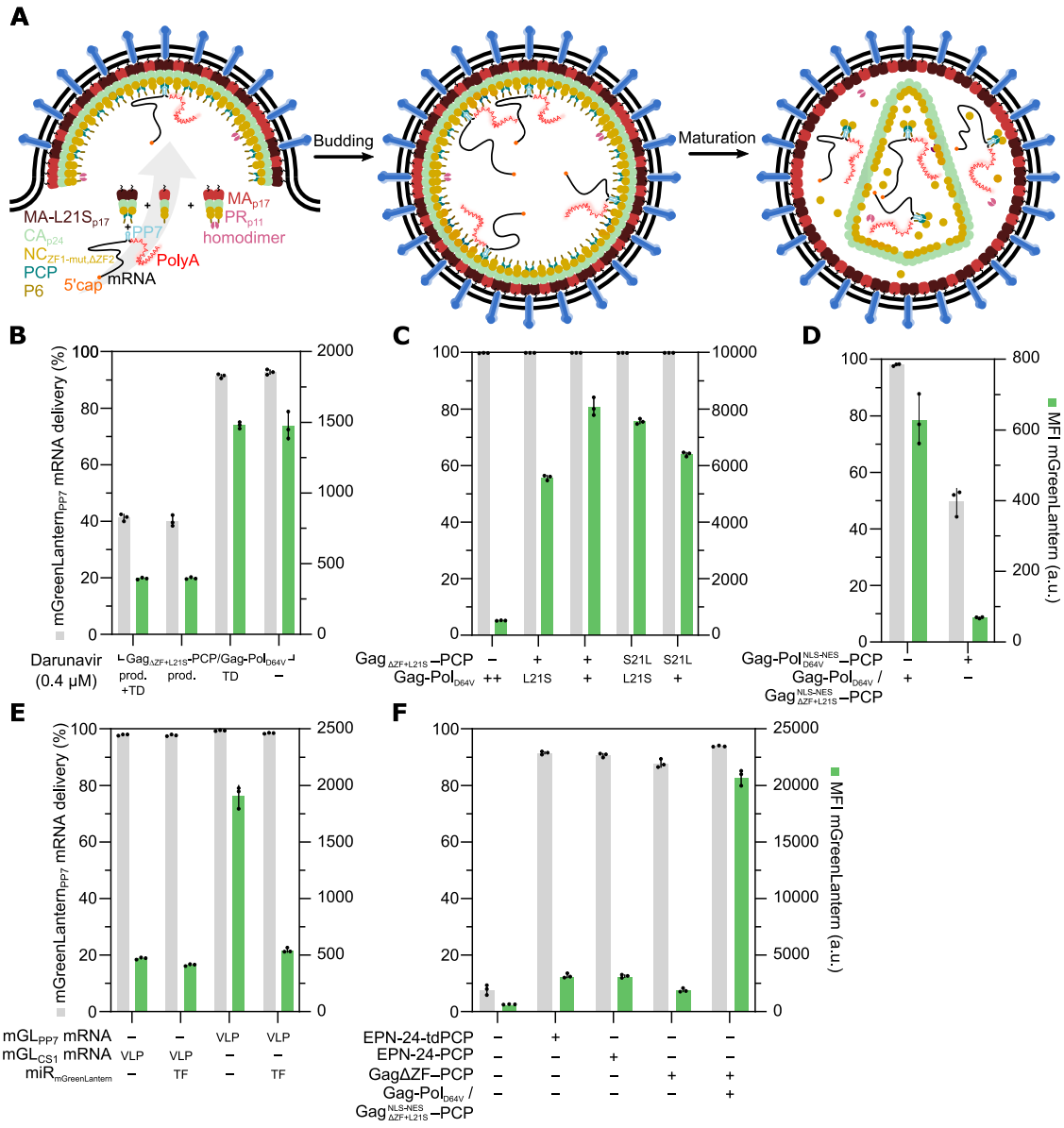

Figure S1. Investigation of relevant factors and general capability of ENVLPE to facilitate mRNA delivery in HEK293T cells, related to design considerations in STAR Methods

(A) Illustration of mRNA packaging using non-shuttling Gag-PCP. The PP7 aptamer is encoded in the 3′ UTR of the cargo mRNA. The VLPs were pseudotyped with VSV-G.

(B) Effect of the protease inhibitor darunavir on mGreenLantern mRNA delivery. Darunavir was added during production (prod.), during transduction (TD), or both (prod. + TD).

(C) Impact of including L21S mutation in the MA domain of Gag when introduced in Gag-PCP or Gag/Gag-Pol$_{D64V}$.

(D) Comparison of mGreenLantern mRNA delivery via Gag-Pol$_{D64V}$-PCP or the mosaic setup using Gag/Gag-Pol$_{D64V}$ and Gag-PCP.

(E) Specificity of Gag-PCP toward PP7-tagged aptamers and the effect of microRNA (miR) transfection (depicted by TF).

(F) Comparison of EPN-24-PCP nanocage variants with Gag-PCP ± Gag/Gag-Pol$_{D64V}$ setups.

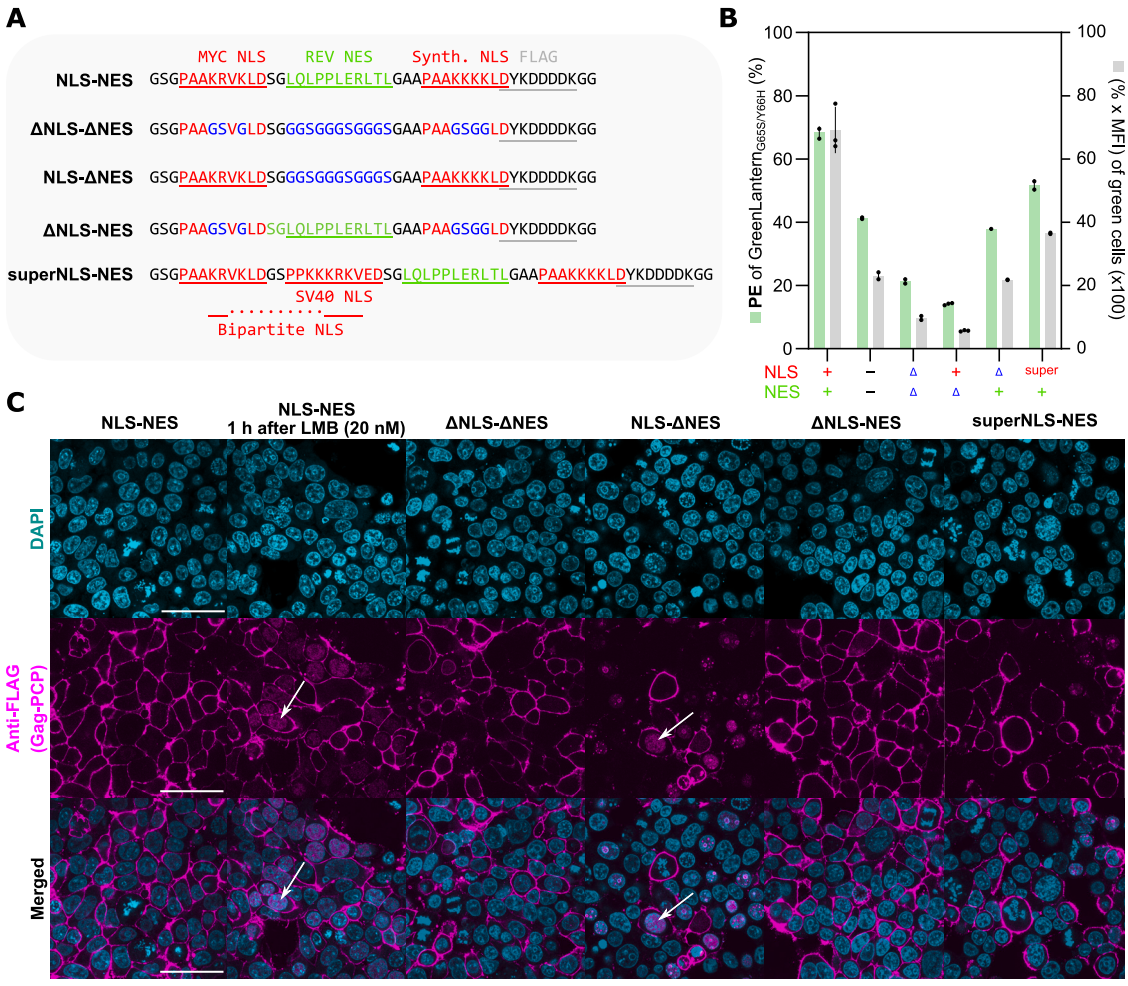

Figure S2. Impact of nucleocytosolic shuttling motifs on VLP-mediated packaging of CRISPR RNPs, related to Figure 1

(A) aa sequences of respective combinations of nuclear localization (NLS) and nuclear export sequences (NES) variants used in (B) and (C).

(B) Evaluation of different combinations of NLS or NES on the delivery of prime editors into the blue mGL HEK293T reporter line.

(C) Immunofluorescence staining of FLAG-tagged Gag variants carrying NLS or NES depicted in (A); 48 h post-transfection into HEK293T cells. Addition of 20 nM leptomycin B (LMB) blocks XPO1/CRM1-mediated nuclear export of HIV-1 REV NES, resulting in nuclear accumulation of a nucleocytosolic shuttling protein (indicated with a white arrow). The scale bar represents 50 μm.

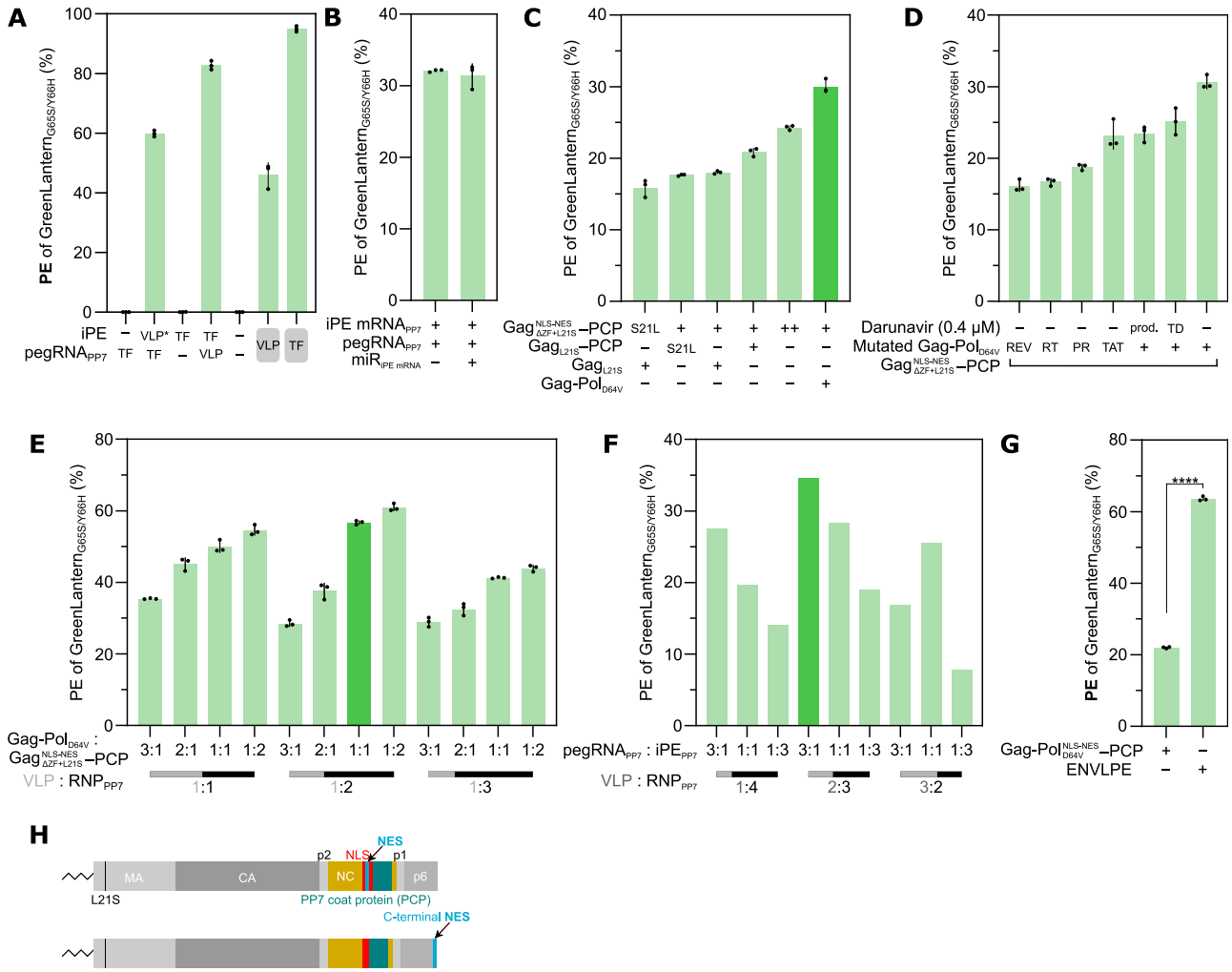

Figure S3. Optimization and characterization of the ENVLPE system for PE-RNP delivery in HEK293T blue mGL cells, related to Figure 1

(A) To determine the limiting component of the prime editor complex, either the mRNA encoding the prime editor protein or the pegRNA was transfected (TF), while the complementary component was transduced (VLP). For the condition where only iPE was delivered via VLP, the iPE mRNA was tagged with a PP7 aptamer to enable recruitment (VLP*).

(B) While being transduced with ENVLPE carrying PE RNPs targeting the blue mGreenLantern reporter, recipient cells were additionally transfected with a miR targeting the 3′ UTR of the iPE mRNA to investigate if any proportion of PE efficacy originated from mRNA delivery instead. miR functionality was independently verified in Figure S1E.

(C) Analysis of the impact on PE delivery when the L21S mutation, as well as the PCP domain, is included in one or both packaging components. To normalize the total amount of packaging plasmid, the amount of an individual plasmid was doubled when used alone (++).

(D) Inactivation of indicated domains encoded in the 2nd generation IDLV packaging vector psPAX2$_{D64V}$ and the impact of the protease inhibitor darunavir.

(E) Co-optimization of mass stoichiometry between Gag/Gag-Pol$_{D64V}$ and Gag-PCP (packaging plasmids) and the ratio between packaging and cargo plasmids. The pegRNA:iPE ratio was set to 3:1 in all conditions.

(F) Co-optimization of mass stoichiometry between pegRNA and iPE (cargo plasmids), and the ratio between packaging and cargo plasmids. Gag/Gag-Pol$_{D64V}$ and Gag-PCP (packaging plasmids) were expressed 1:1 for all conditions.

(G) Effect of inserting the nucleocytosolic shuttling motif and PCP directly into the NC domain of Gag-Pol$_{D64V}$. Bars represent mean ± SD (n = 3 biological replicates). Results of an unpaired t test are shown (****$p < 0.0001$).

(H) Illustration of NES repositioning from NC to C terminus of HIV-1 Gag, as used in Figure 1G.

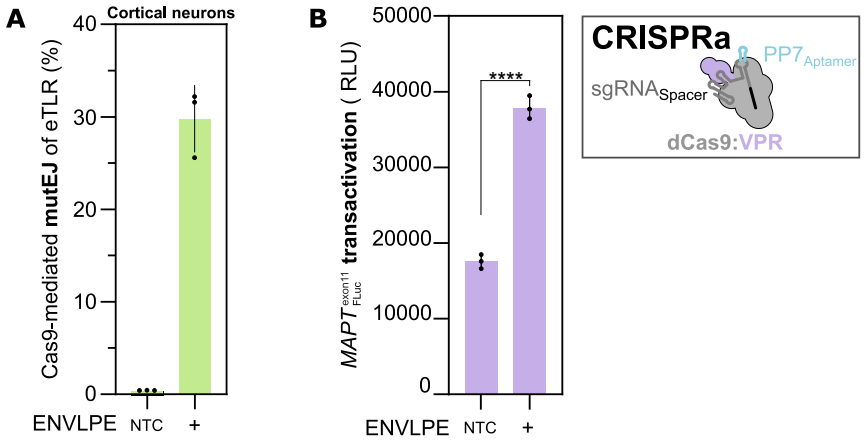

Figure S4. ENVLPE-mediated Cas9 delivery in reporter cortical neurons and transactivation of *MAPT* in HEK293T cells, related to Figure 2

(A) Delivery of Cas9 and PP7-tagged gRNA as RNPs targeting the enhanced traffic-light reporter (eTLRv2); eTLRv2 signals all possible indel events via read-through activation of mGreenLantern in any of the three downstream ORFs. Double-strand breaks (DSBs) were quantified in hiPSC-derived cortical neurons stably expressing eTLRv2 via FC. Bars represent mean ± SD (n = 3 biological replicates).

(B) Relative light units (RLUs) of a *MAPT* HEK293T reporter cell line after transduction with dCas9-miniVPR ENVLPE to induce *MAPT* via CRISPRa. Bars represent mean ± SD (n = 3 biological replicates). Results of an unpaired t test are shown (****$p < 0.0001$).

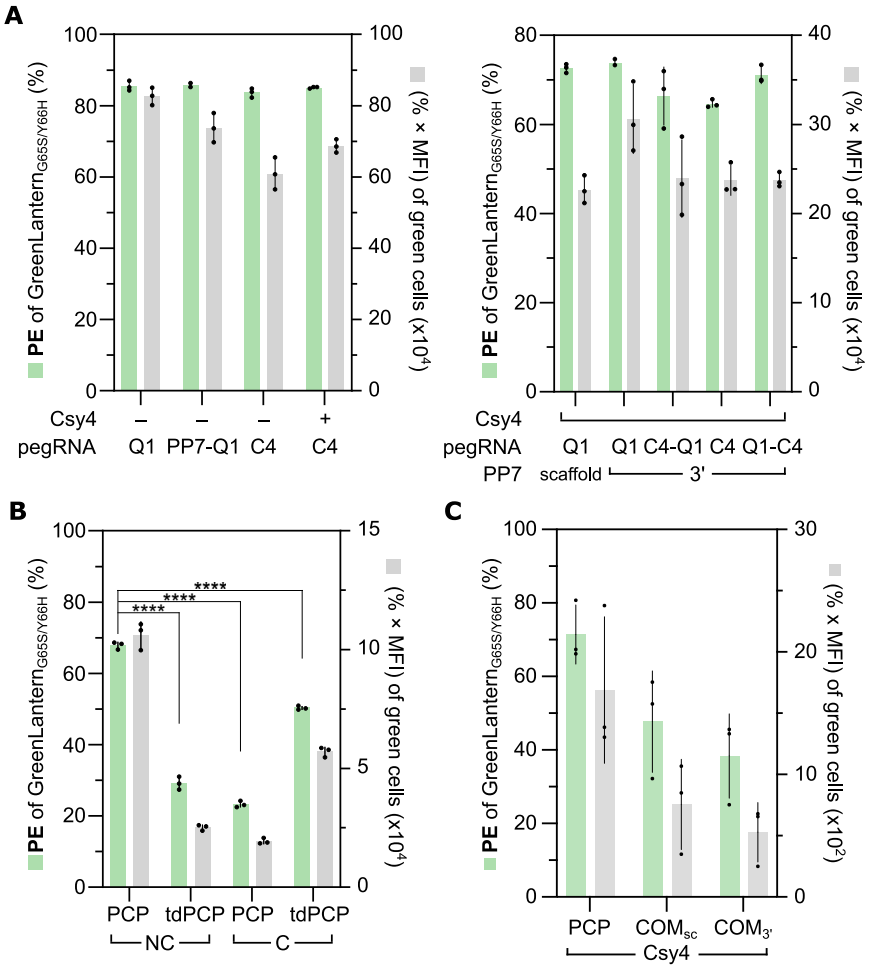

Figure S5. Impact of Csy4/C4 protection in transient transfection settings, validation of PCP-grafting position, and assessment of the versatility of the final pegRNA 3′ configuration, related to Figure 3

(A) PE efficacies in blue mGL reporter HEK293T line transfected with plasmids (i.e., not transduced with ENVLPE) coding for iPE and different pegRNAs with the indicated 3′-modified pegRNAs in the presence or absence of Csy4.

(B) PE efficacies of ENVLPE variants with different grafting positions of PCP (dimeric) and tandem dimers of PCP (monomeric), quantified by FC of the blue mGreenLantern reporter HEK293T cell line. NC indicates the replacement of the NC ZF2 domain with (td)PCP, while C denotes the C-terminal fusion of (td)PCP downstream of Gag after p6. Bars represent mean ± SD ($n = 3$ biological replicates). Selected results are shown of Bonferroni MCT after one-way ANOVA analysis (****$p < 0.0001$).

(C) Checking the *com* aptamer as an alternative to PCP/PP7 under non-saturating conditions (8× dilution). Experiments were performed on the blue mGL HEK293T line. The position of the *com* aptamer in the pegRNA is denoted as sc, scaffold, or 3′, 3′ end. Bars represent mean ± SD ($n = 3$ biological replicates).

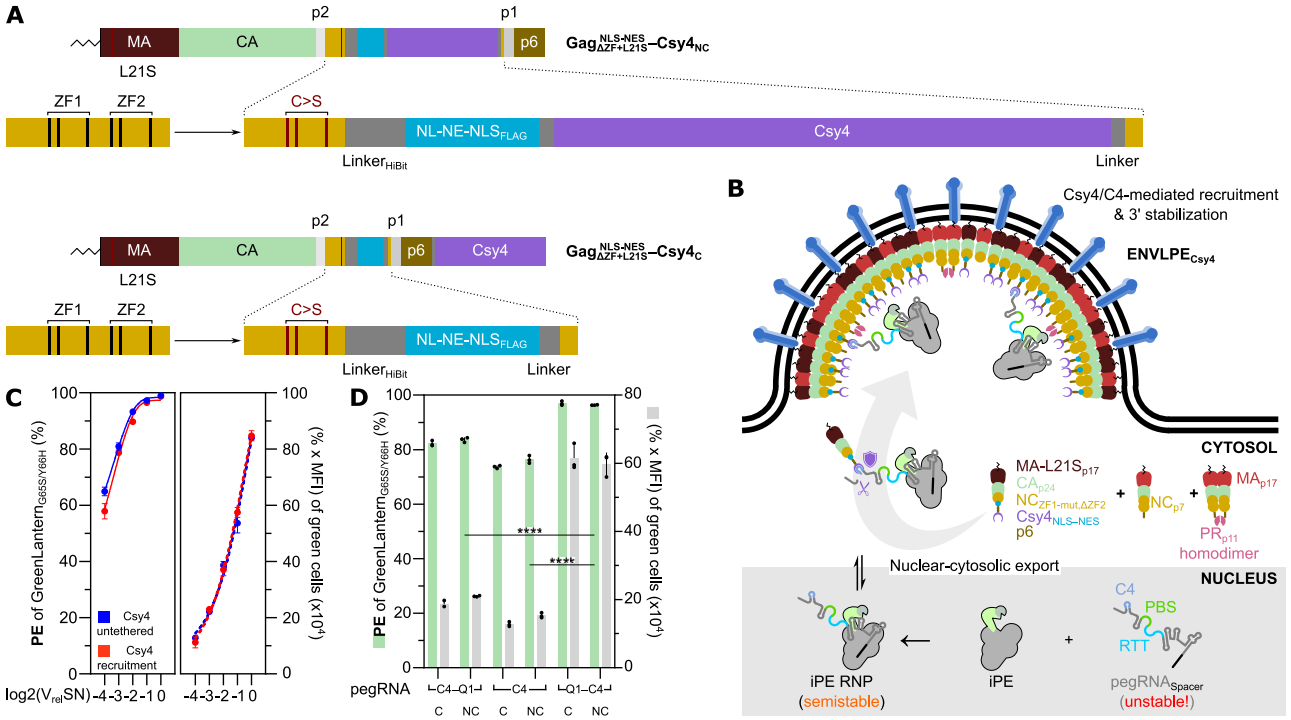

Figure S6. Using Csy4 for simultaneous high-affinity recruitment, related to Figure 3

(A and B) For the ENVLPE$_{Csy4}$ strategy, Csy4 was inserted into Gag NC analogously to ENVLPE in Figure 1A, with the only difference being that an additional C-terminal fusion of Csy4 was tested. In this instance, the Csy4-C4 system can be utilized simultaneously for RNP recruitment and pegRNA stabilization by fusing Csy4 to shuttling Gag, thereby replacing the PCP-PP7 interaction altogether.

(C) Editing efficacy in the blue mGL HEK293T line. The red curves represent ENVLPE$_{Csy4}$ (C-term. fusion), which employs the C4-Csy4 interaction for RNP packaging and pegRNA stabilization, in comparison with ENVLPE$_{PCP}$ in combination with untethered Csy4 for pegRNA protection (blue curves, duplicated from Figure 3B). Log$_2$(V$_{rel}$SN), relative transduction volumes in 2× dilution steps.

(D) Delivery of RNPs for PE via direct fusion of Csy4 to Gag (ENVLPE$_{Csy4}$) to test different orientations of the C4 and Q1 motifs on the pegRNA 3′ end. "NC" denotes Csy4 grafting into the NC domain, "C" denotes fusion to the C terminus of Gag. Experiments were performed on the blue mGL HEK293T line. Bars represent mean ± SD (n = 3 biological replicates). Data were analyzed using two-way ANOVA with Bonferroni MCT (****p < 0.0001).

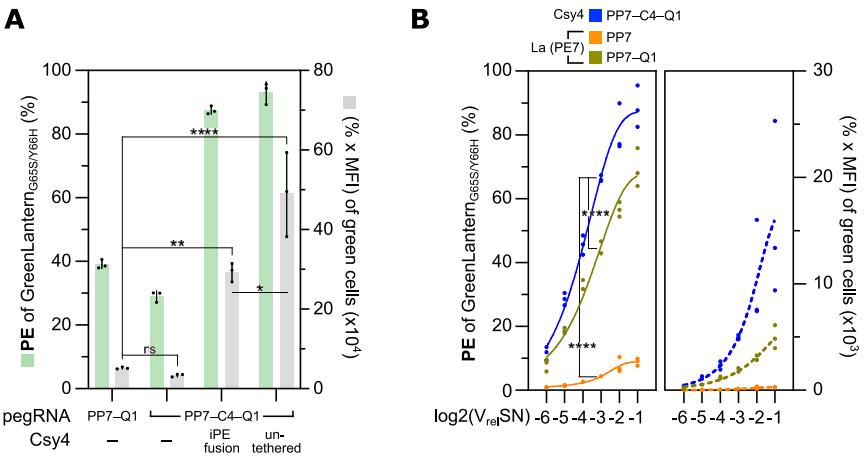

Figure S7. Evaluation of La/SSB-mediated 3′-protection in the context of ENVLPE and context specificity of Csy4/C4 PE-RNP protection system, related to Figure 3

(A) ENVLPE packaged with PE RNPs comprising the final 3′-configuration PP7-C4-Q1 was compared with and without (un)tethered Csy4 expression under non-saturated conditions (8× dilution) for prime editing efficacy on the blue mGL HEK293T line. Selected results of Bonferroni MCT after one-way ANOVA are indicated (****$p < 0.0001$; **$p < 0.01$; *$p < 0.05$; ns $p > 0.05$).

(B) Comparison of ENVLPE-mediated delivery of Csy4/C4-protected prime editors vs. La/SSB-protected prime editors (PE7) across a range of VLP doses on the blue mGL HEK293T line. The PE7 protection system is based on the fusion of an N-terminal fragment (aa 1–194) from La/SSB toward the C terminus of the prime editor to bind and shield the poly(U) stretch of the pegRNA (with or without evopreQ1) from 3′-exonucleolytic attack. $Log_2(V_{rel}SN)$, relative transduction volumes in 2× dilution steps. Points represent $n = 3$ biological replicates (except PE7 PP7-Q1, where $n = 2$).

Selected results of Bonferroni MCT after one-way ANOVA are indicated for the 8× dilution ($log_2(V_{rel}SN) = -3$, ****$p < 0.0001$).

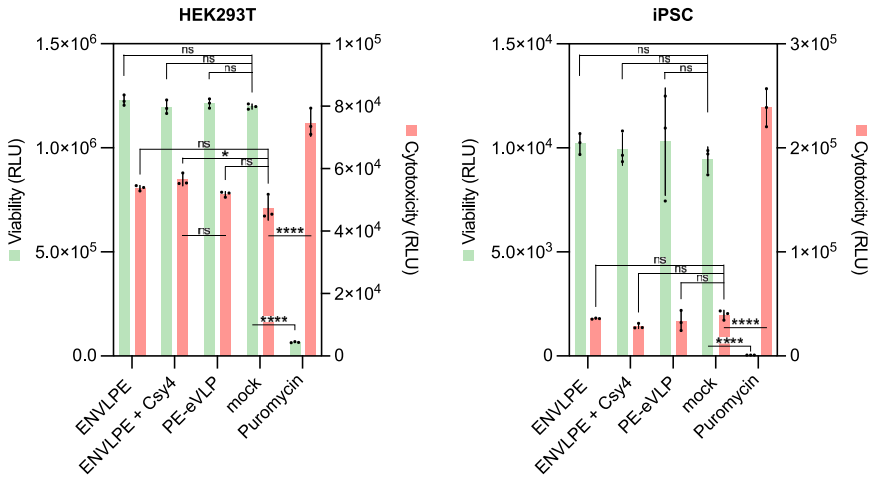

Figure S8. Impact of VLPs on cell viability and cytotoxicity, related to Figure 3

HEK293T cells and hiPSCs were transduced with the indicated VLP systems. 48 h post-TD, cell viability, and cytotoxicity assays were performed. Puromycin 2 μg mL^{-1} was used as a positive control for cytotoxicity. Selected results of Bonferroni MCT after one-way ANOVA analysis are indicated (****$p < 0.0001$; *$p < 0.05$; ns $p > 0.05$).

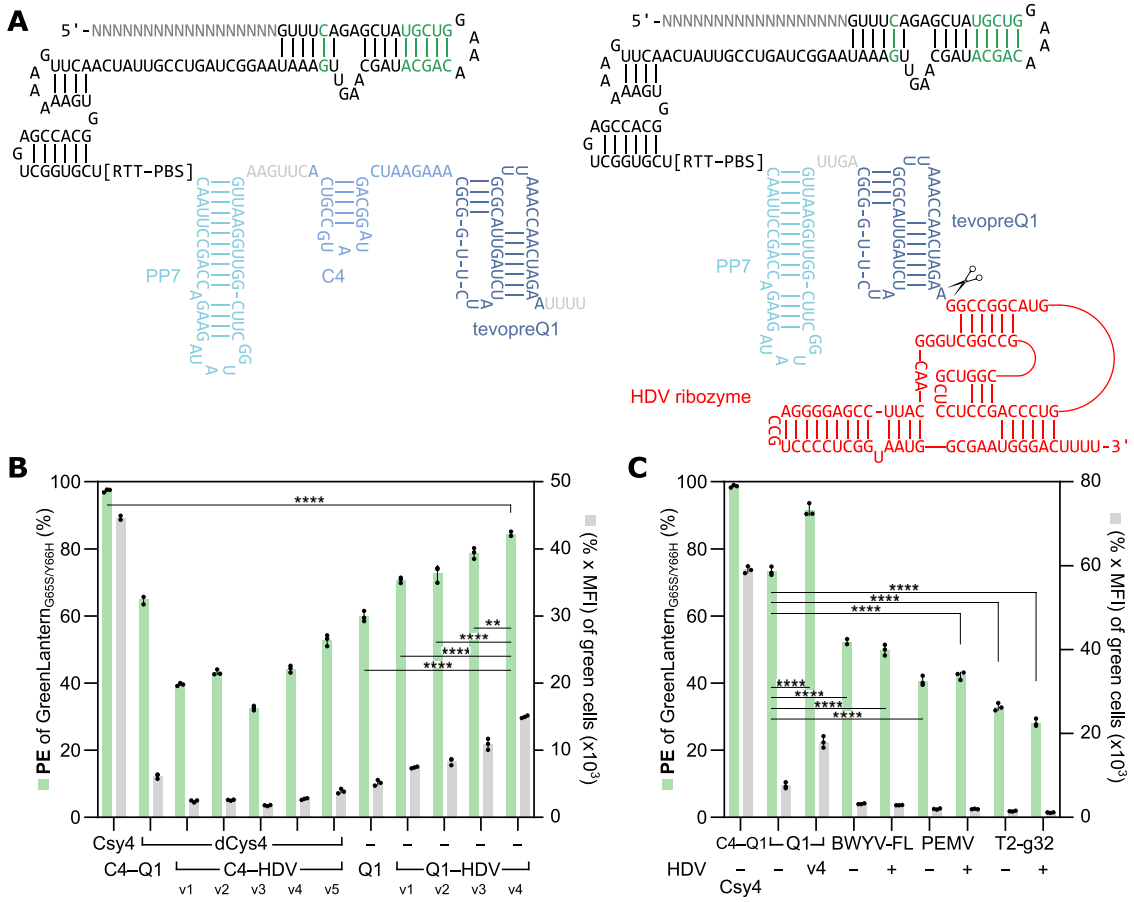

Figure S9. Evaluation of alternative Csy4-independent 3′ stabilization strategies, related to Figure 3

(A) Depiction of the secondary structure of the pegRNA variant carrying PP7-C4-Q1 (left) used throughout the manuscript; and a variant (right) in which truncated evopreQ1 (tevopreQ1) is followed by an HDV ribozyme to remove the 3′-terminal poly(U) stretch, a product of RNA polymerase III promoter termination.

(B) Comparison of the different alternative strategies for 3′-protection from 3′-exonucleolytic attack. dCsy4 indicates a processing-defective variant of Csy4 (H29A), which retains its binding capability for its C4 motif. v1-v4 indicate different minor modifications in the exact placement between C4 or Q1 to the HDV ribozyme with varying nucleotide linkers. Experiments were performed on the blue mGL HEK293T line. Data were analyzed via one-way ANOVA with Bonferroni MCT (****$p < 0.0001$; **$p < 0.01$).

(C) Comparison of a variety of pseudoknot structures with and without a downstream HDV ribozyme as alternative 3′-protection motifs. Experiments were performed on the blue mGL HEK293T line. Data were analyzed via one-way ANOVA with Bonferroni MCT (****$p < 0.0001$).

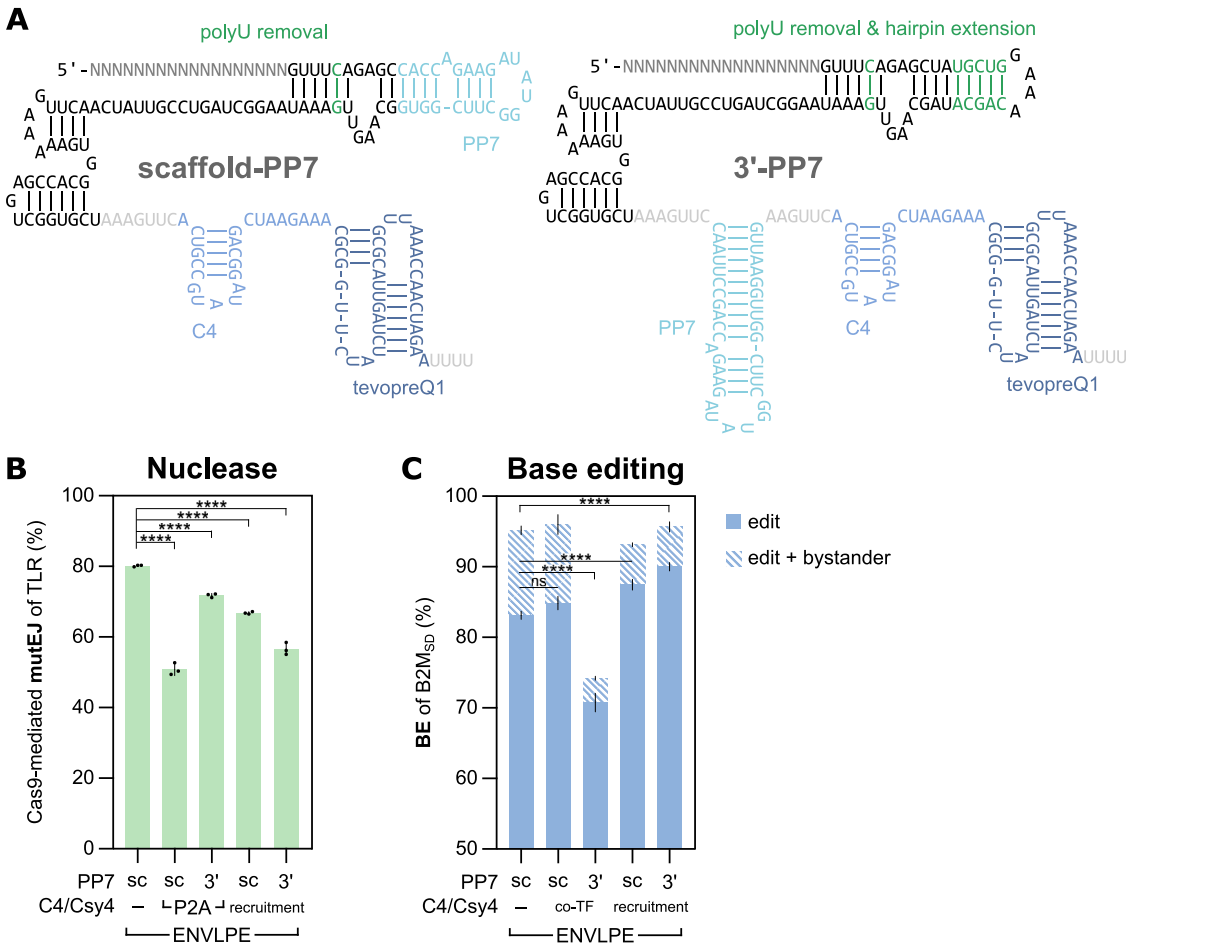

Figure S10. Effect of Csy4 protection on ENVLPE-mediated Cas9 delivery or BE, related to Figure 3

(A) Illustration of sgRNA structures, either with insertion of the PP7 aptamer into the scaffold in combination with the C4 aptamer and downstream tevopreQ1 at the 3′-end or all the components at the 3′-end.

(B and C) Investigation of the effect of the C4/Csy4 protection strategy on ENVLPE-mediated Cas9 and BE delivery using the gRNAs scaffolds depicted in (A). Csy4 was either co-expressed with the Cas9 effector via a 2A peptide ("P2A"), co-transfected as a separate plasmid ("Co-TF"), or fused to ENVLPE ("recruitment"). For (B), indels were quantified via FC analysis of the TLR reporter cell line. For (C), on-target base edits and bystander edits of the endogenous B2M locus in HEK293T cells were quantified via NGS. Results were analyzed via one-way ANOVA; selected results from Bonferroni MCT are indicated by asterisks (****$p < 0.0001$; ns $p > 0.05$). sc, scaffold-PP7; 3′, 3′-PP7.

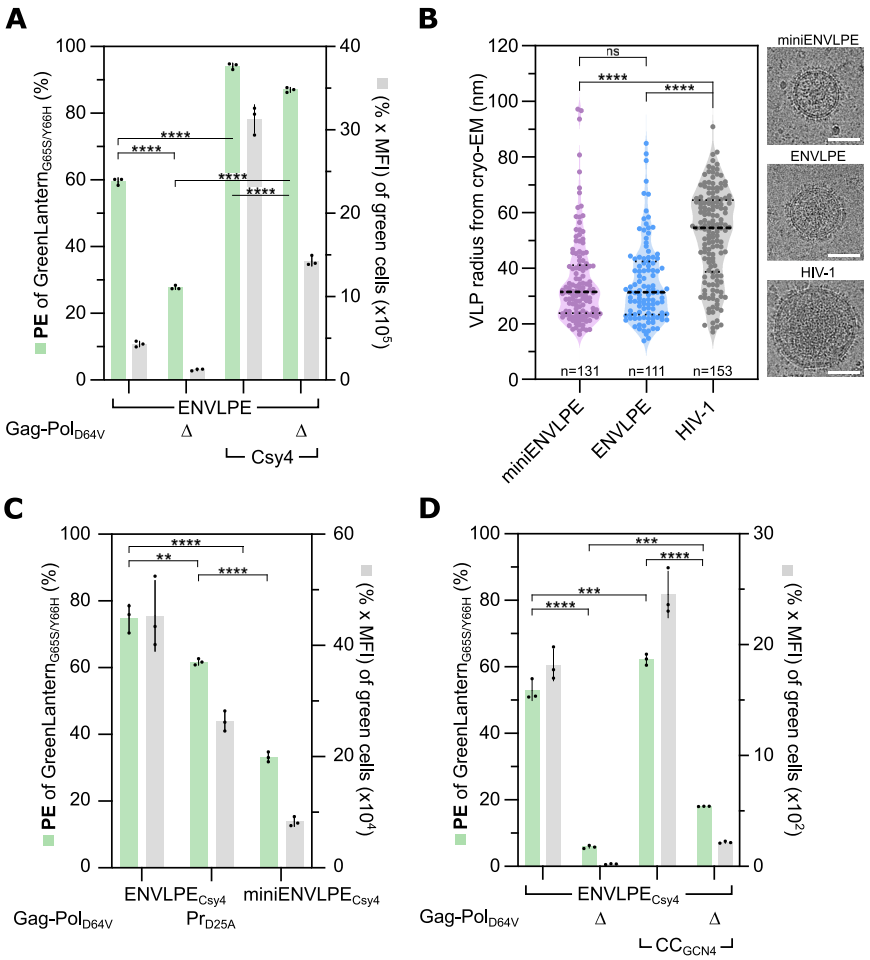

Figure S11. Investigation of the ENVLPE size distribution and release mechanism, related to Figure 4

(A) Analysis of the impact of Gag/Gag-Pol$_{D64V}$ co-expression on PE and PE$_{Csy4}$ efficacy for ENVLPE. Experiments were performed on the blue mGL HEK293T line.

(B) Distribution of VLP radii in comparison with HIV-1 Gag measured by cryoelectron microscopy. The thick dotted line represents the median, while the thin dotted lines constitute the quantiles. Results were analyzed by the Kruskal-Wallis test with Dunn's MCT (****$p < 0.0001$; ns $p > 0.05$). Representative cryo-EM micrographs of the respective species are shown on the right; HIV-1 denotes particles made of HIV-1 Gag/Gag-Pol$_{D64V}$ expressed from psPAX2$_{D64V}$. Scale bar, 50 nm.

(C) Investigating the protease dependence of ENVLPE$_{Csy4}$ by functional inactivation (Pr$_{D25A}$ or omitting Gag-Pol (Δ) under non-saturating conditions (8× dilution). Experiments were performed on the blue mGL HEK293T line.

(D) Benefit of CC$_{GCN4}$ on chimeric and homomeric ENVLPE$_{Csy4}$ assemblies assessed under non-saturating conditions (8× dilution). Experiments were performed on the blue mGL HEK293T line.

For (A), (C), and (D), selected results are shown from one-way ANOVA with Bonferroni MCT (****$p < 0.0001$; ***$p < 0.001$; **$p < 0.01$).

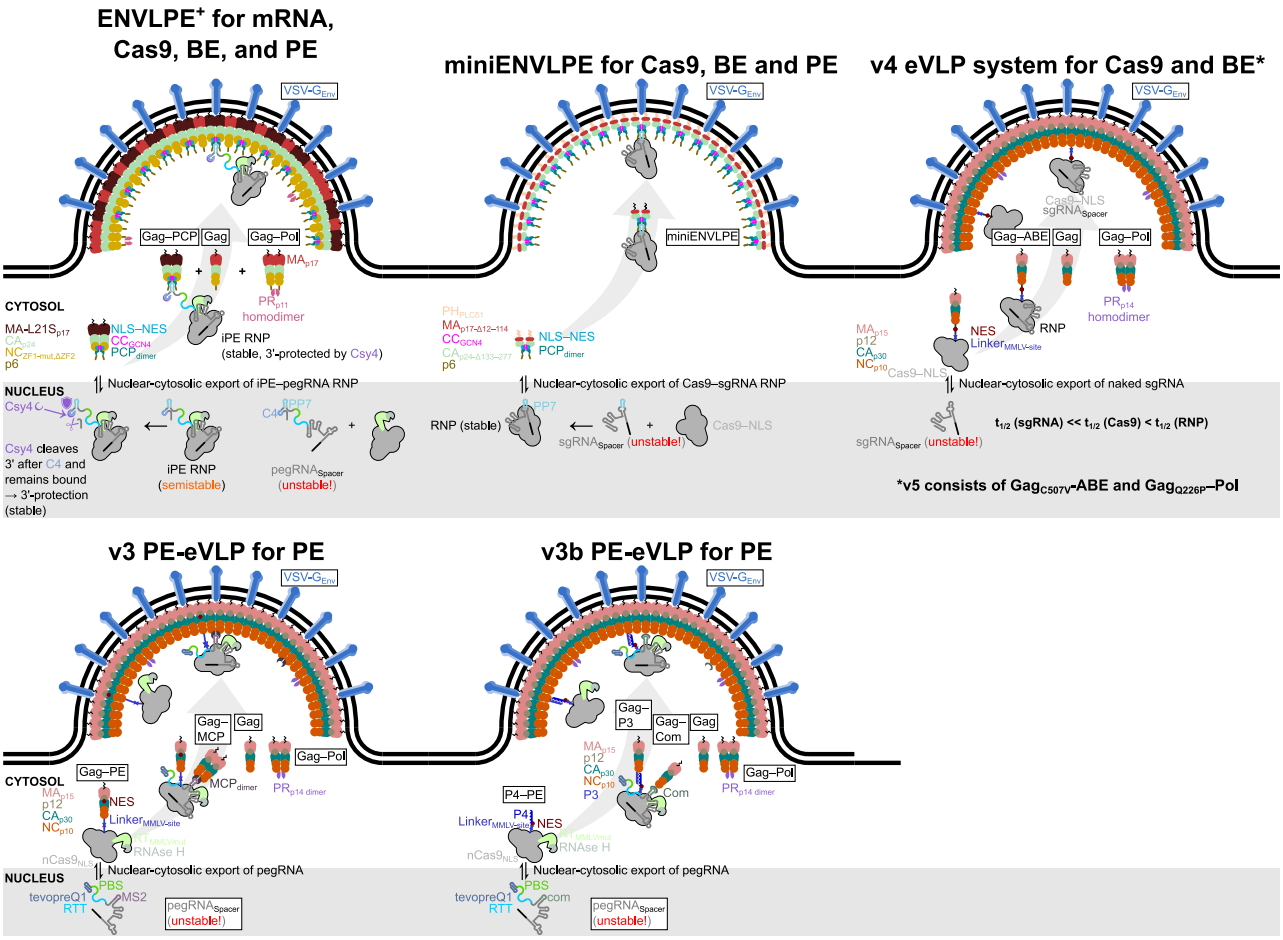

Figure S12. Assembly and RNP recruitment mechanisms in ENVLPE and eVLP variants, related to Figures 5, 6, and 7

The Cas9 effector protein binds the stabilized gRNA-Cas-effector ribonucleoprotein (RNP) complex in the nucleus; nucleocytosolic shuttling (NLS-NES) of Gag-PCP enables binding of the fully assembled RNP via PCP-PP7 interaction. The system enables modular packaging of various RNP complexes and only requires modification of the (pe)gRNA with a PP7 aptamer. Csy4 cleaves and protects the pegRNA in the RNP complex.

v·4 eVLPs consist of an MMLV-Gag fusion to a genome-editing effector protein of choice. The fusion protein shuttles between the nucleus and cytosol to package the unprotected gRNA. In contrast to ENVLPE+, packaging of the Cas *apo*-enzyme (without gRNA) is possible; the genome editor is released after budding only upon proteolytic processing of the Gag polyprotein by the protease encoded in MMLV Gag/Gag-Pol.

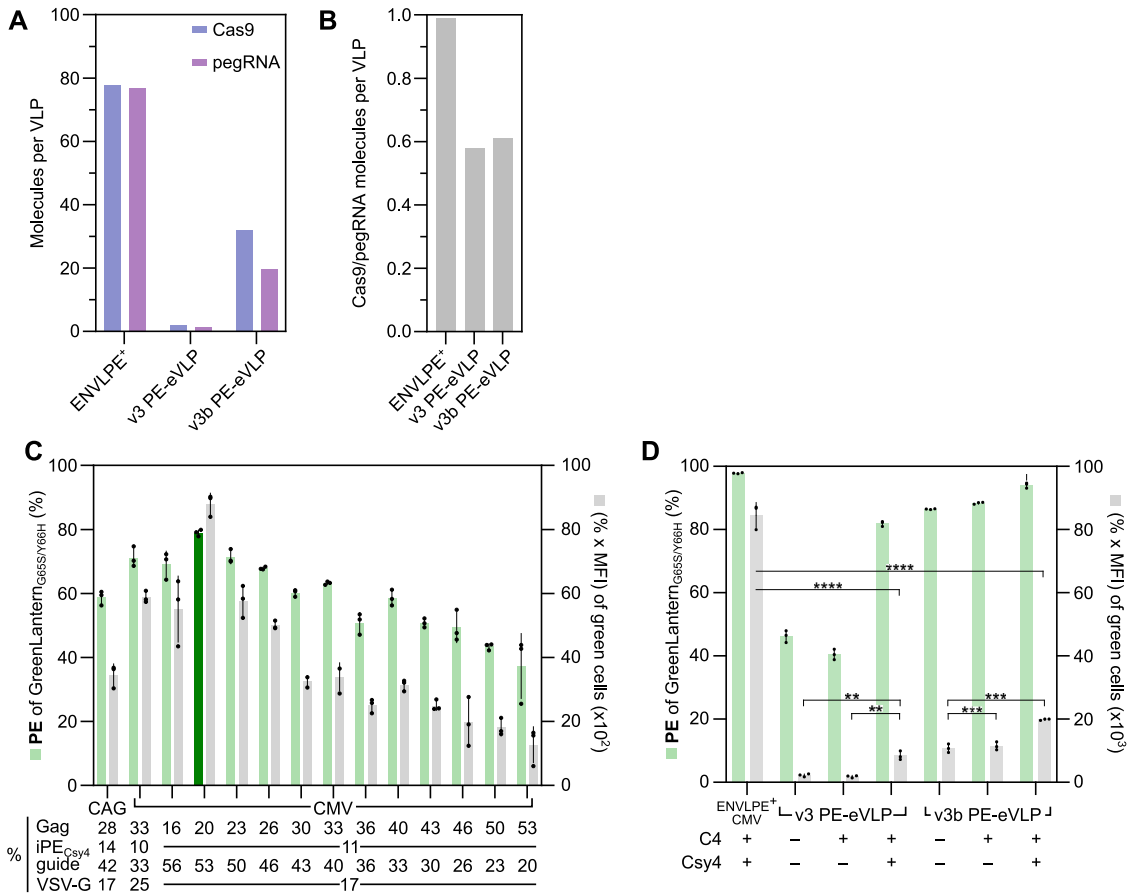

Figure S13. Characterization of RNP loading into different VLP systems, increasing ENVLPE titers by switching from CAG to CMV promoter-driven plasmids, and the benefit of PE_{Csy4} for PE-eVLP-mediated RNP delivery, related to Figures 5, 6, and 7

(A) Quantification of Cas9 molecules per VLP matched with pegRNA molecules per VLP for ENVLPE and v3(b) PE-eVLPs. VLPs produced in 15-cm dishes were purified by ultracentrifugation and resuspended in 1/1,000th of the original volume prior to analysis.

(B) Corresponding Cas9:pegRNA packaging ratios.

(C) Optimization of ENVLPE$^+$ plasmid ratios at non-saturating conditions (8× dilution) after switching ENVLPE$^+$ component expression to CMV promoter-driven plasmids. The chosen ratio for the benchmarking experiments in Figures 5B–5D is indicated in dark green.

(D) To test the compatibility of the Csy4/C4 protection system with v3/v3b PE-eVLPs, Csy4 was supplied as a co-expressing plasmid from a separate plasmid for the PE-eVLP systems. Experiments were performed on the blue mGL HEK293T line. Transduction was performed at 2× dilution. Selected results are shown of Bonferroni MCT after one-way ANOVA analysis (****$p < 0.0001$; ***$p < 0.001$; **$p < 0.01$).

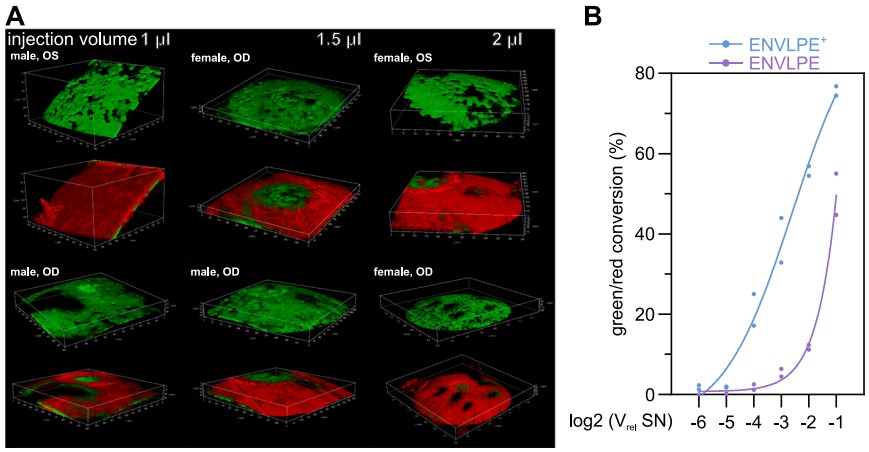

Figure S14. Delivery of Cre_{NLS} mRNA to activate a red/green-reporter locus, related to Figure 7

(A) Cre_{NLS} mRNA-loaded ENVLPEs were injected in different volumes subretinally into the eyes of mT/mG reporter mice (2.53×10^8 particles μL^{-1} in PBS). Two-photon excitation imaging-based 3D reconstruction of the posterior portion of intact mouse eyes are shown, 1 week after subretinal injection. Green-fluorescent cells indicate successful reporter activation by Cre in the red/green-reporter locus. Oculus dexter (OD) indicates the right, Oculus sinister (OS) the left eye. For each reconstruction, the total extent of x and y dimensions is 550 µm.

(B) Quantification of Cre_{NLS} mRNA delivery by ENVLPE vs. $ENVLPE^+$ to a HEK293T reporter cell line carrying a green/red-reporter locus (inverse signal logic compared with A). $Log_2(V_{rel}SN)$, relative transduction volumes in 2× dilution series.

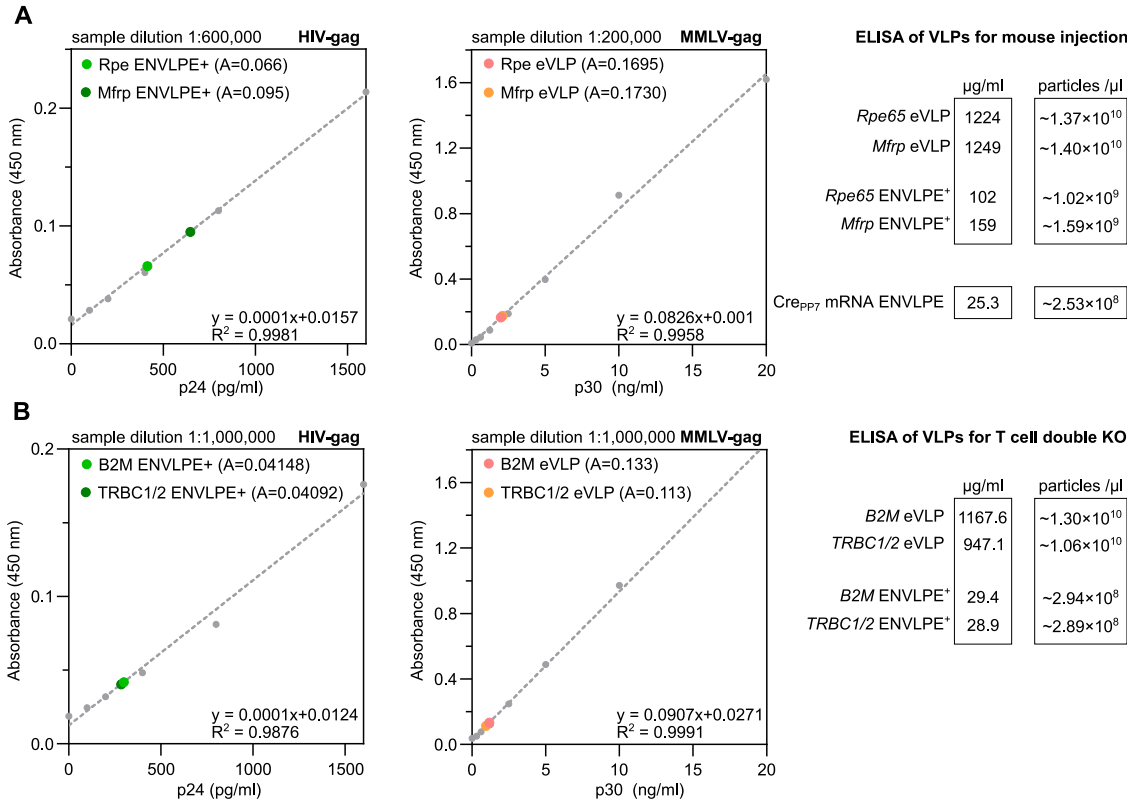

Figure S15. Quantification of VLP titers using anti-p24 (HIV-1) or anti-p30 (MMLV) ELISA, related to Figures 6 and 7

(A) Quantification of ENVLPE$^+$ and v3 PE-eVLP titers after ultracentrifugation prior to subretinal injections. The VLP amount per volume was calculated based on the assumption that 2,500 HIV-1 Gag monomers (or 1,800 MMLV Gag monomers) form the capsid.

(B) Assessment of VLP titers for *ex vivo* BE of T lymphocytes.

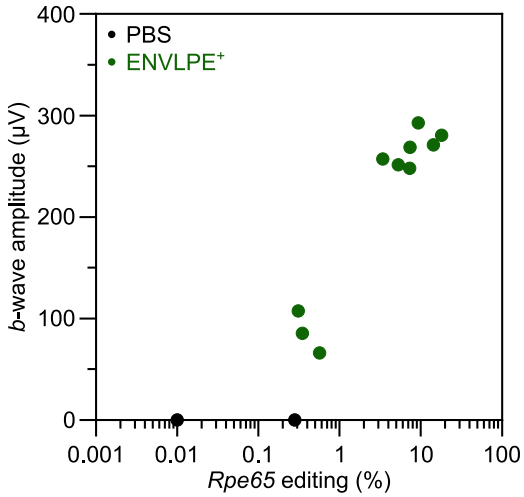

Figure S16. Correlation of *in vivo* editing of *Rpe65* in *rd12* mice with corresponding *b*-waves, related to Figure 7

Correlation plot of *Rpe65* prime editing efficacy and functional restoration quantified by *b*-wave amplitudes in response to a light stimulus after ENVLPE^{+}-mediated iPE$_{Csy4}$ delivery; points correspond to the subset of matching pairs of data points also shown in Figures 7I and 7K.

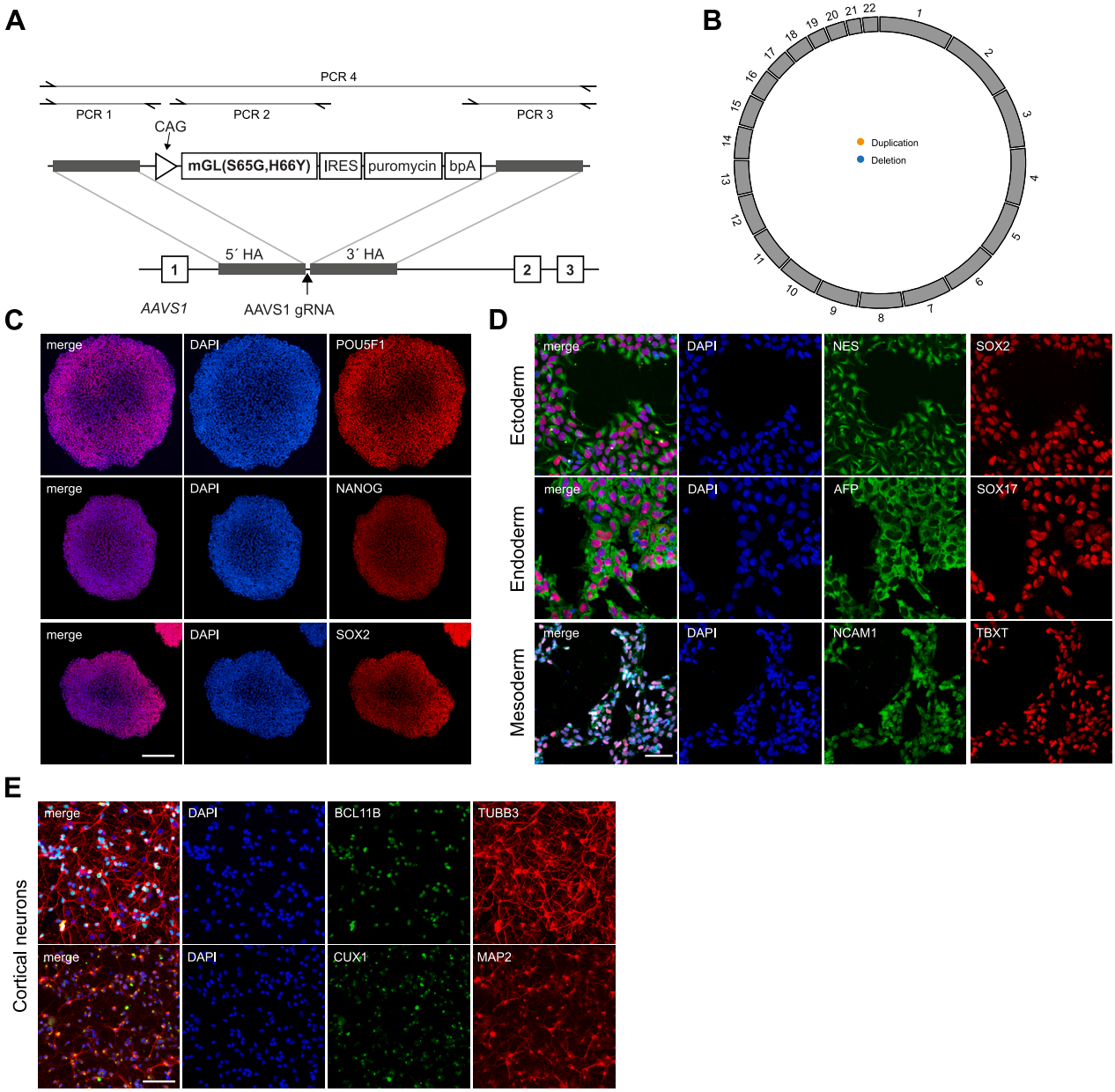

Figure S17. Characterization of pluripotency and neuronal differentiation of the blue mGL reporter iPSC line, related to Figure 1

(A) Schematic illustration of the *PPP1R12C* (*AAVS1*) locus with the inserted cassette encoding the blue mGL reporter as well as a puromycin N-acetyltransferase mediating resistance to puromycin selection.

(B) Analysis of copy-number variation (CNV) in the context of the hiPSC genotype.

(C) Example immunostainings of hiPSC cell markers (POU5F1, NANOG, and SOX2) in the blue mGL cell line after CRISPR-Cas9-mediated knockin. Scale bar, 200 μm.

(D) Immunostaining to show the ability of the generated cell line to differentiate into all three lineages. Scale bar, 50 μm.

(E) Immunostaining of the cell line after differentiation into cortical neurons. Scale bar, 50 μm.

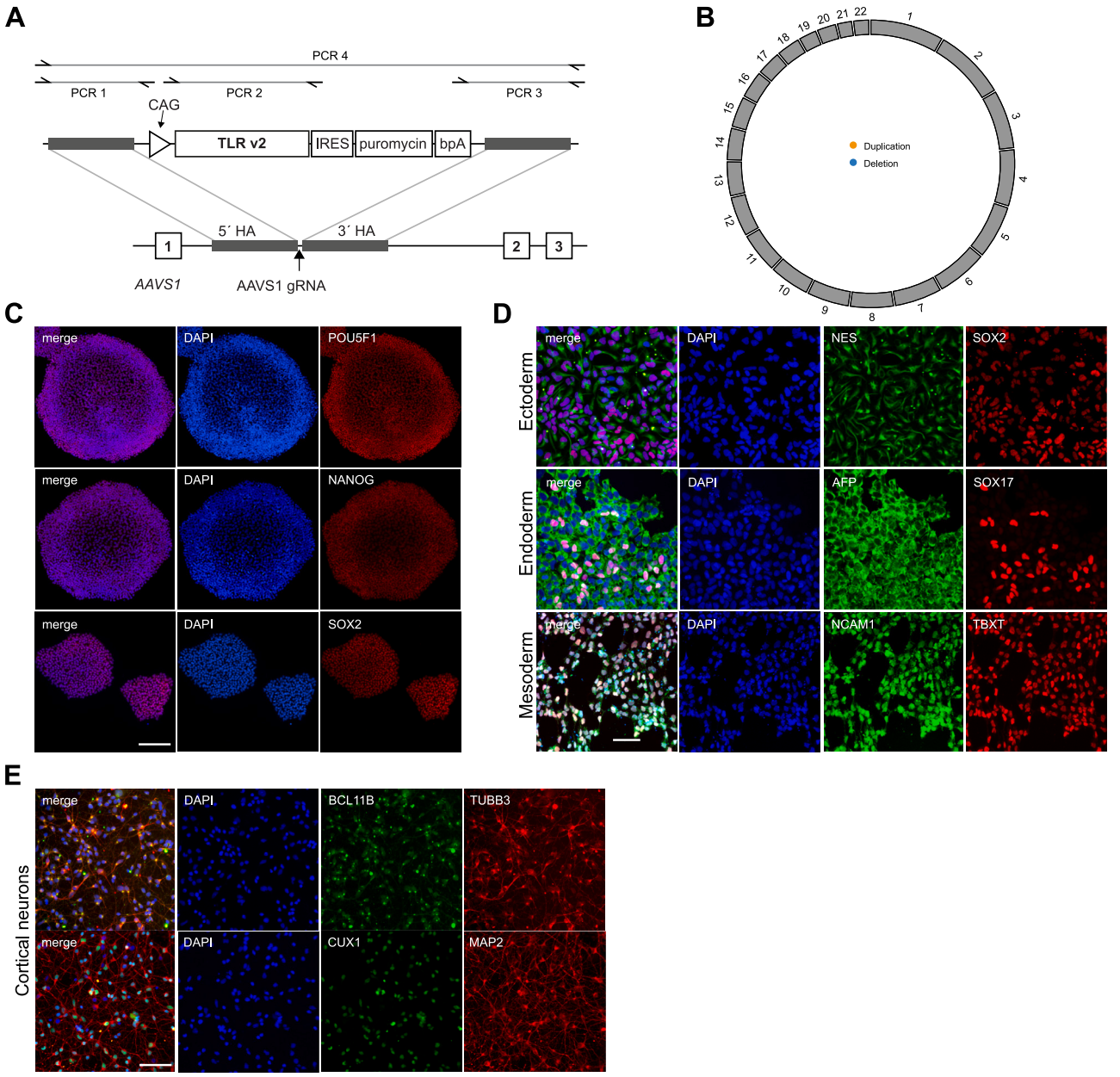

Figure S18. Characterization of pluripotency and neuronal differentiation of the eTLRv2 reporter hiPSC line, related to Figures 2 and S4

(A) Schematic illustration of the *PPP1R12C* (*AAVS1*) locus with the inserted cassette encoding the enhanced traffic-light reporter eTLRv2 as well as a puromycin N-acetyltransferase mediating resistance to puromycin selection.

(B) Analysis of copy-number variation (CNV) in the context of the hiPSC genotype.

(C) Example immunostainings of pluripotency markers (POU5F1, NANOG, and SOX2) in the eTLRv2 hiPSC, after CRISPR-Cas9-mediated knockin. Scale bar, 200 μm.

(D) Immunostaining to show the ability of the generated cell line to differentiate into all three lineages. Scale bar, 50 μm.

(E) Immunostaining of the cell line after differentiation into cortical neurons. Scale bar, 50 μm.

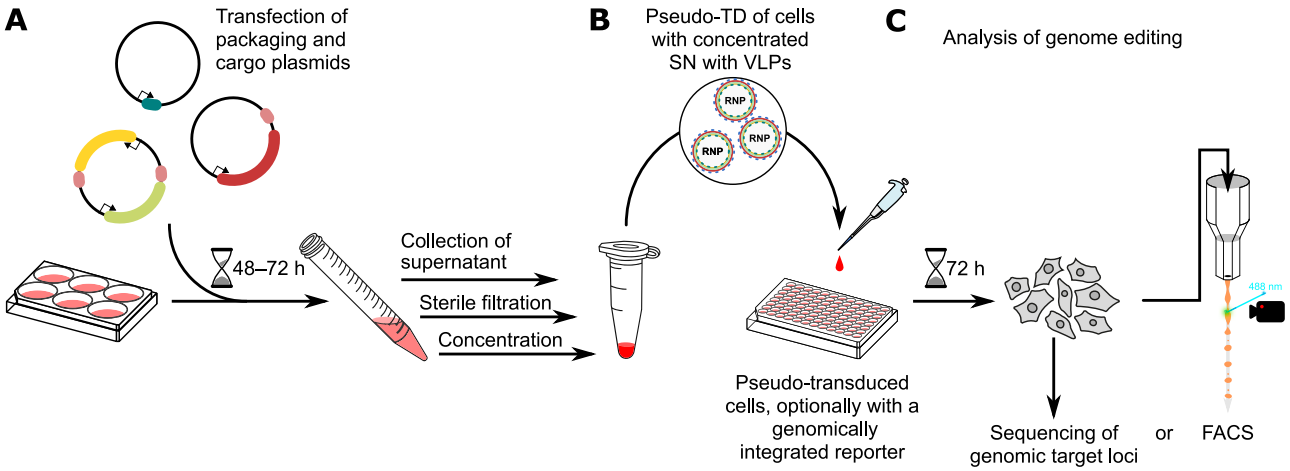

Figure S19. Workflow of ENVLPE particle production, purification, transduction, and analysis, related to VLP production in STAR Methods

(A) Co-transfection of HEK293T cells with packaging, cargo, and glycoprotein plasmids. The cargo plasmids encode a PP7 aptamer-tagged (pe)gRNA and a suitable genome-editing effector. 48–72 h post-transfection of the producer cells, the supernatant (SN) containing the VLPs was collected and sterile-filtered to remove cell debris and leftover transfection reagents. Subsequently, the filtered SN was concentrated using a molecular-weight-cutoff filter (100 kDa).

(B) For pseudo-transduction (pseudo-TD) of the target cells, the supernatant was applied to the cells without exceeding 20% of the total volume of the recipient cell's original growth medium. For simplicity, pseudo-TD is always referred to as transduction/TD.

(C) To optimize the VLP system, cells were analyzed 72 h post-TD via targeted amplicon sequencing of the respective targets or FACS analysis if fluorescence-reporter cell lines were used.